Electronic Spectroscopy of Transient Species
in Plasma Discharges

Inauguraldissertation

Zur Erlangung der Würde eines Doktors der Philosophie vorgelegt der
Philosophisch-Naturwissenschaftlichen Fakultät der Universität Basel

von

Pawel Cias

aus Konskie (Polen)

Basel, 2004

Genehmigt von der Philosophisch-Naturwissenschaftlichen Fakultät

auf Antrag der

Herren Professoren John P. Maier und Jakob Wirz

Basel, den 10 Juni 2004

Prof. Dr. Marcel Tanner

Dekan

- Ile razy zaczna cie napastowac podobne mysli, idz do ktorej z naszych swiatyn i przypatrz sie jej scianom zatloczonym obrazami ludzi, zwierzat, drzew, rzek, gwiazd - zupelnie jak ten swiat, na ktorym zyjemy. Dla prostaka figury podobne nie maja zadnej wartosci i moze niejeden zapytywal: na co one? Po co rzezbia je z tak wielkim nakladem pracy? Ale medrzec ze czcia zbliza sie do tych figur i ogarnawszy je spojrzeniem czyta w nich historie dawnych czasow albo tajemnice madrosci.
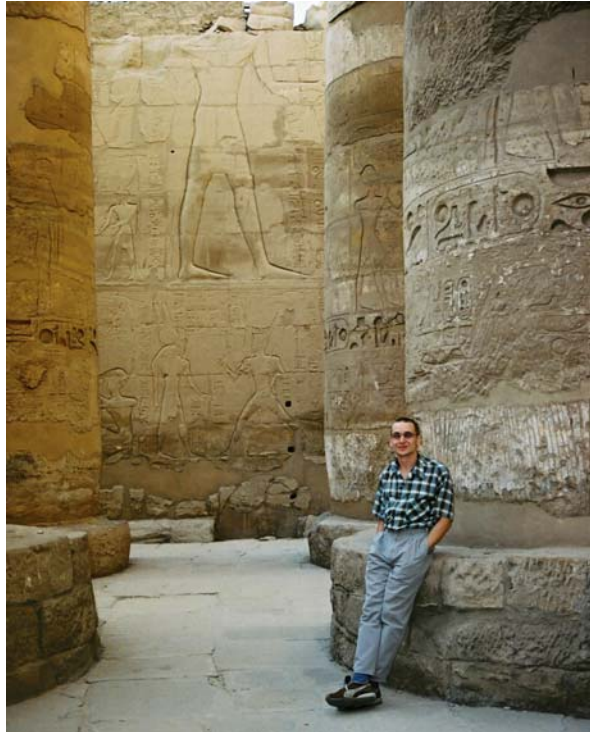
- Whenever these thoughts start to haunt you, go to some of our temples and look carefully at its walls overcrowded with pictures of people, animals, trees, rivers, stars - exactly like the world we live on. For the simpleton these figures are worthless and perhaps not one of them was asking: What are they for? Why are they carved with such an effort? But a wise man approaches them with honor. He sweeps them with his eyes and reads the stories of remote times or the secrets of wisdom.

<div style="text-align:center">

Boleslaw Prus,

Pharaoh

</div>

Acknowledgements

It gives me great pleasure to acknowledge the help and support that I have received during the preparation of this thesis:

I would like to thank Prof. John P. Maier for giving me the opportunity to work in his group. The excellent working environment and the essential resources to learn and do research during the period of my study are greatly acknowledged. I would also like to thank Prof. Jakob Wirz for his courteously agreement to act as my co-referee.

I am also particularly indebted to PD Dr. Harold Linnartz for his guidance and invaluable assistance for the first 2.5 years of my study.

I express my profound gratitude to Tomasz Motylewski for familiarizing me with the experiment and sharing his deep knowledge with me. Similar thanks are directed to Olga Vaizert-Peter.

I would like to express my appreciation to Mitsunori Araki for an invaluable help; and to my colleagues from the crds-lab: Alexey Denisov and Elena Achkasova for very nice collaborative work.

I would like to also thank Lucia Grüter and Patrick Furrer for their fruitful cooperation.

I am also grateful to the people who were technically involved in the experiment for their effort and patience. The generous offer of their experience and knowledge is most deeply appreciated. My special thanks are especially directed to Karl Mutschler from the mechanical workshop for his service and extraordinary skills in constructing sophisticated technical devices; and to Georg Holderied for his help on the field of the electronics. I also feel especially indebted to Jacques Lecoultre not only for synthesizing huge amounts of exotic isotopic substances, which were used in the experiments, but also for priceless lessons and showing me that studio photography is not always so easy as it sometimes seems to be.

Pawel Cias

Contents

0. Introduction

0. 1. Motivation and objectives of this thesis

The first major objective of this work is to expand previous measurements carried out by means of pulsed cavity ringdown experiment toward longer carbon chains of astrophysical relevance. So far cavity ringdown spectroscopy in a supersonic slit jet plasma has been applied to obtain gas phase electronic spectra of a broad range of pure and substituted carbon species. The electronic spectra of the linear chains of the following species were already measured and analyzed: C_n, $C_{2n}H$, $NC_{2n}N^+$, $HC_{2n}N$, $NC_{2n+1}N$, $HC_{2n}H^+$. As the direct absorption measurement does not distort either the shape nor the intensity ratios of measured bands these spectra can be easily used for comparison with diffuse interstellar bands (DIBs). Because these comparisons were not successful so far (no exact match laboratory spectra with DIBs was found), a further effort had to be put in the search of the molecules that could be a carrier of these mysterious interstellar bands. Because recent studies showed that probability of finding the potential carrier is higher in the case of the longer chains, it seemed quite reasonable to try to look for it in the mentioned before group of carbon chains with higher number of carbon atoms.

Especially tempting appeared the idea of obtaining the spectrum of pentaacetylene cation as the matrix experiment results showed that its origin band fits the technical and optical possibilities of the pulsed CRD experimental set-up. The spectrum of $HC_{10}H^+$ could be then compared with the astrophysical data in order to check if there is some match with DIBs or not.

The second major part of this work deals with the search for the gas-phase electronic spectrum of the cyclic B_3 molecule. The molecule is of interest because several of the excited electronic states are degenerate in D_3 symmetry. As a consequence, this should undergo the Jahn-Teller effect. The spectrum of B_3 was already measured in neon

matrix and it showed a complex vibronic structure. Unfortunately, the resolution of the matrix spectra is not sufficient for deep analysis of that effect. Thus a high resolution spectrum in the gas phase is required. As a gaseous precursor could not be used for the production of B_3, there was a need for a modification of the experimental set-up.

This studies on $HC_{10}H^+$ and the technical development of the apparatus leading to the obtaining and analyzing of the cyclic boron trimer gas-phase spectrum will be described in detail later.

0. 2. Structure of the manuscript

In the first chapter the brief description of the diffuse interstellar bands is presented. It gives a summarized state of knowledge about DIBs and a brief compilation of the present hypotheses concerning their possible carriers.

The second chapter is devoted to the supersonic jet technique. The theoretical principles, origin, further development and variety of its applications in the gas phase spectroscopy are briefly described.

The third chapter describes physical principles, origin and applications of cavity ringdown spectroscopy. It shows that this method is a powerful and effective tool in varied branches of modern spectroscopy.

The next chapter covers the description of the experimental set-up used for present studies. At first, the principles of operation are shortly described then the whole set-up is depicted in technical detail.

In the next chapters the results attained by means of cavity ringdown are presented. The brief reviews of carbon cation chains (HC_nH^+), pure boron clusters (B_n) and boron reach clusters studies are presented. They are followed by the results concerning CRD investigations of the $HC_{10}H^+$ and B_3 species.

The last chapter presents a summary of this work.

CHAPTER 1

1. History and a brief description of Diffuse Interstellar Bands

The discovery of visible diffuse absorption bands in stellar spectra dates back to the pioneering years of stellar spectroscopy. In 1922 the original report on the discovery of two spectral features, centred near 5780 Å and 5797 Å in spectra of some spectroscopic binaries was published by Heger [1]. These discovered features were considered as interstellar ones, however, it was only in the 1930s when the works of Merrill [2-4] confirmed this hypothesis. He demonstrated that these puzzling features did not participate in the velocity variations of spectroscopic binaries and furthermore their strength increased with distance and with the degree of the interstellar reddening of the star that furnished the background continuum. That evidence was reinforced by the work of Beals, Blanchet [5], Baker [6], and especially by the extensive study of the feature centred at 4428 Å by Duke [7]. These stationary features were named Diffuse Interstellar Bands (DIB). The term diffuse reflects the common characteristic of all known features; namely their profiles are conspicuously broader than those of interstellar atomic, ionic or molecular lines. This broadening of the profiles of DIBs is presumably due to unresolved rotational structure, possibly compounded by lifetime broadening of the upper states. However, it must be emphasized that they are usually narrower than broad lines originating in atmospheres of fast rotating stars. There exists a great variety in their profiles and intensities so they can not be readily described, classified, or characterized. To the present day no reliable identification of the DIB carriers has been found. Many carriers have been proposed over the years but none of them has withstood general scrutiny. They ranged from dust grains, to free molecules of very different sizes and

structures, even to the hydrogen negative ion [8]. There is a respectable body of opinion that a single carrier can not be responsible for all DIBs. However, it is very hard to estimate how many carriers can produce the observed DIBs. The problem is further complicated by the fact that to this day it is still impossible to find any laboratory spectrum of any substance which would match the astrophysical spectra. The most convenient for study are DIBs observed in spectra of the slightly reddened, bright stars.

These stars are most likely to be obscured by single clouds and one can presume that the obscuring medium is homogeneous, i.e., characterized by narrow range of physical parameters (temperature, column density, velocity, inner structure, shape and size of dust grains, chemical composition, etc). Bright, near-by stars obscured by one cloud would be the most appropriate candidates for the study of DIBs, however, number of such stars is limited. It is essential to mention that accessible early types stars are usually either very distant or slightly reddened, thus the molecular features of spectra are either formed in several clouds along any sightline or are too weak to be measured with proper precision. When several clouds are situated along a sightline, astronomers get the "average spectra" and their interpretation is difficult. The next problem which must be taken under consideration is contamination of interstellar spectra with so called "telluric lines". They are lines and bands of the atmospheric origin. Many of DIBs occur in regions masked by atmospheric O_2 and H_2O lines, so overlying atmospheric structure has to be properly removed. In order to do it, one has to divide a given spectrum by a spectrum of the standard star (e.g. unreddened αPeg or αCyg stars). The number of known DIBs keeps growing. The first survey of DIBs was published in 1937 [9]. In the year of 1975 the major survey of DIBs was published by Herbig [10]. It contained 39 DIBs (twenty of them were observed for the first time) detected in the range of 4400-6700 Å. All these features were clearly seen in the spectrum of the heavily reddened star HD183143. The replacement of photographic emulsion by solid state detectors (CCD) for stellar spectroscopy has resulted in the detection of many new DIBs. Set of few features known in 1930s got much bigger and now the number of DIBs is around of three hundred. In his new survey [11] Herbig placed over 130 features and Krelowski et al. [14] added to this wealth of data yet another 52 weak DIBs. As was said before, there

exist about 300 DIBs, however, existence of some of them is not sufficiently proved. On the other hand, many features still wait for their discovery.

1.1. Parameters of DIBs

The main parameters describing DIBs are:

λ - the wavelength of the feature (approximately central wavelength of band in Å),

A_c - the central depth of the band (described by percent of the continuum level),

FWHM - the full width (in Å) of the band at its half-maximum,

W_λ - the equivalent width in Å or mÅ, (it describes width of a hypothetical line of the same area, of a rectangular profile, and normalized to unity). The ratio of equivalent width reflects the ratio of the oscillator strength when DIBs are due to one carrier.

The profiles of the majority of DIBs are relatively narrow (their FWHM is usually of the order of few Å), however wider bands also can be found in some spectra. The broad 6177 DIB (FWHM ~ 30 Å) in the spectrum of HD183143 star may serve as an example. Most of the DIBs are located in the wavelengths longer than 4430 Å. The central depths of majority of DIBs are of the order of 1-2 % of continuum but there are few exceptions, e.g. the central depth of 5780 DIB in some spectra reaches 30%. The parameters describing DIBs are not stable and vary from one line of sight to another. Jenniskens and Desert in their survey of DIBs [73] showed that value of the equivalent width may change drastically. For the strong 5780 DIB it varies from 0.11 (target star - HD30614) to 0.72 (target star HD183143). It should be noted that there are also differences in values of the parameters obtained by different authors. Comparison of equivalent widths of DIBs collected by Jenniskens and Desert with the data of Herbig shows a small systematic difference.
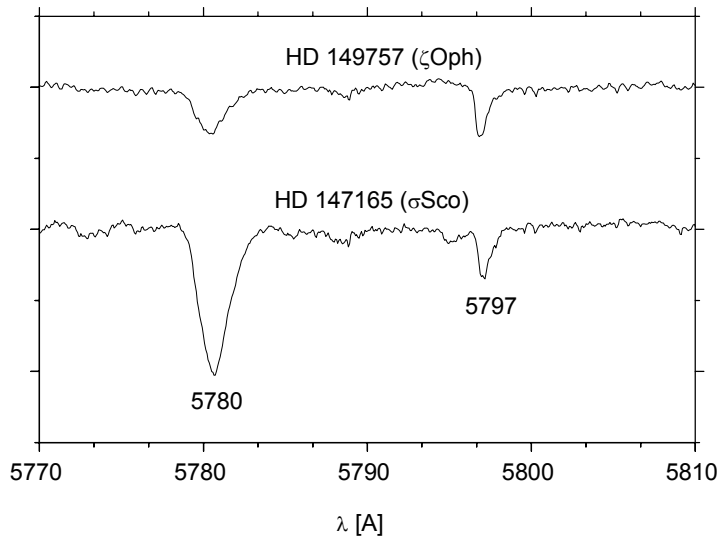
Figure 1.1. DIBs 5780 and 5797 in the spectra of HD 149757 and HD 147165 stars. These bands appeared in the table of the stellar features published by Heger in 1922 [1], and were regarded as "possibly stationary". (Spectra marked by appropriate target stars.)

1.2. Doppler splitting

The problem of the profile determination arose after the CCD new detectors were widely applied to record astrophysical spectra. The high resolution and S/N spectra revealed that the Doppler effect changes the DIB profiles. The broad profiles of the bands are only slightly altered and only in the case of very sharp DIBs the Doppler splitting can be observed.

In 1982 Herbig and Soderblom [15] have shown the composite profiles of 6196 and 6614 DIBs and proved that the Doppler splitting may change the profiles of these narrow bands. There is a great diversity in the velocities and physical properties of the interstellar clouds. That is why the interstellar features in the spectra of distant, heavily reddened stars are permanently contaminated with the Doppler splitting. For example it was observed in the case of the 6196 Å band in the HD102997 spectrum. It was shown that this splitting follows the splitting of the interstellar line D_1 (line of neutral sodium). Precise analysis of the profile of this interstellar atomic line has shown that this star is

obscured by at least seven clouds. The Doppler modification of the 6196 DIB profile is not strictly followed by the same splitting as at in the D_1 line. It may indicate that the carrier of the 6196 DIB is not present in all these clouds containing neutral sodium.

In spite of the fact that astronomers do not really know a true distribution of the DIB carriers in the individual clouds, precise analysis of the interstellar lines is a very useful method of determination of alteration in the DIB profiles.

The sodium D_1 and D_2 lines are very strong and sharp, and that makes them especially handy in the perplexing task of estimating the number of clouds between a target star and an observer. It is established that the Doppler splitting is one of the proofs that DIBs are the features of the interstellar origin. The Doppler effect is not one and only cause of broadening of DIBs. In 1992 Porceddu et al. [16] found the exceptionally broad profiles of 5780 DIB in the spectra of the stars belonging to the Orion Trapezium. The broadening of the bands in this case would have not been explained by the Doppler effect. It seems that a matter surrounding these stars differs substantially in physical and chemical properties from that producing normal diffuse interstellar bands.

1.3. Dependence on reddening

The first careful correlation analysis of dependence of the DIB strength on reddening was carried out by Deeming and Walker in 1967 [17]. They studied DIB 4428. The similar work was done by Murdin [18] for DIB 6283. It appeared that the dependence of one upon the other is not tight.

The advent of digital detectors in the 1980s revolutionized subject of gathering reliable data, however, this major step in the precision of the DIB spectroscopy did not greatly reduce the scatter around a mean regression line relating the DIB strength to colour excess. Nonetheless, it has reinforced the finding that the two are, in the mean, proportional one to another. Despite this dispersion, dependence obtained during the study shows clearly that when E(B-V) diminishes to zero, the strength of DIBs does the same. The colour excess, called also the reddening is defined as a difference in value of extinction measured in two photometrical bands, e.g. B and V (4400 Å and 5500 Å,

respectively). It is the most popular and convenient quantity characterizing the interstellar matter.

1.4. Skin phenomenon

Snow and Cohen were the first to indicate that stars seen through very dense clouds have DIBs weaker than would be expected from their colour excess. In 1974 they concluded that formation of the carrier is inhibited in cloud interiors [19].

This effect known as the "skin phenomenon" is conspicuous, e.g. in heavily obscured stars of the Cyg OB2 association. The study of the DIB behaviour in dense clouds was also carried out by Adamson et al. [20]. They observed the number of stars of different degrees of extinction through the Taurus clouds. The precise investigations of 6 DIBs showed that their normalized equivalent widths (i.e. W/E(B-V)) fell progressively below the diffuse-cloud value as the extinction increased. Adamson et al. believed that this result can be explained only by the concentration of the DIB carriers in the surface layers of the clouds, possibly due to the reduction of the ambient radiation field in the cloud interiors. It is very interesting that the concentration of neutral hydrogen also diminishes as we go towards the centre of the cloud. Since the DIB strength is correlated to the concentration of neutral hydrogen, it seems that the idea of the "skin effect" is well supported. On the other hand, there exist stars whose spectra have DIBs stronger than expected (when inferred from their colour excess). These observations still can not find any reasonable explanation.

1.5. Families of DIBs

The fluctuations in the individual bands strength from one line of sight to another (Figure 1.1.) once again indicate that more than one carrier of DIBs is involved. The first indication of a pattern in these discrepancies was published by Chlewicki et al. in 1986 [21]. They observed a number of early type stars in 3OB associations and divided DIBs into two classes:

I. 5797 and 5850 (well correlated with colour excess),

II. 5780, 6195, 6203, 6269 and 6283 (which showed much weaker dependence on colour excess, but the good correlation with each other).

Krelowski and Walker defined so called families of DIBs, i.e., sets of features observed always together and with the same strength ratios [22]. Each group of related bands ought to be responsible for one carrier so such a division into families seemed very helpful in the eventual identification of that substance. Nevertheless, the correlations between the DIBs are not always tight and convincing.

The groupings proposed by Krelowski and Walker are:

I. Broad and shallow DIBs 4428, 6177, and probably 4882,

II. Relatively symmetric DIBs 4763, 4780, 5362, 5449, 5487, 5780, 6195, 6203, 6269, 6283,

III. Asymmetric DIBs 4726, 5545, 5797, 5849, 6376, 6613, and possibly 5494, 5508, 6379.

They were based on only four stars and not on an analysis of their mutual correlations.

Josefatsson and Snow on the basis of 59 stars carried out an analysis of the mutual correlations, and of the individual correlations with E/(B-V). The region 5690-5870 Å was investigated [23].

Despite such an impressive examination of a large body of data, they did not provide any stronger evidence for the existence of families. They defined only three classes of DIBs:

I. The narrow DIBs 5780, 5797 and 5849 (correlated with each other and with colour excess),

II. Broad bands 5778, 5844 (well correlated with each other but very poorly with E/(B-V)),

III. 5705 (poorly correlated with other DIBs and with colour excess).

The survey of the measurements of stronger DIBs done by Mouton et al. [24] clearly suggests that usually any pair of two DIBs is correlated up to some degree. (The degree of correlation is higher when the widths of two features are similar.) It ought to be mentioned that one has to be very cautious in such a kind of classification. Josefatsson

and Snow placed 5780 and 5797 DIBs into the same family while Krelowski and Walker put them into two different classes. Generally, the limited amount of high quality spectra makes the list of the "family members" very unstable.

1.6. Spacings

The frequency analysis of the wavenumber spacings of DIBs, in search for preferential level separations, did not produce any useful information. Partly because of the concentration of DIBs in certain wavelength regions, and partly because of the gaps in spectra caused by atmospheric and interstellar interferences. Search for the vibrational sequences of the type $v' \leftarrow 0$ did not produce any convincing results either [8]. The only regularities that have been found so far in the DIBs spectra are those noticed by Herbig in the short series of weak, approximately equally spaced DIBs in the 6800 Å region [25], and the similar sequence near 5780 Å recognized by Jenniskens and Desert [26]. Although such regularities may turn out to be helpful, there is no strong evidence that these sequences exist for real. The proper investigations are complicated by the possible existence of multiple overlapping features which makes any results not convincing.

1.7. Review of the proposed carriers

One carrier can not be responsible for all known DIBs. That fact is widely accepted, however, the open questions are: how many carriers may be involved in producing all of the DIBs, and what is the phase of that mysterious substance. Dust grains or free molecules were usually proposed as the potential carriers of DIBs, however, now it seems that scientist should search for the carriers somewhere "in between." The carriers may be crucially important in interstellar chemistry: they may constitute a significant fraction of all chemically bonded matter in the interstellar gas, and many may be molecules larger than any so far identified. Nowadays it is believed that they are long carbon chains or polycyclic aromatic hydrocarbons. Although additional theory and

astronomical observations are needed, the identity of the carriers is now essentially a problem in laboratory astrophysics. Here is a brief review of the proposed carriers. Some of them are rather outdated and gone into oblivion, while others (e.g. carbon chains or PAHs) are still intensively studied and investigated as the potential carriers of DIBs. However, even in that case, no convincing proof had been found so far.

1.7.1. Solid particles

It has long been known that some solids, such as crystals doped with metal ions, can produce narrow absorption lines at low temperatures. In 1979 Duley [27] studied the spectra of Cr^{3+} ions in MgO crystals, for which certain transitions between levels of the ground state were expected to produce narrow lines in the 7000 Å region. However, no interstellar lines at these wavelengths have been found [8], and in fact there is no evidence that interstellar crystalline MgO exists in the quantity required [28-29].

The ion Fe^{3+} also has been proposed as a potential carrier of few stronger DIBs [30], however, mineral in which they were doped (garnet) is an implausible constituent of the interstellar grains because of the conditions under which it is formed on the Earth [31]. A more appealing idea was that the DIB carriers might be dispersed as an impurity through the spherical dust particles and the electric field of the crystal lattice in which such an atom would be imbedded could shift and split the atom's energy levels. It should be noticed that such theories do not specify what the impurity atom might be. In 1969 Duley and Graham [32] carried out experiments in which Ca atoms in a matrix of solid benzene produced a broad absorption feature near 4500 Å. (Ca resonance line is located at 4227 Å). The molecules of Ca_2 in benzene and other hydrocarbons showed a variety of absorptions, some of which lie not far from the positions of known DIBs. All these laboratory experiments, however, produce absorption bands which are much broader than the broadest DIBs. These nonconclusive experimental data are not the only reason to doubt that DIBs originate in the dust grains. Lack of tight correlation between the strength of DIBs and colour excess suggests that the grains of different sizes should be involved in producing DIBs. On the other hand it stands in contradiction to well proved constancy of the DIB profiles in many different interstellar environments. Furthermore,

the absence of the detectable change in interstellar polarization across some of stronger DIBs shows that these features do not originate in the aligned grains responsible for polarization of light in the optical region [33].

1.7.2. Free molecules

The detection of the first interstellar diatomic molecules (CN and CH) came few years after the interstellar origin of DIBs was demonstrated. Stimulated by that discovery, a number of the specific molecular carriers were proposed. Some of these proposals were based on near-agreement with gas-phase laboratory wavelengths, while others have come from a less direct reasoning. The list of specific molecules that had been suggested is very long, however, none of these have received enthusiastic support. Table 1.1. contains some examples of molecules suggested as the potential carriers of DIBs. The reason to favour gas-phase molecular carriers is the possibility of explanation of the difusseness of DIBs. It is very reasonable to suspect that the widths of DIBs represent the unresolved rotational structure. If so, then excited rotational levels of the lower state must remain populated at temperatures and densities of diffuse clouds. Danks and Lambert [34] estimated such closely spaced rotational levels of a hypothetical, large molecule and came to conclusion that such conditions would be met for the lowest 10-20 levels. So they tried to reproduce the observed profiles of the relatively narrow DIBs at 5780 Å and 5797 Å. The attempt to fit the contour of the much broader 4428 Å turned out to be unsuccessful. The second explanation of the widths of DIBs could be that the upper energetic states of the molecule have very short lifetime. In 1955 Herzberg [35] remarked that the ionization potentials of negative ions such as O^- or C^- are low enough so the preionization transitions would occur in the optical region, but the laboratory experiments carried out by Ensberg and Jefferts in 1979 [36] found no transitions of O^- or C^- at the wavelengths of several prominent DIBs.

Molecule	Author and year of publication.
CO_2	Swings, 1937
Na_2, NaK	Saha, 1937
$(O_2)_2$	McKellar, 1960
NH_4	Herzberg, 1955
O^-, C^-	Herzberg, 1955
CH_4^+	Herzberg, 1955
H^-	Rudkjobing, 1969
$HCOOH^+$	Herzberg, 1988

Table 1.1. Free molecules considered as the potential carriers of DIBs.

Herzberg also mentioned the possibility that the predissociation of some polyatomic molecules could produce diffuse bands in the optical region, however, the predissociation itself would have to destroy the absorber. To maintain its sufficient concentration, a fast process of recombination would have to exist. Unfortunately under interstellar conditions no efficient process of such a recombination had been known. This difficulty became less severe when the importance of the very rapid ion-molecule reactions for interstellar chemistry was recognized.

1.7.3. Polycyclic aromatic hydrocarbons

In the 1980s many specialists proposed polycyclic aromatic hydrocarbons (PAHs) as potential carriers of DIBs. This idea was put forward independently by Van der Zwet and Allamandola [37] and by Leger and d'Hendecourt [38]. The possibility of ionized PAHs being the carriers of DIBs was proposed by Crawford, Tielens and Allamandola [39]. The essential points that make PAHs very promising molecules are:

- the survivability of the larger PAHs molecules against photodissociation in the interstellar radiation field,

- abundance of carbon in the interstellar medium sufficient enough to account for the DIB strength,
- neutral, and particularly ionized PAHs are known for the strong electronic transitions in the optical region.

The efforts to obtain astronomically relevant data are nowadays mostly focused on the investigations of the following molecules:
- naphthalene ($C_{10}H_8$) and its cation ($C_{10}H_8^+$),
- pyrene ($C_{16}H_{10}$) and its cation ($C_{16}H_{10}^+$),
- phenantrene cation ($C_{14}H_{10}^+$),
- coronene ($C_{24}H_{12}$) and its cation ($C_{24}H_{12}^+$),
- ovalene ($C_{32}H_{14}$) and its cation ($C_{32}H_{14}^+$).

Neutral naphthalene does not absorb in the visible region, but the cation produces series of bands, the strongest at 6741 Å, followed by weaker features at 6520 Å and 6151 Å [40]. However, none of the more prominent DIBs are matched by these peaks obtained in the laboratory. In 1999 Romanini et al. obtained the first gas-phase electronic absorption spectrum of an ionized naphthalene. This study showed that there is no correspondence between the DIBs and strong absorption bands of $C_{10}H_8^+$ [41].

Neutral pyrene also does not absorb in the visible region, however, its cation exhibits more promising possibility. In the neon matrix the spectrum is dominated by a strong absorption band centred at 4395 Å, while in the argon matrix this peak is slightly shifted longward to 4435 Å. Although this result is interesting (very good coincidence of latter peak with 4428 DIB), one should be cautious in interpretations. Authors of the experiment were inclined to state that this coincidence might be due to chance [40]. Absorption spectra of coronene, ovalene, and their cations have been described by Ehrenfreund et al. in 1992 [42]. Similar experiments were carried out by Salama and Allamandola in 1993 for phenantrene cation [43]. Unfortunately, none of the features found in the optical region match any of the DIBs wavelengths. All those investigations focused on specific PAHs, but in the interstellar clouds a mixture of compounds might be expected as well. Taking that fact into account Ehrenfreund et al. examined the

absorption spectrum of a neutral coal pitch extract deposited in a solid neon matrix [44]. This material was distilled from coal, and consisted of a mixture of about 150 different aromatic molecules among which compounds such as C_mH_n (where m = 14-24, and n = 10-14) were present in percentages of 2% or more. Only few discrete bands were found between 3800 and 4700 Å, and there were no convincing coincidences with known DIBs. This result is interesting, however, it stands in contradiction to the results of the earlier works that firmly showed that PAHs' ions are expected to have the strong transitions in the optical region. Sarre suggested that negative ions of PAHs might be also responsible for the DIB origin [45]. Supporting calculations made by Lepp and Dalgarno [46] showed that in the cloud interiors, negative PAHs' ions might be comparable in abundance with neutral PAHs. This calculations depend on an assumed value for the rate of cosmic-ray ionization, which provides the free electrons. However, there is a strong objection to that idea. Namely, as Snow and Cohen noted, the DIB concentration is lowest in cloud interiors [19]. Nevertheless, the laboratory studies of the spectra of some plausible anion of PAHs might be very interesting.

1.7.4. Carbon chains

In 1977 Douglas suggested that polycarbon chains such as C_5, C_7 and C_9 might survive under interstellar conditions [47]. He remarked that the means by which it might happen is the internal conversion. That process enables the radiationless transition to take place from the excited level to vibrational levels of the same or another electronic state, following which the absorber returns to the ground state by a series of infrared transitions. Douglas also suggested that such carbon chains should produce strong diffuse absorption bands in the 4000-5000 Å region. The hypothesis that carbon chains might be a carrier of some of the DIBs was strongly supported by the fact that these species fulfill the requirements which are imposed on the potential carrier. The advantages of this hypothesis are following:
-   the carriers are associated with stable molecules, which are composed of one of the most abundant element in the interstellar space

- carbon chains absorb in the visible region
- these species exist at least in some interstellar regions

These suggestions were firstly pursued in the laboratory by Kratschmer, Sorg, and Huffman in 1985 [48] and subsequently by Kurtz and Huffman in 1990 [49]. Carbon molecules obtained by vaporization of graphite (C_n, where n = 4-9) and then deposited into a cold argon matrix produced a series of absorption bands centred at 2471 Å (the strongest), 3079, 3490, 4470 Å (weaker) and 4930, 5860 Å (very weak). Since the matrix shift estimated by Kratschmer et al. is about 50 Å, the band 4470 Å matches DIB 4428 very well.

In 1998 Tulej et al. measured the gas-phase electronic spectra of several carbon chain anions [50]. They obtained spectra of C_6^-, C_7^-, C_8^-, and C_9^- containing many narrow bands which appear to match some DIBs. Most intriguing coincidence was found for the bands of C_7^- anion and several DIBs where the DIBs have similar widths and relative intensities. However, new data obtained by McCall et al. in 2001 showed that C_7^- must be rejected as a potential carrier of DIBs [51]. There were strong chemical arguments against this hypothesis: chemical models of Ruffle et al [52] were unable to reproduce necessary abundance of C_7^-, even with the most favorable assumptions. New measurements of DIBs positions showed that the origin band of C_7^- does not match 6270 DIB either in wavelength or profile. Some vibronic bands also do not match perfectly DIBs. Additionally, one of the DIBs, attributed to the vibronic band of C_7^- turned out to be a stellar line.

Mitchell and Huntress went a bit further and proposed hydrocarbon chain molecules of up to $C_{12}H_m$ (where m was unspecified) as the species that might be responsible for at least some of the DIBs [53]. Laboratory investigations of the analogous molecules were also carried out by Motylewski et al. Using the cavity ring down spectroscopy combined with the supersonic slit nozzle discharge they obtained spectra of C_8H and $C_{10}H$ chains. Although numerous absorption bands were observed, their coincidence with known DIBs is not too convincing [54]. In 1994 Freivogel et al. obtained the spectra of carbon-chain anions [55]. The $C_nH_m^-$ anions (where n = 14, 16 and m < 3) spectra show many correspondences with some of the DIBs. Particularly

striking are coincidences in the region 7000-8000 Å where nine bands match very well DIBs listed by Herbig and Leka [8]. However, it must be again emphasized that with the accuracy of measurements of the matrix and astrophysical spectra these overlaps may be only coincidences.

In 2004 Maier et al. [56] summarized the current situation in the context of laboratory studies carried out in recent years on not only bare carbon chains, but also their ions and simple derivatives containing hydrogen or nitrogen. The results of their analysis led to interesting conclusions about the role of carbon chains as potential carriers of the diffuse interstellar bands. First, it was suggested that the abundance and oscillator strength of shorter chains (approximately up to 10 atoms) are too small to account for the stronger DIBs. Second, because of the electronic configurations of these open-shell species, the lowest energy - transition does not have a large oscillator strength but the higher energy one in the UV does, and the chains would have to be prohibitively long for these absorptions to shift into the DIB 4000 - 9000 A wavelength region. The exceptions are closed-shell systems such as the odd-numbered bare carbon chains, and the ones in the C_{15} - C_{31} size range that have their very strong transitions in this region.

1.7.5. Fullerenes

After the laboratory detection of fullerene C_{60} in 1985, the extensive study of that large molecule started to take place. Because of the readiness with which fullerens can be produced under a variety of laboratory conditions, it seemed reasonable that such molecules could also occur in the interstellar medium. For this reason Kroto et al. [57] speculated that fullerene C_{60} might be the potential carrier. This idea was very appealing because such heavy molecules could easily explain the broadening of DIBs. Their small rotational constants make it possible for a large number of rotational levels to be populated at interstellar temperatures. Thus their absorption bands would appear as diffuse and unresolved. Unfortunately, the laboratory experiments carried out by Leach et al. [58] showed that there is no agreement in position between the laboratory spectrum of C_{60} and the known DIBs.

Ballster, Antoniewicz, and Smoluchowski proposed that DIBs can be produced by the resonance lines of common neutral atoms (e.g. Si or Mg) trapped in the C_{60} cages [59]. These resonance lines would be shifted to the longer wavelengths on account of the depression of the upper state by the electric field of the cage. Since the ionization potential of C_{60} is about 7.6 eV, so most of these molecules should be singly ionized under interstellar conditions. That is why the cation C_{60}^+ also has been proposed as the DIB carrier. Unfortunately, Fulara et al. showed that there is no laboratory evidence for the strong C_{60}^+ transitions between about 3100 and 9000 Å, so this cation can not be responsible for DIBs in the optical region [60].

In the early 1990s it was also suggested that $C_{60}H_m$ (where $m \geq 1$) might be an appropriate molecule, but the spectrum of $C_{60}H_2$ obtained by Henderson and Cahill showed that there are no significant differences from that of pure C_{60} [61]. However, McIntosh and Webster have estimated that under interstellar conditions m may be somewhere between about 10 and 30 [62], therefore potential spectra would be changed more radically, but to this day no laboratory spectra of such species are known.

1.7.6. Porphyrins

One of the more unusual proposals as to the identity of the DIB carrier was advanced by Johnson in 1972 [63]. He suggested that bis-pyridyl-magnesium-tetrabenz-porphyrin (MgTBPp) might be the feasible molecule. In his experiment (the MgTBPp molecule was suspended in a frozen hydrocarbon matrix) he obtained the spectrum containing three strong absorption bands centred at 4428 Å, 6284 Å, and 6174 Å that matched very well the prominent DIBs. Johnson claimed that the wavelengths of 25 DIBs could be reproduced by transitions between the vibronic levels of that molecule. Similar work was done for H_2TBP and MgTBP molecules [64]. The drawback of these schemes is that temperature of the interstellar medium is much lower than those required to make such an excitation possible.

In 1980 Donn and Khanna [65] repeated the laboratory experiments of Johnson. They confirmed the existence of strong absorption bands near 4400 Å and 6300 Å, however, the band centred at 6174 Å was not detected. Despite these results, authors of

the experiment were inclined to state that such a complicated molecule as MgTBPp could not form and survive under interstellar conditions, particularly at the temperatures required by Johnson's hypothesis. In 1993 Miles and Sarre noted [66] that molecule of dihydroporphyrin ($C_{20}N_4H_{16}$) has a strong electronic transition that in the supersonic jet lies at about 6284 Å which matches very well the 6283 DIB. In a polystyrene matrix, the same feature occurs at 6381 Å, and by applying the same matrix shift to a number of weaker bands, Miles and Sarre found a near agreement with the wavelengths of the 6177 and 6010 DIBs.

1.7.7. Conclusions about carriers

This brief review of the proposed carriers clearly indicates that despite intensive astrophysical observations and laboratory study all of them may be regarded as mere "putative" ones. It must be emphasized, however, that of all proposed carriers two of them seem to outrun the rest in feasibility. Namely, carbon chains and polycyclic aromatic hydrocarbons. It is now clear that the DIBs can not be explained by the early concept of a single carrier owing to the large number of bands detected and the lack of correlation between the bands. The present consensus, based on high-resolution astronomical observations, is that the carriers are large carbon-bearing gas phase molecules in either the neutral or/and ionized forms and that these molecular carriers are part of an extended size distribution of the interstellar dust. At the moment it is difficult to say which group of the molecules could be really responsible for DIBs (PAHs or carbon chains), however, it looks like they should be involved into the "business" of DIBs carriers. They both are relatively large carbon-containing molecules with a variety of the intense absorption bands in the IR-VIS region and both are ubiquitous in diffuse interstellar clouds. It should not be forgotten, however, that the high density of DIBs in the optical region makes any accidental coincidence very possible. It becomes even more conspicuous when one takes into account both the tolerance of a wavelength match, as well as the uncertainties in the DIB wavelengths themselves. So one should be cautious in formulating radical conclusions as to what molecules the DIBs carriers really are. It

seems that the only reasonable and undoubted conclusion in this matter is a humble statement that the full solution of this intriguing problem is still down the road.

1.8. Relations between the continuous extinction and DIBs

The extinction produced by interstellar matter refers to the combined effects of the scattering and absorption of electromagnetic radiation by the matter along sight lines through the interstellar space. The interstellar extinction curve depicts the absorption and scattering due to various interstellar dust components and spans from the near infrared to the far ultraviolet (Figure 1.2.).

It is described by the equation:

$$F(\lambda) = E\,(\,\lambda\text{-V}) / E\,(\,\text{B-V}),$$

Where:

F(λ) - normalized extinction,

E (λ-V) - colour excess

E (B-V) - colour excess

Customary the value of the interstellar extinction is plotted against the inverted wavelength, i.e., $1/\lambda$ which is expressed in μm^{-1}.

The average interstellar extinction curve for the diffuse cloud medium exhibits a nearly linear rise from 1 μm^{-1} to the 2.25 μm^{-1} "knee" where the slope changes. In the ultraviolet region there is a pronounced extinction bump near 4.6 μm^{-1} (2175 Å) followed by the broad minimum and the steep non-linear rise in extinction to the shortest wavelengths. For wavelengths shorter than ca. 5500 Å, the interstellar extinction curve exhibits considerable variations in the shape from one line of sight to another. In addition, the strength variations and the width (FWHM) of the 2175 Å bump has been observed to vary by more than a factor of two from 360 Å to 770 Å with the average width about 480

Å. In contrast, the central position of the bump does not change so drastically. The most extreme variations in extinction value are found in the far ultraviolet region.
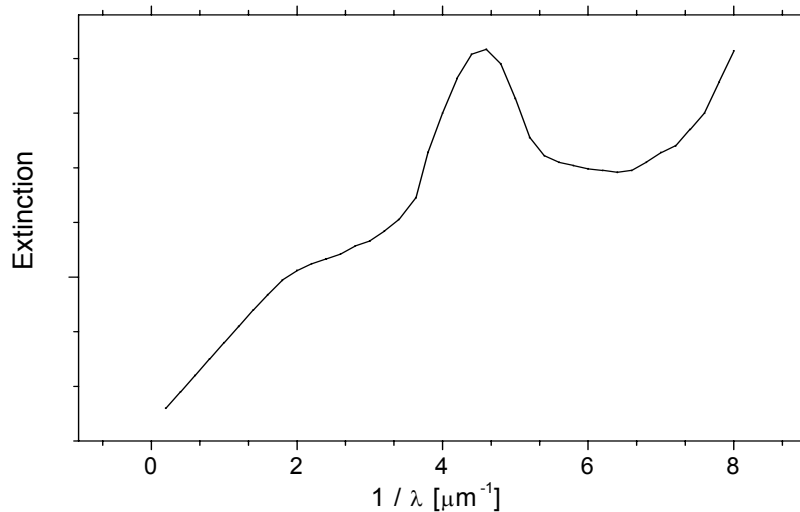
Figure 1.2. The interstellar extinction curve observed in the spectrum of HD149757 star.

The different models of the interstellar dust were developed to account for the extinction curve. The long wavelength extinction usually is explained by the absorption and scattering from classical Van de Hulst [67] grains which size is about 0.1-0.2 μm. In the model of Hong and Greenberg [68], they consist of silicate cores and a mantle of material which absorbs strongly in the visual region. In 1989 Duley et al. proposed condensations of carbon atoms into an amorphous carbon directly from the gas phase on the silicate grains [69]. Jenniskens and Greenberg analysed the parameters of 115 ultraviolet extinction curves [70] published by Aiello et al. [71]. They decomposed them into the linear rise, bump, and the far ultraviolet rise. These analyses did show that a shape of the extinction curve up to 6000 Å is determined by the big grains absorbing in the optical region. At about 6000 Å particles responsible for the linear rise start to affect the extinction curve. They must have sizes as small as about 0.01μm or less because at short wavelengths the extinction of the classical grains saturates. The 2175 Å bump is usually explained by the amorphous carbon grains or their mixtures with larger molecules.

Large molecules like PAHs also have been proposed as the carriers of the bump as well as more general molecules containing alkene and alkyne bands [72]. Linear polyynes and cyanopolyynes should in principle be regarded as good candidates for the ultraviolet interstellar absorption. In particular, polyynes C_8H_2, $C_{10}H_2$, and cyanopolyynes HC_7N, HC_9N and $HC_{11}N$ have a strong absorption line close to the region of 2000-2200 Å. Unfortunately, all these molecules have strong vibrationally allowed bands in the near ultraviolet region which would make difficult a good fitting of the strong interstellar maximum at 2175 Å without undesirable absorptions at shorter wavelengths. The carrier of the far ultraviolet non-linear rise has not yet been identified, however, its correlation with CH abundance has been reported [73].

The interstellar extinction law has been shown to be not identical toward different lines of sight. The varying shape of the 2175 Å bump and the strongly variable slope at the far ultraviolet segment suggest varying physical properties of the interstellar clouds. In 1988 Krelowski and Westerlund noticed that spectra of two stars, σSco and ζOph, showing very different ratios of the strong DIBs 5780 and 5797, are associated with very different shapes of vacuum ultraviolet extinction curves [74].
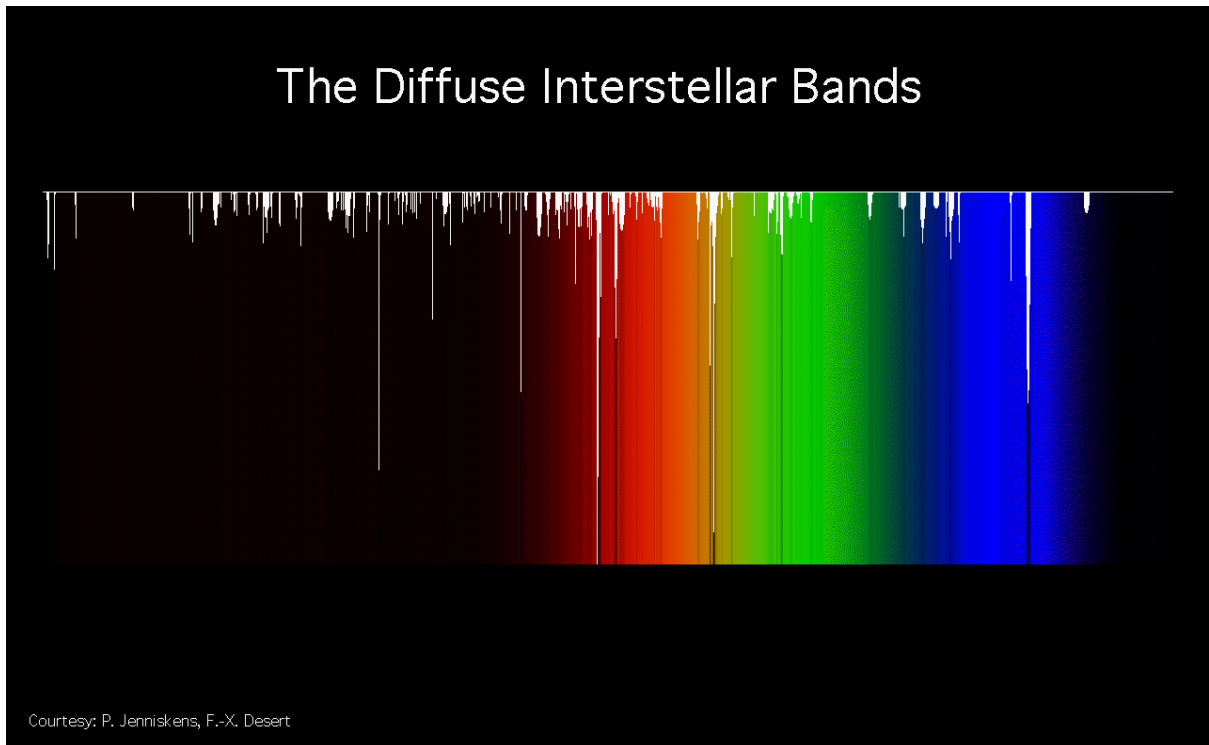
Figure 3.1. The spectrum of DIBs (Ref. 76).

The curves of ζOph type is characterized by the steep far ultraviolet rise while in those of σSco type such a rise is not observed. It may suggest that carriers of the narrow 5797 DIB are related in some way to the carrier of the far ultraviolet extinction rise. However, statements made by the authors are only qualitative ones. Similar relationship between the strength of DIBs and the ultraviolet extinction curve behavior was found in the case of 5844 Å band [75]. A couple of lists of Diffuse Interstellar Bands have been made over the years. The most important and reliable catalog is published in the review of Jenniskens and Desert [76]. This thorough catalog was updated by discoveries of Krelowski et al. [77] and Jenniskens et al [78]. The results of this work can be found on the internet [79]. Another survey of DIBs with precise wavelengths can be found on the website of Galazutdinov [80].

References

[1] M.L. Heger (1922), *Lick. Obs. Bull.*, **10**,146

[2] P.W. Merrill (1934), *PASP*, **46**, 206

[3] P.W. Merrill et al. (1937), *ApJ*, **86**, 174

[4] P.W. Merrill, O.C. Wilson (1938), *ApJ*, **87**, 9

[5] C.S. Beals, G.H. Blanchet (1937), *PASP*, **49**, 224

[6] E.A. Baker (1949), *Edinburgh. Pub.*, **1**, 15

[7] D. Duke (1951), *ApJ*, **113**, 100

[8] G.H. Herbig, K.D. Leka (1991), *ApJ*, **382**, 193

[9] P.W.Merrill, R.F. Sanford, O.C. Wilson, G.G. Burwell (1937), *ApJ*, **86**, 274

[10] G.H. Herbig (1975), *ApJ*, **196**, 129

[11] G.H. Herbig (1995), *ARA&A*, **33**, 19

[14] J. Krelowski, C. Sneden, D. Hiltgen (1995), *Planet. Sci.*, **43**, 1195

[15] G.H. Herbig, D.R. Soderblom (1982), *ApJ*, **252**, 610

[16] I. Porceddu, P. Benvenuti, J. Krelowski (1992), *AAp*, **260**, 391

[17] T.J. Deeming, G.A.H. Walker (1967), *ZsfAp*, **66**, 175

[18] P. Murdin (1972), *MNRAS*, **157**, 461

[19] T.P. Snow, J.G. Cohen (1974), *ApJ*, **194**, 313

[20] A.J. Adamson, D.C.B. Whittet, W.W. Duley (1991), *MNRAS*, **252**, 234

[21] G. Chlewicki, G.P. van der Zwet, L.J. van Ijzendoorn, J.N. Greenberg (1986),
    ApJ, **305**, 455

[22] J. Krelowski, G.A.H. Walker (1987) *ApJ*, **312**, 860

[23] K. Josafatsson, T.P. Snow (1987) *ApJ*, **319**, 436

[24] C. Moutou, J. Krelowski, L. d'Hendecourt, J. Jamroszczak (1999) *AAp*, **351**, 680

[25] G.H. Herbig, (1988), *ApJ*, **331**, 999

[26] P. Jenniskens, F.X. Desert (1993), *AAp*, **274**, 465

[27] W.W. Duley (1979), *ApJ*, **227**, 824

[28] D. Massa, B.D. Savage, E.L. Fitzpatric (1983), *ApJ*, **266**, 622

[29] J.A. Nuth, B. Donn (1984), *ApSpSci.*, **103**, 357

[30] J. Dorschner (1970), *AN*, **292**, 107

[31] J. Dorschner (1971), *Natue Phys. Sci.*, **231**, 124

[32] W.W. Duley, W.R.M. Graham (1969), *Nature*, **224**, 785

[33] A.J. Adamson, D.C.B. Whittet (1992), *ApJ*, **398**, L69

[34] A.C. Danks, D.L. Lambert (1976), *MNRAS*, **174**, 571

[35] G. Herzberg, (1955), *Mem. Soc. Roy. Sci. Liege*, **15**, 291

[36] E.S. Ensberg, K.B. Jefferts (1979), *ApJ*, **195**, L89

[37] G.P. van der Zwet, L. J. Allamandola (1985), *AAp*, **146**, 76

[38] A.Leger, L. d'Hendecourt (1985), *AAp*, **146**, 81

[39] M.K. Crawford, A.G. Tielens, L.J. Allamandola (1985), *ApJ.*, **293**, L45

[40] F. Salama, L. J. Allamandola (1992), *ApJ,* **395**, 301

[41] D. Romanini, L. Biennier, F.Salama, A. Kachanov, L.J. Allamandola, F. Stoeckel, (1999) *Chem. Phys. Lett.* **303**, 165

[42] P. Ehrenfreund, L. d'Hendecourt, L. Verstraete, A. Leger, W. Schmit, D. Defourneau (1992a), *AAp*, **259**, 257

[43] F. Salama, L. J. Allamandola (1993), *J.Chem.Soc. Faraday Trans.*, **89**, 2277

[44] P. Ehrenfreund, L. d'Hendecourt, C. Joblin, A. Leger (1992b), *AAp*, **266**, 429

[45] P.J. Sarre (1980), *J.Chem. Phys.*, **77**, 769

[46] S. Lepp, A. Dalgarno (1988), *ApJ*, **324**, 553

[47] A.E. Douglas (1977), *Nature*, **269**, 130

[48] W. Kratschmer, N. Sorg, D.R. Huffman (1985), *Surf. Sci.*, **156**, 814

[49] J. Kurtz, D.R. Huffman (1990), *J. Chem. Phys.*, **92**, 30

[50] M. Tulej, D.A. Kirkwood, M. Pachkov, J.P. Maier (1998), *ApJ*, **506**, L69

[51] B. J. McCall, J. Thorburn, L. M. Hobbs, T. Oka, D. G. York, (2001) *ApJ*, **559**, L49

[52] D. P. Rufle, R. P. A. Bettens, R. Terzieva, E. Herbst, (1999)) *ApJ*, **523**, 678

[53] G.F. Mitchell, W.T. Jr. Huntress (1979), *Nature*, **278**, 722

[54] T. Motylewski, H. Linnartz, O. Vaizert, J.P. Maier, G.A. Galazutdinov, F.A. Musaev, J. Krelowski, G.A.H. Walker, D.A. Bohlender (2000), *ApJ .* **531**, 312

[55] P. Freivogel, J. Fulara, J.P. Maier (1994), *ApJ*, **431**, L151

[56] J. P. Maier, G. A. H. Walker, D. A. Bohlender (2004), *ApJ,* **602**, 286

[57] H.W. Kroto, J.R. Heath, S.C. O'Brien, R.F. Curl, R.E. Smalley (1985), *Nature*, **318**, 162

[58] S. Leach et al. (1992), *Chem. Phys*., **160**, 451

[59] J.L. Ballster, P.R. Antoniewicz, R. Smoluchowski (1990), *ApJ*, **356**, 507

[60] J. Fulara, M. Jakobi, J.P. Maier (1993), *Chem. Phys. Lett*., **211**, 227

[61] C.C. Henderson, P.A. Cahill (1993), *Science*, **259**, 1885

[62] A. McIntosh, A. Webster (1992), *MNRAS*, **255**, 37P

[63] F.M. Johnson (1972), *Ann. Bull. N.Y. Acad. Sci*., **187**, 186

[64] F.M. Johnson (1991), *B.A.A.S.*, **23**, 933

[65] B. Donn, R.K. Khanna (1980), *Ap. Sc. Sci*., **68**, 19

[66] J.R. Miles, P.J. Sarre (1993), *JChem. Soc. Faraday. Trans*., **89**, 2269

[67] H.C. Van de Hulst (1957), *Scattering by small particles*, New York: J.Wiley

[68] S.S. Hong, J.M. Greenberg (1980), *A&A*, **88**, 194

[69] W.W. Duley, A.P. Jones, D.A. Williams (1989), *MNRAS*, **236**, 709

[70] P. Jenniskens, J.M. Greenberg (1993), *A&A*, **274**, 439

[71] S. Aiello, B. Barsella, G. Chlewicki, J.M. Greenberg, P. Patriarci, M. Perinotto (1988), *A&AS*, 73, 195

[72] M. Braga, S. Larsson, A. Rosen, A. Volosov (1991), *A&A*, **245**, 232

[73] P. Jenniskens, P. Ehrenfreund, F. X. Desert (1992), *A&A*, **265**, 1

[74] J. Krelowski, B. Westerlund (1988), *A&A*, **190**, 339

[75] J. Krelowski, T. P. Snow, J. Papaj, C.G. Seab, B. Wszolek (1993), *ApJ*, **419**, 692

[76] P. Jenniskens, F.-X. Desert (1994), *AApS*, **106**, 39

[77] J. Krelowski, C. Sneden, D. Hiltgen, (1995) *Planet. Space. Sci*. **43**, 1195

[78] P. Jenniskens, I. Porceddu, P. Benvenuti, F.-X. Desert, (1996) *A&A* **313**, 649

[79] http://leonid.arc.nasa.gov/DIBcatalog.html

[80] http://www.sao.ru/hq/coude/DIBwavelength.htm

CHAPTER 2

2. Supersonic jet phenomenon and its application in spectroscopy of transient radical species

The emission or absorption spectra of large organic molecules are usually broad and their structure is not always clear. This is caused primarily by two factors. One of them is Doppler broadening. Another one is high population of excited rovibronic levels in the ground electronic state of the molecule at high temperature. The result is a spectrum that is congested and difficult to interpret. In order to cope with this problem, there is a tendency toward measurements of spectra of isolated molecules which are cooled to a very low temperature. The excellent tool that provides for extensive cooling of translational and internal degrees of freedom of molecular gases is a supersonic free expansion. In this method a neutral carrier gas containing vapour of the substance of interest is expanded into the vacuum chamber through a nozzle. As a result of the adiabatic expansion of the gas (at pressure p_0 and temperature T_0) into the vacuum, conversion of internal energy of the gas into kinetic energy takes place. This leads to sharpening of the Maxwell-Boltzman distribution of molecular velocities and to translational cooling to temperature T. Hence, the Doppler broadening is significantly reduced. The cooling of large molecules in the supersonic jet is effective when the diameter of the nozzle is relatively large with respect to the mean free path of the molecules.

Owing to partial cooling of rotational and vibrational degrees of freedom of the molecules, only the lowest rovibronic levels in the ground electronic state are populated. This simplifies the spectra enormously as the number of lines is noticeable reduced. With a very effective cooling most "hot transitions" do not take place and as a result the analysis of the spectra is much easier.

The parameters of state of an ideal gas expanding under adiabatic conditions are given by the equation:

$$\frac{T}{T_0} = \left(\frac{p}{p_0}\right)^{\frac{\kappa-1}{\kappa}} = \left(\frac{\rho}{\rho_0}\right)^{\kappa-1} = \left[1 + \frac{(\kappa-1)M^2}{2}\right]^{-1}$$

Where:

M - the Mach number,

T_0 - the initial temperature in the nozzle,

p_0 - the initial pressure of gas in the nozzle,

ρ_0 - the initial density of gas in the nozzle,

κ - c_p / c_v (c_p, c_v - heat capacities at constant pressure and constant volume, respectively).

T, p, ρ, and M are the parameters at a given point of the jet.

Free jet expansions prove useful in producing interesting radicals which are usually transient species and can not be produced effectively by other methods. Low densities attained in jet allow these unstable molecules to survive long enough for studying. The radicals and ions prepared in nozzle expansions are amenable to investigation by a range of spectroscopic techniques, ranging from optical spectroscopy with high dispersion grating instruments and photographic plate detection to mixed optical-microwave spectroscopy with modern klystrons and lasers. A long-lasting problem in analyzing spectra is that of locating each band origin, corresponding to the energy of the transition if the molecule were not rotating or vibrating. These band origins are more easily identified in spectra of very cold molecules Many examples of spectral structure simplifying upon cooling of rotations can be found in the review papers of Engelking [1] and Levy [2].

Studeis carried out by Kantrowitz [3] showed that low rotational and translational temperatures could be attained without necessarily aggregating molecules or quenching internal vibrations. It was also recognized that the translational velocity distribution

would become narrow, with the overall bulk motion away from the nozzle becoming a bit over the initial speed of sound in the preexpanded gas. This was a significant improvement in molecular beam characteristics over that available with an effusive source, since a narrow velocity distribution could be achieved automatically, without having to introduce a mechanical velocity selector in the beam path. Several proposals were made to utilize an expansion for a molecular beam source [4-6].

2.1. Circular nozzles

Most studies use an unconstrained free jet expanding into a vacuum chamber from a circular hole, without introducing skimmers for separating out a free molecular beam. Since most researchers do not have infinite pumping speed available, the jet expands into a low pressure. Much work has been done on the aerodynamics of a similar situation, a rocket exhaust plume at high altitude [7, 8]. A good deal of theoretical and experimental work on axial symmetric jets has been summarized by Love [9].

Many of the theoretical predictions of flow structure have been experimentally confirmed by methods of shock visualization and Pitot tube pressure measurement. Recently, optical tomography of Cl_2 expansions using arc lamp UV sources have directly confirmed predictions of the density distribution in the flow [10].

The basic structure of the expansion consists of subsonic hydrodynamic flow on the high-pressure side of the nozzle toward the constricting throat. At the throat, the flow conditions becomes sonic and, subsequently, supersonic in the expansion into the vacuum. More detailed description of the circular nozzle can be found in the next subchapters.

2.2. Planar nozzles

Nozzle geometry need not be cylindrically symmetric about the flow axis. Recently, planar nozzle geometries have been introduced to attempt to match the properties of the expansion to the needs of the spectroscopist. The engineering literature

refers to these as "slot" nozzles; molecular spectroscopists lean toward the term "slit" nozzles.

Flows from slit nozzles have been experimentally studied [11] and summarized [12]. The density in an expansion from a thin slit falls off only inversely with distance from the nozzle, leading to milder cooling over longer dimensions than in a jet from a circular nozzle. This has been useful in reducing the rate of cooling [13].

On first examination, a planar jet would appear to offer the advantage of a longer path length for absorption studies, which have now been conducted over the electromagnetic spectrum from IR [14] to VIS-UV [15]. A careful study of this question by Veeken and Reuss [16] shows that the column density along a path parallel to the long dimension of the slit increases by only 17% over that offered by a circular nozzle operating at the same mass throughput. Column densities of molecules is not the major advantage of a planar nozzle.

Veeken and Reuss point out a more subtle advantage of the slit nozzle. Because the velocity components parallel to the long dimension are more uniform and smaller, the resulting Doppler line width is correspondingly narrower. This has two effects: first, individual spectral lines can be better resolved; second, the optical density at the line maximum increases. Thus, the slit nozzle is preferable for high resolution measurements.

While slit nozzles have been predominantly used for studies of stable molecules and clusters, investigators studying molecular ions at high resolution [17] have shown the suitability of planar nozzles also for ion spectroscopy [18].

2.3. Continuous and pulsed jets description

The description of molecular beams from nozzle sources cannot be separated from free-jet behavior, since the properties of jets are skimmed and reflected in those of beams. Moreover, free jets and nozzle beams are often encountered in the same fields of basic and applied research: studies of translational, rovibrational, and even electronic relaxation, atomic and molecular spectroscopy, scattering processes in gas-gas, gas-photon, or gas-surface interactions, gas or isotope separation by aerodynamic or laser methods, gas dynamic or chemical lasers, condensation phenomena, physics and

chemistry of van der Waals complexes or clusters, nuclear fusion, molecular beam epitaxy, flow phenomena, aerospace studies, etc. In most of these important applications, it is of interest to obtain, as much as possible, narrow velocity spreads (or very low temperatures) in the jet or the beam, high density or intensity in the molecular beam, and a variable kinetic energy from the thermal to the electronvolt range. All these jet and beam characteristics can be improved by increasing the quantity P_0D^* where P_0 is the nozzle stagnation pressure and D^* is the nozzle diameter. This product represents the total number of two-body collisions undergone by a given molecule during the expansion process and, consequently, characterizes the degree of cooling. The extent of this flow cooling may also be limited by the formation of unwanted van der Waals complexes determined by the number of three-body collisions scaling roughly as $P_0^2D^*$. Also the nozzle stagnation temperature T_0 and the nozzle shape, governing together with D^* the expansion rate, allow one to control the condensation process.

2.3.1. Continuous Jets at Low Pressure ($P_1 \sim 10^{-3}$ - 10^{-4} Torr)

The pioneering experimental work on continuous jets and beams is due to Becker and co-workers [19]. Much credit for their development at low pressure P_1 must go to Fenn and his associates [20, 21]. Their nozzle skimmer system can be operated easily with any gas at any temperature, due to relatively weak disturbances from the background gas and the skimmer. Nevertheless, the small mass throughput acceptable by diffusion pumps, or cryopumps, limits the quantity P_0D^* and, consequently, the jet and beam performance. This pumping problem is encountered mainly with pure or seeded light gases, also with most of the common gases (in particular if heating is used to prevent condensation), and finally in cluster beam generation. On the contrary, for a number of gases expanded from room temperature, the extent of cooling is not limited by pumping requirements but by the onset of formation of undesirable van der Waals complexes ($\propto P_0^2D^*$). At least in this case, Fenn's technique is certainly appropriate.

A schematic diagram of the free-jet and molecular beam source of the Fenn type is presented in Figure 2.1. Due to the decrease of the collision frequency in the jet of relatively low density, the transition from continuum to free molecular flow $(x_S)_{max}$

occurs and the expansion becomes frozen [20, 21] at a distance from the nozzle much smaller (< 1/10) than the distance

$$X_M = 0.67D*(P_0/P_1)^{1/2} \qquad (1)$$

at which the Mach disk of a free jet shock wave structure would be formed in a continuum flow field obtained with the same nozzle and expansion ratio (see in Figure 1 the virtual Mach disk location). Because of the limitations mentioned above, these low density continuous systems are not easily perfected but they are sufficient for a wide variety of applications.

The region available for spectroscopic purposes within the isentropic expansion core typically starts around 5-10 nozzle diameters downstream from the nozzle and extends to the mach disk. For example, for an expansion of 1000 Torr into a chamber of 0.1 Torr out of a nozzle of 0.1-mm diameter, one expects to find the mach disk at 6.7 mm downstream. Thus, a 5-mm long region, extending between 1 and 6 mm downstream from the nozzle is available. Only moderate vacua are needed whenever experiments are conducted here, in the core of the expansion in front of the nozzle, and for these cases a mechanical blower pump, as pioneered by Campargue [22] is often the choice of pumping apparatus. Some experiments involve actual molecular beams, requiring chamber pressures 10^{-6} Torr or lower. These high vacua are most easily achieved with diffusion pumps. Although the volume throughput of a diffusion pump is large, the overall mass throughput is limited, and many diffusion pumped expansions have pulsed nozzles, first pioneered by Gentry [23, 24].
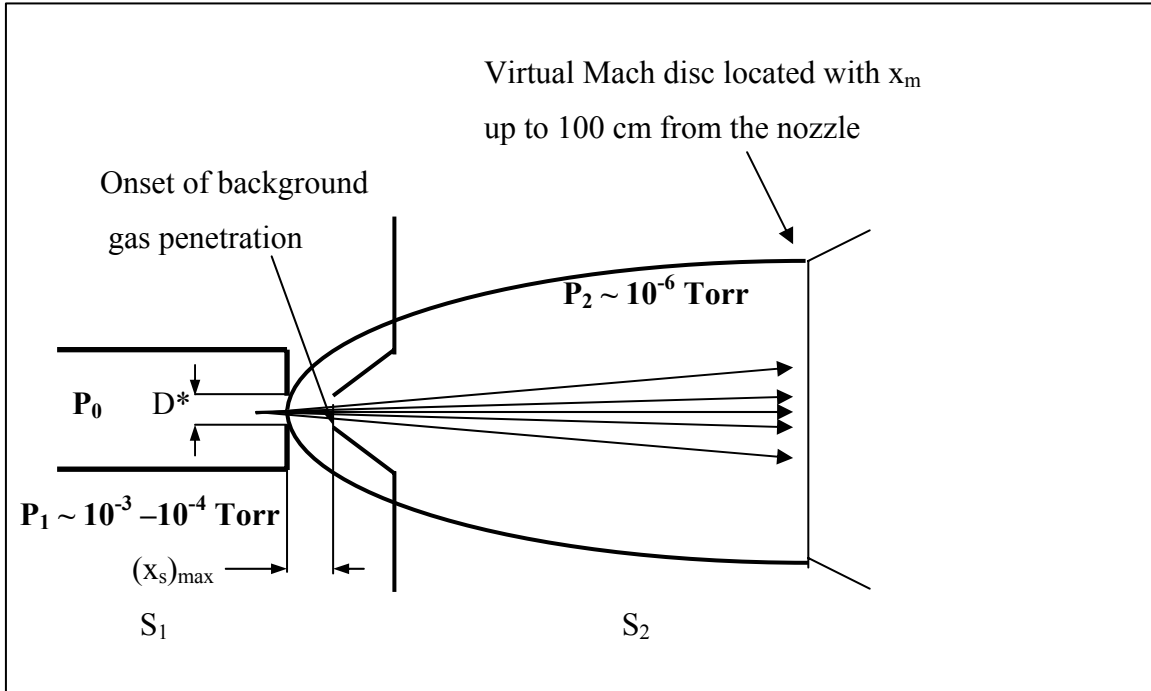
Figure 2.1. Schematic diagram of a continuous nozzle beam source operated at low background pressure in the expansion chamber (Fenn type).
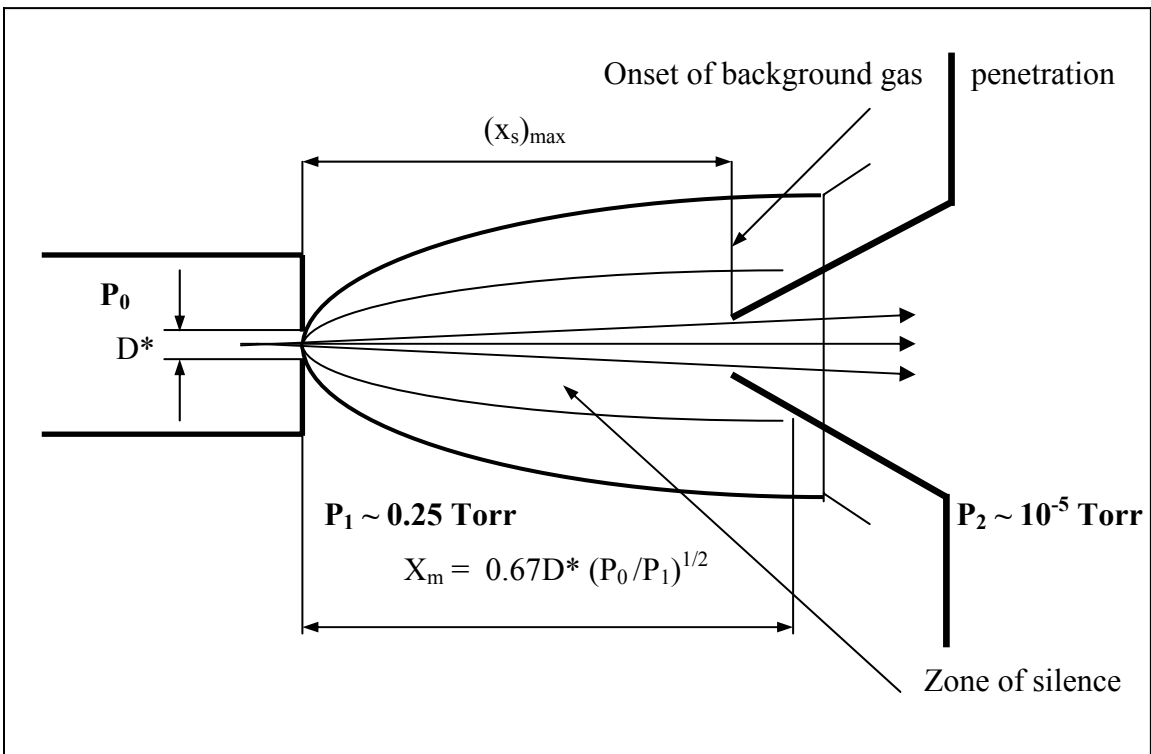
Figure 2.2. Schematic diagram of a nozzle beam source operated by skimming in the region of overexpansion of a free jet zone of silence (Campargue type).

Infrequent, short, gas pulses allow low ultimate pressures to be attained without overloading the average pumping speed. Pulse duration must be sufficient to allow development of hydrodynamic flow through the nozzle; the time required to establish steady flow has been investigated by Saenger and Fenn [25].

2.3.2. Pulsed Jet and Beams ($P_1 \sim 10^{-4}$ - 10^{-6} Torr)

In the absence of limitations due to condensation effects, the conventional approach to the pumping problem can be improved significantly by the use of a pulsed nozzle [26]. Thus, the gas flows only during the pulses into an expansion chamber sufficiently large and continuously evacuated by a large diffusion pump, or cryopump, in order to ensure that the warm background gas does not disturb the cold pulsed jet. Consequently, the pumping capacity determines the repetition rate but does not affect the expansion.

The advantages of pulsed jets and beams are due to their economical properties (gas consumption, pumping speed) and very high performance in particular in beam intensity and low temperature. Nevertheless, they may present a few drawbacks linked to their limited duty cycle, relatively large physical size, possible lack of stability and reproducibility, etc. Also pulsed nozzles are not operated at high temperatures in the present state of the art. However, preliminary experiments have been performed in our laboratory by operating a high-temperature, high-pressure source with a pulsed valve located in the downstream vicinity of the nozzle orifice.

2.3.2.1. Alternative Approach Based on the Creation of a Free-Jet Zone o Silence in a Relatively High-pressure Environment ($P_1 \sim 10^{-2} - 1$ Torr).

In the nozzle beam method developed at Saclay [27-32] the interaction of the supersonic flow with the ambient gas produces a well-defined free-jet shock wave system. Such a structure was observed recently by using electron beam fluorescence equipment available in the SR3 wind tunnel of the Laboratoire d'Aerothermique at Meudon [33]. This flow visualization has been obtained for helium by operating nozzle skimmer device in the wind tunnel with the same pressures P_0, P_1, and P_2 (in the post-skimmer region) as used at Saclay for achieving maximum helium beam performance at room temperature [31, 32].

For a given pressure ratio P_0/P_1, the shock waves are fixed in place as P_1 decreases, but their thickness (approximately several mean free paths of the molecules under the post-shock conditions) increases to form a diffuse system which finally vanishes at low pressures, $P_1 \leq 10^{-3}$ Torr, as used in the conventional molecular beam sources (Figure 2.1). In this case, the effect of the background gas on the jet molecules is simple scattering [20] which affects the largest part of the jet. Also scattering is possible when a shock barrel is present but diffuse enough for allowing penetration of the background molecules mainly into the final stages of the free-jet expansion [28-30]. It has been found that this invasion effect is strongly mass selective in favour of the light species of a gas mixture surrounding the shock wave structure [28, 29]. This is the basic principle of the jet membrane process for gas and isotope separation [34, 35].

At sufficiently high pressures P_0 and P_1, the cold isentropic core of the jet appears to be completely unaffected by the warm background gas along the total length X_M, as defined by relation (1), from the nozzle to the Mach disk [28, 30] Thus, the supersonic expansion produced in such a created zone of silence is exactly the same as that obtained in the ideal conditions as a perfect vacuum. Also, as shown clearly by flow visualization,

the jet is overexpanded upstream of the Mach disk down to densities which are considerably less than the background gas density outside the shock structure. This offers the possibility of achieving extremely low temperatures (to 6×10^{-3} K) in very compact systems.

This alternative approach for improving the nozzle beam technique has appeared initially from our semiempirical relation [28, 31] giving the experimental conditions for maximum beam intensity (Figure 2.2):

$$(X_s/D^*)_{max} = 0.125[(1/Kn_0)(P_0/P_1)]^{1/3} \tag{2}$$

where X_s/D^* is the nozzle-skimmer distance in D^* units, $Kn_0 = \lambda_0/D^*$ is the nozzle Knudsen number, and λ_0 is the nozzle stagnation mean free path. Also at the distance $(X_s/D^*)_{max}$ appears the limit of the zone of silence, as indicated by the onset of background gas penetration into the stream tube subtended by the skimmer orifice. Obviously this distance from the nozzle must be increased as much as possible for extending the cooling in the undisturbed part of the jet and the skimmed molecular beam [36].

At constant nozzle flow rate ($\propto P_0 D^{*2}$) and background pressure P_1, the volumetric pumping speed in the nozzle chamber

$$S_1 \propto P_0 D^{*2}/P_1 \propto X_M \tag{3}$$

also is constant and relation (2) can be rewritten for a given gas in the form:

$$(X_s/D^*)_{max} \propto [P_0 D^*(P_0/P_1)]^{1/3} \propto 1/D^* \tag{4}$$

which confirms the virtue of using miniature nozzles.

Finally, for a given gas, nozzle, and pumping speeds S_1, it is easily found that

$$(X_s/D^*)_{max} \propto (P_0^2/P_1)^{1/3} \tag{5}$$

This simplification shows clearly the effect of increasing the absolute pressures on the effective length of the zone of silence and finally on the jet and beam performance [30, 32]. The great interest of this approach results from its possibility of eliminating the background gas disturbance and extending the flow cooling by the same way. Also, for a given pump size, operation in the range of 10^{-1} to 1 Torr (at a density much higher than in the terminal part of the jet due to the overexpansion leads to an increase of several orders of magnitude in the nozzle mass flow rate ($P_0 D^{*2}$) over that traditionally available.

In conclusion, the free jet zone of silence appears as an extremely efficient way for cooling continuously with the only limit due to condensation. In particular, helium free jets provide ideal media largely used for simplifying the laser spectroscopy of molecules which are cooled with He in the gas phase to extremely low temperature [37-40]. The exploration of only the supercooled and undisturbed core of the jet is possible and the shock waves do not affect the propagation of light. On the contrary, as shown below, skimming very high Mach numbers in a free-jet zone of silence (Figure 2.2.) is technically much more difficult than skimming in the Fenn free jets (Figure 2.1.). This difficulty has limited the application of the nozzle beam technique developed at Saclay. Also this was the reason why very high Mach numbers (~180) predicted and obtained already in 1968 in He free jets were not measured until 1974 by the molecular beam time-of-flight (TOF) technique [31], after successively different improvements in optimising the geometry of the skimmer were performed.

2.4. Spectroscopy of cold radicals

Radicals and molecular ions are among the most chemically reactive species known and play a key role in chemistry ranging from the upper atmosphere [41-43] to molecular synthesis in the interstellar medium [44-46]. The vast majority of chemical reactions proceed via elementary reactions involving highly unstable transients such as radical and molecular ions. This has stimulated longstanding efforts toward developing high resolution spectroscopic tools for detailed characterization of these highly reactive species in the gas phase [47-54]. Generally speaking, two universal experimental problems to overcome are first generation of sufficient densities for detection (such

transient species are usually very difficult to maintain at sufficient concentrations to probe experimentally) and second successful extraction and analysis of high resolution spectra in the presence of much higher concentrations of precursor molecules.

The most widely tools used for generation of transient radical species have been based on electrical discharges. Several groups have exploited these methods to study a variety of small radicals with coherent light sources from the microwave to the ultraviolet spectral region [55-57]. Of particular interest has been the application of direct absorption laser techniques for high-resolution spectroscopy of radicals/molecular ions present in electrical discharges, where these reactive molecules can be maintained at relatively high steady state concentrations.

A promising technique has been the combination of an electrical discharge and a supersonic expansion. Such discharge expansion sources provide an extremely powerful tool for ion or radical spectroscopy under jet-cooled conditions. The method was initially pioneered by Engelking and coworkers [58], who developed a sharp tungsten tip 'Corona' discharge ionization source behind the pinhole of a continuous wave (cw) expansion nozzle. These Corona sources yield appreciable densities of rotationally cold radicals (with $T_{rot} < 15$ K) at the expansion orifice, which simplifies the spectroscopic analysis and has proved useful for a variety of emission and laser-induced fluorescence studies [1].

The problem of low densities of radical species, which made direct absorption difficult to observe was significantly reduced by development discharge methods allowing relatively high densities of species to be achieved. These discharge sources of radicals combined the long path length of a slit with the high densities accessible in a pulsed supersonic expansion. The examples of such sources can be found in the works of Davis et al. [59, 60] and Anderson et al. [61].

On the other hand the applications of more and more sensitive methods of probing radicals under laboratory conditions increased noticeably the number of very interesting results. So far, high resolution laser spectroscopic studies have been successfully performed on an impressively large class of important molecular ions and radicals [62]. Among the various methods of high resolution study of transient radical and molecular ion species [63-65], electric discharge sources combined with supersonic expansion and

sensitive detection methods have played an especially important role [66]. The further progress in the study of transient species came with the invention and development of sensitive method – cavity ringdown. Especially their combination with a pulsed slit nozzle appeared to be very fruitful in the studies of the unstable species. Detailed description of the method and its applications is given in the next chapters.

References

[1] P. C. Engelking, Chem. Rev. 91 (1991) 399

[2] D. H. Levy, Ann. Rev. Phys. Chem. 31 (1980) 197

[3] A. Kantrowitz, J. Chem. Phys. 14 (1945) 150

[4] A. Kantrowitz, J. Grey, Rev. Sci. Instrum. 22 (1951) 328

[5] G. B. Kistiakowsky, P. Schlichter, Rev. Sci. Instrum. 22 (1951) 333

[6] J. B. Fenn, J. Deckers, Rev. Sci. Instrum. 34 (1963) 96

[7] T. C. Adamson, Jr., in "Supersonic Flow Chemical Processes and Radiative Transfer", D. B. Olfe and V. Zakkay, Eds., Pergamon, New York, 1964, p 177

[8] J. Bowyer, L. D'Attorre, and H. Yoshihara, in "Supersonic Flow Chemical Processes and Radiative Transfer", D. B. Olfe and V. Zakka , Eds., Pergamon, New York, 1964, p 201

[9] E. S. Love, "Experimental and Theoretical Studies of Axi-symmetric Free Jets", NASA TR R-6, 1959

[10] G. W. Faris, R. L. Byer, Opt. Lett. 11(1986) 413

[11] A. E. Beylich, Z. Flugwiss, Weltraumforsch. 3 (1978) 48

[12] O. F. Hagena, Surf. Sci. 106 (1981) 101

[13] M. Silkes, C. Jouvet, S. A. Rice, Chem. Phys. Lett. 87 (1982) 515

[14] C. M. Lovejoy, D. J. Nesbitt, J. Chem. Phys. 86 (1987) 3151

[15] A. Amirav, J. Jortner, J. Chem. Phys. 82 (1985) 4378

[16] K. Veeken, J. Reuss, Appl. Phys. B 38 (1985) 117

[17] I. W. Milkman, J. C. Choi, J. Hardwick, J. T. Moseley, J. Chem. Phys., 86 (1987)

1679

[18] I. W. Milkman, J. C. Choi, J. Hardwick, J. T. Moseley, Rev. Sci. Instrum. 59 (1988) 508

[19] E. W. Becker and K. Bier, Z . Naturforsch. A , 9, 975 (1954); K. Bier and O. F. Hagena, "Rarefied Gas Dynamics", 3rd Symposium, Vol. I, J. A. Laurmann, Ed., Academic Press, New York, 1963.

[20] J. B. Fenn, J. Deckers, "Rarefied Gas Dynamics", 3rd Symposium, Vol. I, J. A. Laurmann, Ed., Academic Press, New York, 1963; J. B. Fenn, J. B. Anderson, "Rarefied Gas Dynamics", 4th Symposium, Vol. 11, J. H. De Leeuw, Ed., Academic Press, New York, 1966; J. B. Anderson, R. P. Andres, J. B. Fenn, G. Maise, "Rarefied Gas Dynamics", 4th Symposium, Vol. 11, J. H. De Leeuw, Ed., Academic Press, New York, 1966

[21] J. B. Anderson in "Molecular Beams and Low Density Gasdynamics", P. P. Wegener, Ed., Marcel Dekker, New York, 1974

[22] R. Campargue, J. Phys. Chem. 88 (1984) 4466

[23] W. Gentry, C. F. Giese, Rev. Sci. Instrum. 49 (1978) 595

[24] W. Gentry, C. F. Giese, J. Chem. Phys. 67 (1977) 5389

[25] K. L. Saenger, J. B. Fenn, J. Chem. Phys., 79 (1983) 6043

[26] K.Bier and 0. F. Hagena, "Rarefied Gas Dynamics", 4-th Symposium, Vol. 11, J. H. De Leeuw, Ed., Academic Press, New York, 1966; W. R. Gentry and C. F. Giese, Rev. Sci. Instrum. 49 (1978) 595; M. G. Livermann, S. M. Beck, D. L. Monts, and R. E. Smalley, "Rarefied Gas Dynamics", 11-th Symposium, Vol. 11, R. Campargue, Ed., CEA, Paris, 1979

[27] R. Campargue, Rev. Sci. Instrum. 35 (1964) 111

[28] R. Campargue, Thesis, Paris, (1970)

[29] R. Campargue, J. Chem. Phys., 52 (1970) 1795

[30] R. Campargue and J. P. Breton, Entropie, 42 (1971) 18

[31] R. Campargue, A. Lebehot, "Rarefied Gas Dynamics", 9th Symposium, Vol. 11, M. Becker and M. Fiebig, Eds., DFVLR Press, Porz-Wahn, F.R.G., 1974

[32] R. Campargue, A. Lebehot, and J. C. Lemonnier, "Rarefied Gas Dynamics", 10-th Symposium, Vol. 11, J. Leith Potter, Ed., AIAA, New York, 1977

[33] G. Dupeyrat, Thesis, Paris, 1979

[34] R. Campargue, J. B. Anderson, J. B. Fenn, B. B. Hamel, E. P. Muntz, J. R. White in "Nuclear Energy Maturity", P. Zaleski, Ed., Pergamon Press, Oxford, 1975

[35] J. W. Brook, V. S. Calia, E. P. Muntz, B. B. Hamel, P. B. Scott, T. L. Deglow, J. Energy 4 (1980) 199

[36] H. Ashkenas and F. S. Sherman, "Rarefied Gas Dynamics", 4-th Symposium, Vol. 11, J. H. De Leeuw, Ed., Academic Press, New York, 1966

[37] R. E. Smalley, D. H. Levy, and L. Wharton, Laser Focus, 40, Nov. (1975)

[38] R. E. Smalley, L. Wharton, and D. H. Levy, J. Chem. Phys. 63 (1975) 4977

[39] D. H. Levy, L. Wharton, and R. E. Smalley in "Chemical and Biochemical Applications of Lasers", C. B. Moore, Ed., Academic Press, New York, 1977;

[40] D. H. Levy, Annu. Rev. Phys. Chem. 31 (1980) 197

[41] E.E. Ferguson, Acc. Chem. Res. 14 (1981) 327

[42] C.A. Smith, L.T. Molina, J.J. Lamb, M.J. Molina, Intern. J. Chem. Kinetics 16 (1984) 41

[43] S. Solomon, R.R. Gareia, R.S. Rowlans, D.J. Weubbles, Nature 321 (1986) 755

[44] E. Herbst, W. Klemperer, Astrophys. J. 185 (1973) 505

[45] T. Oka, M.J. Jogod, J. Chem. Soc. Faraday Trans. 89 (1993) 2147

[46] O.L. Polyansky, B.M. Dinelli, C.R. Le Sueur, J. Tennyson, J. Chem. Phys. 102 (1995) 9322

[47] T. A. Miller, Ann. Rev. Phys. Chem. 27 (1976) 127

[48] R. J. Saykally, R. C. Woods, Ann. Rev. Phys. Chem. 32 (1981) 403

[49] T.J. Sears, J. Chem. Soc. Faraday Trans. 832 (1987) 111.

[50] E. Hirota, Int. Rev. Phys. Chem. 8 (1989) 171

[51] P.F. Bernath, Ann. Rev. Phys. Chem. 41 (1990) 91

[52] E. Hirota, Annual Reports, The Royal Society of Chemistry Section C, (1994)

[53] P. Davies, Spectrochim. Acta Part A 55 (1999) 1987

[54] E.J. Bieske, O. Dopfer, Chem. Rev. 100 (2000) 3963

[55] E. Hirota, Chem. Rev. 92 (1992) 141

[56] P. F. Bernath, Ann. Rev. Phys. Chem. 41 (1990) 91

[57] C. Demuynck, J. Mol. Spectrosc. 168 (1994) 215

[58] P.C. Engelking, Rev. Sci. Instr. 57 (1986) 2274

[59] S. Davis, D. T. Anderson, G. Duxbury, D. J. Nesbitt, J. Chem. Phys. 107 (1997) 5661

[60] S. Davis, M. Fárník, D. Uy D. J. Nesbitt, Chem. Phys. Lett. (2001) 23

[61] D.T. Anderson, S. Davis, T.S. Zwier and D.J. Nesbitt , Chem. Phys. Lett. 258 (1996) 207

[62] M.E. Jacox, Vibrational and electronic energy levels of polyatomic transient molecules, American Chemical Society and American Institute of Physics, Gaithersburg, MD, 1994, in: J.P. Maier (Ed.), Ion and Cluster Ion Spectroscopy and Structure, Elsevier, Amsterdam, (1989) 483.

[63] H. Petek, D.J. Nesbitt, P.R. Ogilby, C.B. Moore, J. Phys. Chem. 87 (1983) 5367

[64] D.W. Kohn, H. Clausberg, P. Chen Rev. Sci. Instrum. 63 (1992) 4003

[65] H. Linnartz, D. Verdes, T. Speck, Rev. Sci. Instrum. 71 (2000) 1811

[66] P.B. Davies, Chem. Soc. Rev. 24 (1995) 151

CHAPTER 3

3. Cavity ringdown method - principles and applications

The study of molecular absorption and emission of radiation is of a great importance in modern science. Much of information about the geometrical and electronic structure of various molecules and molecular clusters comes from optical absorption studies performed on either bulk samples or, more recently, in molecular beam expansions. In some cases, especially involving small diatomic and triatomic species, emission measurements can be more sensitive since the appearance of a tiny signal is measured rather than a small change in a large one. The most established techniques for making such measurements are laser-induced fluorescence (LIF) and resonance-enhanced multiphoton ionization (REMPI), and both have been employed successfully in a large number of studies. Unfortunately for many applications involving large polyatomic molecules absorption measurements are potentially superior to those based on emission, due to rapid internal conversion, predissociation, or other dynamical processes which significantly reduce the emission quantum yield. Even for small systems, the vibronic band intensities are often contaminated by intramolecular relaxation dynamics; in such cases, these techniques cannot be used for reliable intensity measurements. For clusters that exhibit rapid photofragmentation, depletion spectroscopy can be employed quite effectively to measure their vibronic structure, but again, dynamic effects complicate the interpretation of spectra. The problem is that direct absorption methods are generally orders of magnitude less sensitive than those based on emission, therefore, difficult to apply to transient species, such as clusters or radicals.

For many applications, such as atmospheric pollution studies or flame probing the use of direct absorption measurements is often impractical since the absorbing species is present only in trace amounts or the sample path-length is pretty short. In the limit of weak absorption, the transmitted optical intensity decreases exponentially with absorption path length according to Lambert-Beer's law:

$$I = I_0 e^{-\sigma n l}$$

where:

σ- wavelength dependent absorption cross section proportional to the transition dipole moment,

n - volume density of molecules,

l - absorption path-length

The ability to measure the I/I_0 ratio with a high accuracy typically limits the measurement to minimum losses of $0.01 - 0.001$ %. In addition such precision absorption measurements require very sophisticated optical systems and sources which have a stable output intensities. Usually the high stability is obtained using several types of continuous lasers used in experimental configurations which employ some form of frequency modulation to discriminate against the low frequency noise. The examples are infrared lasers [1-5], diode lasers [6] and tunable cw dye lasers [7].

When it comes to the experimental systems based on pulsed lasers the same degree of accuracy of the measurement has not yet been possible. The pulse to pulse amplitude variation of most pulsed laser sources is around 10% which requires a greater detector dynamic range and this way reducing the effective signal resolution. In addition, the short pulse widths of such lasers (10-30 ns) makes it very difficult to modulate the frequency for differential analysis. Because of this limitations, sensitive absorption measurements have not been made over the full spectral range accessible using nonlinear frequency conversion techniques.

For the applications in which fluorescence emission analysis is not practical, some means of increasing the sensitivity of absorption detection is required. Lambert-Beer's law says that in the limit of very weak absorption, when the density of the sample is low,

the signal can be increased proportionally by lengthening the absorption path for example using a multipass configuration. However, in practice getting more than 100 passes is not possible as the light beam diverges and gets weaker with every reflection [8-12].

The problem is more severe in the case of other applications e.g., molecular beams where the geometrical cross-sections are really small. Here the same small volume has to be repeatedly probed. Although several innovative examples of optical multipass systems suitable for the molecular beams have been proposed [3, 12, 13], most of them allow only a few passes and even the most promising designs can not give more than 100 [12]. The situation changed drastically in 1988 when O'Keffe and Deacon reported the invention of a new technique which allows an increase of several orders of magnitude in sensitivity over existing methods for the wide spectral region accessible with tunable pulsed lasers. The method is based not on the measurement of the absorbed signal strength, but upon the measurement of the decay rate of a light pulse confined to a highly reflective closed optical cavity [14]. The principles of the new method henceforth called cavity ringdown are described below.

3.1. Principles of cavity ringdown

The method is based on measurement of the time rate of decay of a pulse of light trapped in a high reflectance optical cavity. In practice, pulsed laser light is injected into an optical cavity that is formed by a pair of highly reflective plano-concave mirrors (R > 99.9 %, f=100cm). The small amount of light that is trapped inside the cavity reflects back and forth between the two mirrors, with a small fraction transmitting through each mirror with each pass. The resultant transmission of the circulating light is monitored at the output mirror as a function of time and allows the decay time of the cavity to be determined. This signal has an envelope which is simply a first order decay $\exp[-t/\tau]$. The time required for the cavity to decay to 1/e of the initial output pulse is called the "cavity ringdown" time.

It can be easily seen that the ring down time, τ, is determined by the following equation:

$$\tau = \frac{d}{c(1 - R + \alpha l)}$$

where:

d - the optical length of the cavity,

c - the speed of light,

R - the averaged reflectivity of the two mirrors

αl – the absorbance for a sample present in the cavity with absorption coefficient α and length l.

The idea of the cavity ringdown method is described graphically in the Figure 3.1.

When no absorbing medium is present in the cavity the ringdown time is a function of only the mirror reflectivities (R) and cavity dimensions (d). The absorption $\alpha l = 0$ and as a result τ is relatively long (black line in the figure). When the molecule absorbs the laser light the ringdown time decreases and it depends on the absorbance of a medium which is present in the cavity. The exponential decay is much stepper because the product αl is not equal 0 anymore (red line in the figure). Absolute absorption intensities are obtained by subtracting the base-line transmission of the cavity, which is determined when the laser wavelength is off-resonance with all molecular transitions. As the ring down time reflects the rate of absorption rather than the magnitude of the absorption and as such it has important advantages compared with conventional absorption techniques. The method is immune to pulse-to-pulse fluctuations in the laser power and the very long absorption pathlengths that are obtained by confining the light pulse several microseconds in the cavity make this technique ideal to study unstable species.

Figure 3.1. The principles of cavity ringdown method.

$$\tau = d \,/\, c \,(1 - R + \alpha \, l)$$

Intensity

Time μs
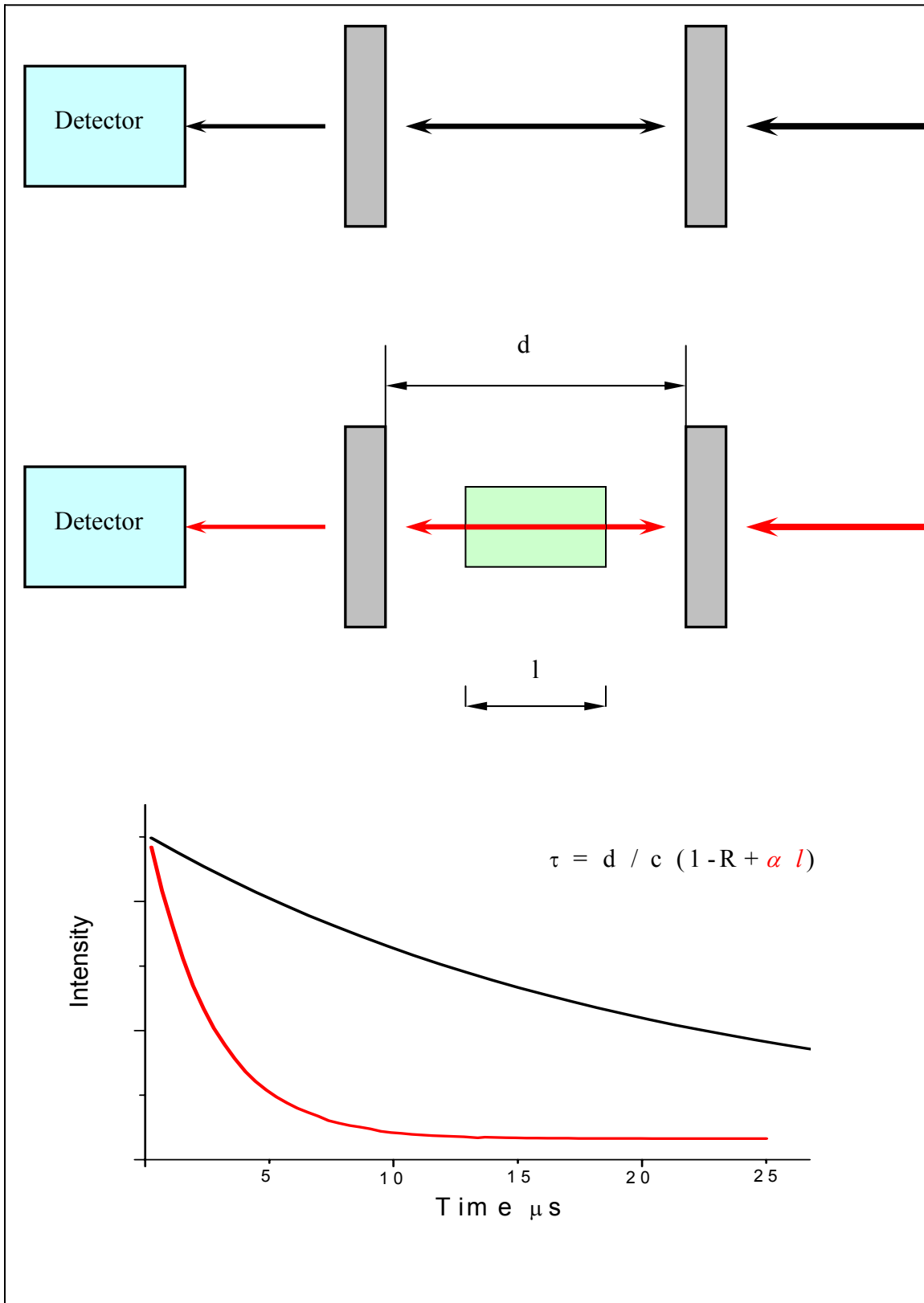
3.2. Applications of cavity ringdown method

Cavity ring down method was applied to study of the radicals produced in the discharge sources. In 1996 Kotterer et al. reported experiments where they comprised a hollow cathode discharge within a cavity ringdown system. Using this approach the A $^2\Pi$ - X $^2\Sigma_g^-$ (6-0) transition of N_2^+ [15] and the $^2\Pi$ - X $^2\Pi$ transition of C_6H were measured [16].

As the cavity ringdown measurements have proved very effective in the detection of carbon chains, the results of the method have been of astrophysical relevance. It has been suggested that carbon chains may be potential carriers of some of the diffuse interstellar bands [17]. Following that suggestion and arguments by Douglas [18] this concept have been supported by the detection of molecules with a charbon-chain skeleton in dense interstellar clouds by microwave spectroscopy. However, the ultimate test could be only made by comparing the astronomical data with spectra measured in the laboratory under conditions which closely imitate those in the interstellar medium. This could be done by means of cavity ringdown method. The experimental set-up which could be use for this studies was described by Motylewski and Linnartz [19]. It consisted of a standard cavity ringdown unit sampling the plasma generated in a pulsed supersonic slit jet expansions. In 2000 Motylewski et al. compared the laboratory gas-phase spectra of neutral and cationic linear carbon-chain radicals they measured with astronomical diffuse interstellar bands [20]. The origin bands of the strong electronic transitions of the studied species, $C_{2n}H$ (n=3-6), $HC_{2n}H^+$ (n=2-4), $NC_{2n-2}N^+$ (n=3, 4), did not coincide with detectable DIBs, except for $HC_{2n-1}N^+$ (n=3), which possibly matches a weak feature. The profile change and the shift of the maxima of the absorption bands with temperature were also illustrated.

Appendix to chapter 3

Numerous researchers have employed and developed cavity ringdown technique for various purposes, including the spectroscopic study of molecules and clusters. Shortly after the initial gas cell measurements of O'Keefe and Deacon [14], cavity ringdown was developed for molecular beam spectroscopy by O'Keefe et al. [21]. In this work, vibronic spectra were obtained for a variety of transition metal clusters, including the copper dimer and trimer systems. In this application of cavity ringdown to the study of laser-generated molecular beams, several potential difficulties were addressed. The transient nature of the molecular beam, high plasma density, and large shot to shot fluctuations typical of laser vaporization sources were of primary concern. Although these factors did in fact limit the attainable sensitivity to 5-10 ppm (fractional absorption) per pass, this work demonstrated the suitability of the ringdown technique for molecular beam spectroscopy and underscored the potential of the method for other applications. These molecular beam investigations have since been extended to include a number of metal cluster and metal silicide studies.

The next application of the ringdown technique was demonstrated in 1991 by Benard and Winker [22], who utilized a novel variation of the approach to detect either the optical gain or loss in a laser-induced chemical reactor. In that experiment, the active volume of a CO_2 laser pumped-flow reactor was situated at the center of a confocal ringdown cavity (d = 50 cm), at right angles to both the gas flow and CO_2 laser pump axes. The ringdown measurement was performed with an excimer-pumped dye system and detected with a fast photodiode and oscilloscope at the exit mirror. A delay between the photolysis laser and ringdown probe laser facilitated buildup of a population inversion in BiF before spectral interrogation.

In 1993 Yu and Lin [23] reported the first development of the ringdown technique for kinetics studies. In that work, phenyl radical was generated by laser photolysis of nitrobenzene, followed by spectral interrogation with the pulsed cavity ringdown technique. The exponential decay of the photolyzed product was accounted for by replacing the absorption term in the ringdown expression with an absorption

(concentration) exponential decay factor given by A = A$_o$ exp(-k't'), where k' is the pseudo-first-order decay constant of phenyl and t' is the time after firing of the photolysis laser. The absolute values of the second-order rate constants were then determined from the slopes of the linear k' vs concentration plots. The validity of this approach stemmed largely from the fact that the lifetime of the photolyzed product (5-10 ms) was orders of magnitude longer than the associated ringdown times (ca. 25 μs). Lin and co-workers have tested the accuracy of the cavity ringdown approach described above for kinetics studies by measuring the rate constant of the NH_2 + NO reaction via the NH_2 absorption spectrum at 537 nm [24]. These studies have since been extended to include the C_6H_5 + NO $\rightarrow$ C_6H_5NO reaction [23], wherein the C_6H_5 absorption band at 505 nm was monitored, the C_6H_5 + CCl_4 reaction (in the presence of O_2) wherein the $C_6H_5O_2$ product was investigated via its 510 nm absorption band [25] and further experiments of the NH_2 + NO reaction, again studied via the NH_2 absorption at 537 nm [26]. The experiments of Lin and co-workers demonstrated the feasibility of using the ringdown method for kinetics studies. In theory, this approach could be extended to faster kinetics processes than those explored above, as long as the chemical dynamics are significantly slower than the fitted time region of the ringdown decay. This same application of cavity ringdown for kinetics studies has also been recently implemented by Zhu and Johnston [27] for studying the reaction of vinoxy radical with molecular oxygen.

Romanini and Lehmann [28, 29] have used cavity ringdown to obtain overtone spectra of HCN in static gas cells, in search of chaotic behavior in highly excited vibrational states. In these experiments, the cavity ringdown spectral intensities for the HCN (105) overtone were found to be different from those obtained in photoacoustic studies, but were in agreement with ab initio calculations. In these experiments, a novel boxcar scheme was utilized to measure the ringdown signal, and a Brillouin cell was located before the cavity to reject the input laser ASE, which in some cases could otherwise lead to a reduction in the extracted absorption intensities.

Meijer et al. [30] have extended cavity ringdown into the UV in a study of the 300 nm band of OH obtained in a small Bunsen burner flame. Absorption spectra were obtained with a multimode dye laser (~1.2 GHz bandwidth) and used to calculate the temperature of an atmospheric pressure methane-air flame. Mirror reflectivities used in

that work were ca. 99.5%, resulting in very fast decay times and subsequent lower sensitivity. In the case of flame spectroscopy, small ringdown cavities combined with small burner dimensions helped to minimize thermal lensing effects (e.g., beam walking), which can significantly degrade cavity alignment. These effects are more severe at shorter wavelengths since they are dominated by nonresonant processes that typically scale exponentially with frequency. In this same study, experiments were performed wherein narrow band (~5 MHz) cw laser light was coupled into cavities of on- and off-confocal geometry, which revealed the transverse and longitudinal mode structure of the ringdown cavity. The researchers then measured the visible absorption spectrum of iodine with a pulsed laser and nonconfocal cavity geometry and interpreted the absence of distorted or missing spectral features as being explicitly due to the near-continuous mode spectrum of the cavity.

Meijer and co-workers have since utilized the cavity ringdown method for the detection of trace species in the gas phase [31] and have also used the absorption measurements in a static gas cell to determine the absolute transition strength of the 206 nm Cameron band of CO [32]. Boogaarts and Meijer [33] have also used ringdown spectroscopy in conjunction with a mass spectrometer and laser desorption apparatus to estimate the number density of desorbed diphenylamine molecules.

Zalicki et al. [34] have employed cavity ringdown to detect the methyl radical in a hot filament flow reactor via the 216 nm band. The spatial dependence of the methyl concentration in the vicinity of the filament was derived from the associated intensity of the absorption spectrum. In this work, an absorption sensitivity of 20 ppm was reported, and the broad vibronic band spectra obtained exhibited a signal to noise ratio roughly four times better than that of previous conventional absorption measurements and comparable to that obtained in atmospheric pressure flames with the method of degenerate four wave mixing (DFWM) reported by Sick and co-workers [35]. These flow reactor studies were further employed to gain insight into the chemistry of diamond film growth.

Scherer et al. [36] have extended cavity ringdown into the 1.6 and 3.3 μm regions of the mid-infrared. In that work, a single mode optical parametric oscillator (OPO) laser system was employed to obtain Doppler limited spectra in static gas cells. In these

studies, the high mirror reflectivities (R > 99.95%) allowed a sensitivity of better than 3 ppm (fractional absorption per pass) to be obtained. Comparison of IR-cavity ringdown overtone spectra of acetylene obtained in the 1.6 μm region with state-of-the-art photoacoustic data demonstrated nearly 1 order of magnitude greater sensitivity for IR-cavity ringdown. IR-cavity ringdown has also been implemented by Scherer et al. as a nonintrusive diagnostic of chemical species in low pressure flames in the 1.6-4 μm region [37]. In this work, sensitivity, spectral congestion in high-temperature hydrocarbon flame environments, and the ability to operate in moderately sooting flames was explored. Additionally, comparison of the IR-cavity ringdown flame spectra to those obtained by other infrared methods demonstrated at least 1 order of magnitude greater sensitivity for IR-cavity ringdown. Cavity ringdown has also been used by Scherer and Rakestraw to determine the HCO radical concentration in a low pressure flame [38].

Engeln and Meijer [39] have reported the combination of visible cavity ringdown with a Fourier transform (FT) spectrometer. In this demonstration, broadband laser light is first coupled into the ringdown cavity and then directed into a commercial FT instrument. Obtaining an interferogram in combination with the intensity decay of the resonator allows a spectrum to be obtained with comparable sensitivity to that of currently available FT systems that employ multipass configurations.

Giles et al. [40] have used cavity ringdown method to obtain the doubly forbidden $^3\Delta$-X $^1\Sigma$ vibronic transitions in diacetylene in the 396-342 nm region, and Pearson et al. [41] have employed cavity ringdown for the study of the J-dependent line broadening in the A-X system of HNO.

These and some other applications of cavity ringdown technique are discussed in more details in the review article published in 1997 [42].

In 1998 Berden et al. applied cavity ringdown in the environment that is usually difficult to access, e.i., high magnetic field [43]. They recorded the rotationally resolved spectra of the b $^1\Sigma^+_g$ (v=0) - X $^3\Sigma^-_g$ (v=0) band of molecular oxygen in magnetic fields up to 20 T. Measurements were performed in a 3-cm-long cavity, placed in the homogeneous field region inside a Bitter magnet. Cavity ringdown absorption spectra were measured with linearly and circularly polarized light, leading to different ΔM selection rules in the molecular transition, thereby aiding in the assignment of the spectra.

Dispersion spectra were obtained by recording the rate of polarization rotation, caused by magnetic circular birefringence, using the polarization-dependent CRD detection scheme.

Similar experiments have been carried out by Romanini et al. in 1999 [44] but the studied species was naphthalene cation. It was produced in a slit jet coupled with an electronic discharge, and cavity ring down was used to obtain its absorption spectrum in the region 645–680 nm. Two of the strongest $C_{10}H_8^+$ bands previously characterized by matrix isolation spectroscopy were found, both with a fractional blue shift of about 0.5%. This was the first gas-phase electronic absorption spectrum of an ionized polycyclic aromatic hydrocarbon (PAH) and opened the way for a direct comparison of laboratory PAH spectra with the diffuse interstellar bands. These experimental results represented an important step in the spectroscopy of large aromatic ions or radicals in the gas phase.

In 2003 Bieniier et al. obtained the gas-phase electronic absorption spectra of the naphthalene and acenaphthene cations in the visible range in a free jet planar expansion using the same approach [45]. The direct absorption spectra of two out of four bands measured of the gas-phase cold naphthalene cation along with the gas-phase vibronic absorption spectrum of the cold acenaphthene cation were reported for the first time. This experiment enabled the intrinsic band profiles to be measured, a key requirement for astrophysical applications.

Interesting applications of cavity ringdown was described in 2002 by Brown et al. [46]. They used this method to the simultaneous concentration measurement of nitrate radical, NO_3, and dinitrogen pentoxide, N_2O_5 in the ambient atmosphere. The sensitivity for detection of both NO_3 and N_2O_5 was very high (comparable to or better than previous measurements) and time resolution was significantly better. Furthermore, direct measurement of N_2O_5 represented a previously unavailable capability. Concentrations of both species were measured simultaneously in two separate flow systems and optical cavities pumped by the same pulsed dye laser at 662 nm. One of the flow systems remained at ambient temperature for detection of NO_3, while the other was heated to 80 °C to induce thermal decomposition of N_2O_5 providing a measurement of the sum of the NO_3 and N_2O_5 concentrations. In this experiment for the first time NO_3 was measured in the tropospheric concentration.

Recently cavity ringdown method was used in the studies of photochemically relevant triplet species [47]. Despite their importance, molecular triplet states have received relatively little attention in spectroscopic studies. This was primarily due to the challenge of detecting the spin-forbidden $T_n \leftarrow S_0$ transitions. Drucker et al. overcame these difficulties by applying the CRD method. They measured the vibronically resolved singlet-triplet spectra of some organic compounds (acrolein, diacetylene, butadiene and some of the cyclic enones). This success underscored the versatility of the CRD technique in cases where a very high sensitivity is needed.

In 1997 Romanini et al. employed for the first time a commercial tunable CW single-frequency laser to demonstrate a new version of the cavity ringdown experiment [48]. They measured a section of the weak acetylene overtone transition near 570 nm, and compared to existing photoacoustic data. Their high quality and reproducible Doppler-limited spectra displayed showed that the CW cavity ringdown is as good as a pulsed CRD. Most interesting applications of CW-CRDS include high resolution spectroscopy at low pressure, sub-Doppler absorption spectroscopy in a supersonic jet, and trace-gas detection using compact diode laser sources. In another experiment they also proved that even the broad and weak absorption bands could be measured by means of CW-CRDS. It was demonstrated by the obtaining the absolute absorption spectrum of a weak and broad overtone transition in CHF_3 [49].

In 1998 He et al. demonstrated the extension of diode laser CW-cavity ringdown spectroscopy into the 1300 nm region, with a simple scheme for frequency matching the cavity [50]. The technique had a very high instrumental resolution in the sub-MHz range and was extremely sensitive. In their work they measured the $\Sigma - \Sigma$ band $\nu_1 + 3\nu_3$ of N_2O around 7780 cm^{-1}. The obtained spectra had a well-defined and reproducible baseline, which was important for quantitative measurements and for observing very weak absorbances. Absorption bands of $CHCl_3$ between 7700 and 7750 cm^{-1} have also been observed. While the assignment for $CHCl_3$ must remain preliminary, they demonstrated once again that the cavity ringdown technique provides both high resolution and absolute frequency and intensity accuracy.

CW cavity ringdown method was also successfully applied to measure electronic spectra of cold carbon chain radicals at very high spectral resolutions. In 2002 Birza et al.

recorded the rotationally resolved origin band spectrum of the A $^2\Pi_g$ - X $^2\Pi_u$ electronic spectrum of triacetylene cation [51]. The spectrum was recorded before, using both pulsed cavity ringdown and cw frequency plasma modulation approaches [52]. The experiment showed that the achievable resolution attained using CW-CRD method is significantly higher.

All of these studies have clearly established the widespread applicability of cavity ringdown for sensitive spectroscopic measurements and foreshadow the increased use of this rapidly developing technique. Cavity ringdown is a direct absorption technique and is therefore relatively free from the complications and limitations associated with the molecular internal conversion and excited state predissociation. As a result the method can be used for studying also systems comprising larger number of atoms. The most compelling attributes of the method are its simplicity and versatility, combined with an extraordinarily high sensitivity. This brief description of wide applications of CRD method shows clearly that the last word has not yet been said.

References

[1] A. S. Pine, W. L. Lafferty, J. Chem. Phys. 78 (1983) 2154

[2] N. Ohashi, A. S. Pine, J. Chem. Phys. 81 (1984) 73

[3] Z. S. Huang, K. W. Jucks, R. E. Miller, J. Chem. Phys. 85 (1986) 3338

[4] C. M. Lovejoy, M. D. Schuder, D. J. Nesbitt, Chem. Phys. Lett. 127 (1986) 374

[5] G. T. Fraser, A. S. Pine, W. L. Lafferty, R. E. Miller, J. Chem. Phys. 87 (1987) 1502

[6] C. Yamada, K. Nagai, E. Hirota, J. Mol. Spectrosc. 85 (1981) 416

[7] H. Petek, D. J. Nesbitt, D. C. Darwin, C. B. Moore, J. Chem. Phys. 86 (1987) 1172

[8] J. W. White, J. Opt. Soc. Am, 32 (1942) 285

[9] D. R. Herriot J. Schulte, Appl. Opt. 4 (1965) 883

[10] A. R. W. McKeller, N. Rich, V. Soots, Appl. Opt. 9 (1970) 222

[11] W. R. Trutna, L. R. Byer, Appl. Opt. 19 (1980) 301

[12] P.G. Lethbridge, A. J. Stace, Rev. Sci. Instrum. 58 (1987) 2238

[13] T. E. Gough, G. Gravel, Rev. Sci. Instrum. 52 (1981) 802

[14] A. O'Keefe, D. A. G. Deacon, Rev. Sci. Instrum. 59 (1988) 2544

[15] M. Kotterer, J. Conceicao, J.P. Maier, Chem. Phys. Lett. **259** (1996) 233

[16] M. Kotterer, J.P. Maier, Chem. Phys. Lett. **266** (1997) 342

[17] The Diffuse Interstellar Bands, eds. A. G. G. M. Tielens and T. Snow, Kluwer, Dordrecht (1995)

[18] A. E. Douglas, Nature 269 (1977) 130

[19] T. Motylewski, H. Linnartz, Rev. Sci. Instrum. 70 (1999) 1305

[20] T. Motylewski, H. Linnartz, O. Vaizert, J.P. Maier, G. A. Galazutdinov, F. A. Musaev, J. Krelowski, G. A. H Walker, D. A. Bohlender, ApJ, 531 (2000) 312

[21] A. O'Keefe, J. J. Scherer, A. L. Cooksy, R. Sheeks, J. Heath, R. J. Saykally, Chem. Phys. Lett. 172 (1990) 214

[22] D. J. Benard, K. B. Winker, J. Appl. Phys. 69 (1991) 2805

[23] T. Yu, M. C. Lin, J. Am. Chem. Soc. 115 (1993) 4371

[24] T. Yu, M. C. Lin, J. Phys. Chem., 98 (1994) 2105

[25] T. Yu, M. C. Lin, J. Phys. Chem. 98 (1994) 9697

[26] E. W. Diau, T. Yu, M. A. G. Wagner, M. C. Lin, J. Phys. Chem. 98 (1994) 4034

[27] L. Zhu, G. Johnston, J. Chem Phys. 99 (1995) 15114

[28] D. Romanini, K. K. Lehmann, J. Chem. Phys. 99 (1993) 6287

[29] D. Romanini, K. K. Lehmann, J. Chem. Phys. 102 (1995) 633

[30] G. Meijer, M. G. H. Boogaarts, R. T. Jongma, D. H. Parker, A. M. Wodtke, Chem. Phys. Lett. 217 (1994) 112

[31] R. T. Jongma, M. G. H. Boogaarts, I. Holleman, G. Meijer, Rev. Sci. Instrum. 66 (1995) 2821

[32] R. T. Jongma, M. G. H. Boogaarts, G. Meijer, J. Mol. Spectrosc. 165 (1994) 303

[33] M. G. H. Boogaarts, G. Meijer, J. Chem. Phys. 103 (1995) 5269

[34] P. Zalicki, Y. Ma, R. N. Zare, E. H. Wahl, T. G. Owano, J. S. Harris, C. H. Kruger, Chem. Phys. Lett. 234 (1995) 269

[35] V. Sick, R. L. Farrow, Opt. Lett. 11 (1995) 111

[36] J. J. Scherer, D. Voelkel, D. J. Rakestraw, J. B. Paul, C. P.Collier, R. J. Saykally, A. O'Keefe, Chem. Phys. Lett. 245 (1995) 273

[37] J. J. Scherer, D. Voelkel, D. J. Rakestraw, Appl. Phys. B: Lasers Opt. 64 (1997) 699

[38] J. J. Scherer, D. J. Rakestraw, Chem. Phys. Lett. 265 (1997) 169

[39] R. Engeln, G. Meijer, Paper presented at the 51st Ohio State University Symposium on Molecular Spectroscopy, 1996.

[40] B. Giles, C. A. Arrington, F. C. Hagemeister, T. S. Zwier, Paper presented at the 51st Ohio State University Symposium on Molecular Spectroscopy, 1996.

[41] J. Pearson, A. J. Orr-Ewing, M. N. R. Ashfold, R. N. J. Dixon, Chem. Soc., Faraday Trans. 92 (1996) 1283

[42] J. J. Scherer, J. B. Paul, A. O'Keefe, R. J. Saykally, Chem. Rev. 97 (1997) 25

[43] G. Berden, R. Engeln, P. C. M. Christianen, J. C. Maan, G. Meijer, Phys. Rev. A 58 (1998) 3114

[44] D. Romanini, L. Biennier, F. Salama, A. A. Kachanov, L. J. Alalmandola, F. Stoeckel, Chem. Phys. Lett. 303 (1999) 165

[45] L. Biennier, F. Salama, L. J. Alalmandola, J. Chem. Phys. 118 (2003) 7863

[46] S. S. Brown, H. Stark, S. J. Ciciora, R. J. McLaughlin, A. R. Ravishankara, Rev.

Sci. Instrum. 73 (2002) 3291

[47] S. Drucker, J. L. Van Zanten, N. D. Gagnon, E. J. Gilles, N. R. Pillsbury, J. Mol. Struct. in press

[48] D. Romanini, A. A. Kachanov, N. Sadeghi, F. Stoeckel, Chem. Phys. Lett. 264 (1997) 316

[49] D. Romanini, A. A. Kachanov, F. Stoeckel, Chem. Phys. Lett. 270 (1997) 546

[50] Y. He, M. Hippler, M. Quack, Chem. Phys. Lett. 289 (1998) 527

[51] P. Birza, T. Motylewski, D. Khoroshev, A. Chirocolava, H. Linnartz, J.P. Maier, Chem. Phys., 283 (2002) 119.

[52] D. Pfluger, T. Motylewski, H. Linnartz, W.E. Sinclair, J.P. Maier, Chem. Phys. Lett. 329 (2000) 29

CHAPTER 4

4. Experiment

The experimental set-up consists of a standard cavity ring down unit sampling the plasma generated in a pulsed supersonic slit jet expansion. The latter is located in a large stainless-steel cross-piece, evacuated by a roots blower system. The tunable radiation is generated by an excimer pumped dye laser system. The light exiting the ring down cavity is detected by a photodiode. This signal is displayed on a 300 MHz 8-bit digital oscilloscope. A spectrum is recorded by measuring τ as function of the wavelength of the laser (running at 30 Hz). Typically 45 ring down events are averaged at each wavelength before the digitized data are downloaded to a workstation, that is also used to control the scanning procedure. The main layout of the experimental set-up is shown in Figure 4.1 and the detailed description of main parts of it is given below.

4.1. Lasers

As a source of the tunable light the SCANmate 2E laser (Lambda Physik) was used. It offered a tuning range from about 340 nm to 900 nm using a variety of dyes. As a solvent methanol (Fluka, "rein") and DMSO (Merck, "for synthesis", dried with molecular sieves) were used. The dye laser was pumped by a pulsed 308 nm XeCl excimer laser (COMPEX 110 Lambda Physik) with the energy of the pulse around 120 mJ. The resulting power depended strongly on the used dye, range, alignment and presence of an etalon in the oscillator cavity. Typical value of output energy was ~0.5 - 3.0 mJ. The linewidth (FWHM) of the dye laser was about 0.1 - 0.15 cm^{-1} without intracavity etalon and ~ 0.04 cm^{-1} with the etalon inserted into the cavity.
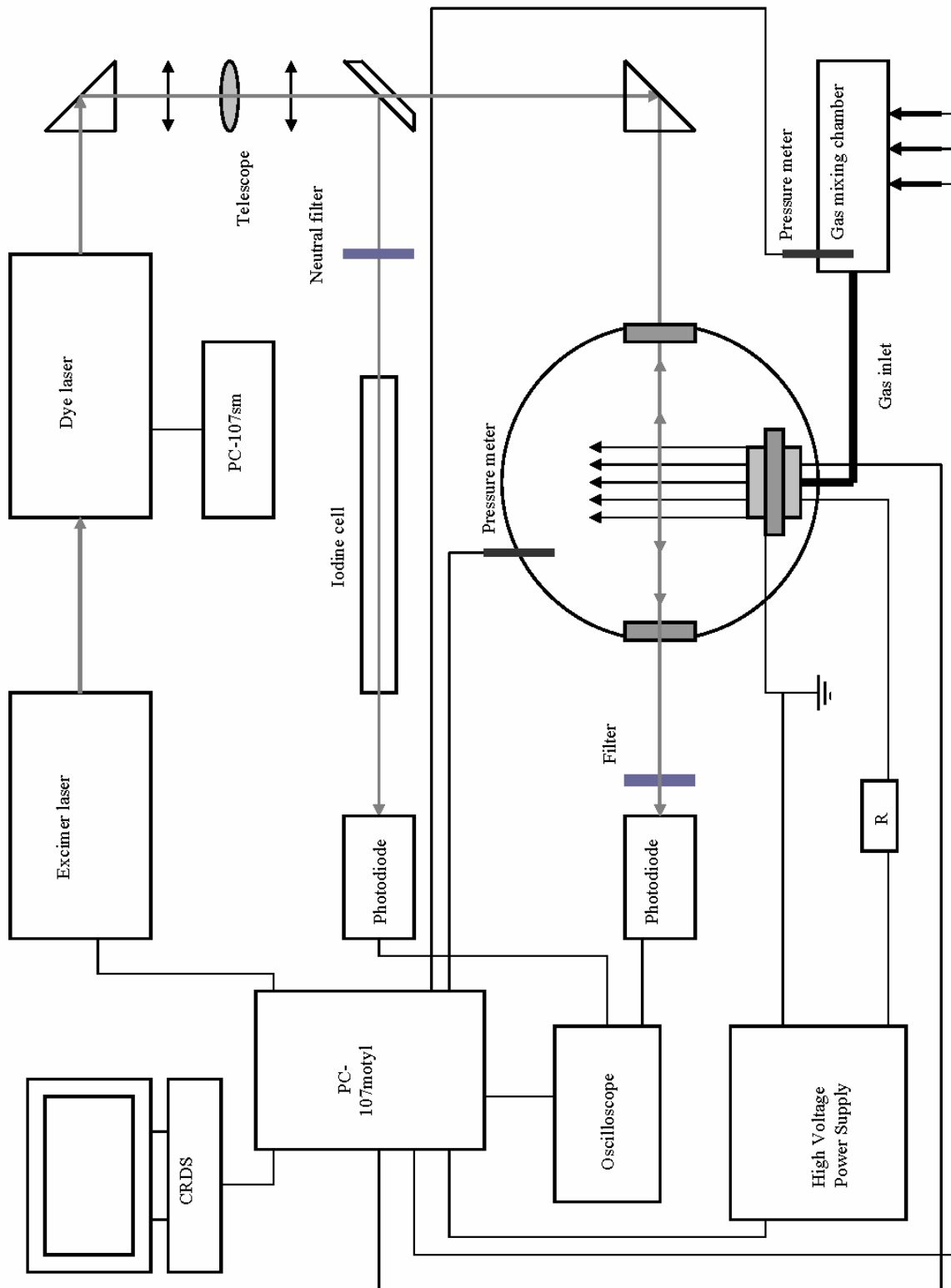
Figure 4.1. Experimental setup.

The laser was tuned by turning the diffraction grating (and optionally also the etalon). The SCANmate was communicating with the computer via a multimode optics fiber interface using Lambda Physic protocol. The commands were sent by the "scanmate" program delivered by Lamda Physik running under DOS 6.22. To attain greater flexibility and immunity instead of serial connection (RS 232) TCP/IP Ethernet connection was used. The "scanmate" program was run in a DOS emulator environment running under Linux. It received commands via a virtual serial port connected to an intermediate Linux process rgpib_svc (remote GPIB server) which in turn communicated with the scan control program lcmeter using TCP/IP/RPC pcontrol. Etalon scans require manual finding of the etalon so called "normal positions" and synchronizing the etalon with the grating set to the desired wavelength. During this alignment the spectral purity of the generated laser light was optimized by a monitor etalon. (One looked through the monitor etalon at the laser light dispersed through a lens and cast on a sheet of white paper.) Both etalon single mode operation and the intensity of ASE (amplified spontaneous emission) could be checked easily this way.

The output beam from the dye laser was directed into the chamber by a special optical system consisting of two prisms and a telescope (Two CC lenses with f=150mm). The telescope was equipped with the 100 µm pinhole. Such a system allowed the laser beam to be spatially filtered only for TEM_{00} mode and focused exactly inside the cavity where absorption process took place.

4.1.1. Calibration

Mainly two independent methods were used to calibrate the wavelength. A reference most frequently used was the absorption spectrum of I_2 vapor. The spectrum of I_2 was measured simultaneously with the CRD spectrum. Approoximately 10 % of the laser light was reflected through a beamsplitter towards a 1 m long cell filled with saturated I_2 vapor at room temperature. Before the beam entered the cell it passed through a neutral filter, passing ~0.5-5% of the light to avoid power saturation of absorption lines. The light was detected by a Hamamatsu ST336-44BQ photodiode which

was connected to the second channel of a digital LeCroy 9310 oscilloscope (1MΩ input impedance) in parallel with a 100 nF capacitor and the 330 Ω resistor. The capacitor was necessary to elongate the detected pulse to the time scale of 10-20 μs comparable with the ring-down signal recorded on the first input of the oscilloscope and to avoid signal saturation.

Iodine absorption spectrum could be observed in the range of 490 - 650 nm. The recorded I_2 spectra were loaded into the xmgr program and shifted together until measured iodine spectrum overlaped with the "reference I_2 spectrum". The reference spectrum was generated by iod.perl program from a list of the lines positions and intensities [2]. The accuracy of the iodine calibration was around 0.1 cm^{-1} for low resolution spectra and 0.01-0.02. cm^{-1} for the high resolution (with the intracavity etalon).

Outside of the range of 490 - 650 nm I_2 lines were to weak to be detected. Hence, other calibration methods had to be used. In most cases absorption lines of excited rare gas atoms (He, Ne) could be found in the vicinity (a few nm distance) of the region to be calibrated. Usually lines on both sides of the calibrated region were used and the spectrum was corrected by the average shift of the atomic absorption lines measured in the supersonic expansion excited by the discharge. The resulting accuracy of this calibration was ~0.3 cm^{-1}.

4.2. CRD Cavity

The high finesse optical cavity is the most characteristic of the CRDS experiment. It consisted of two plano-concave dielectrically coated mirrors facing each other. The mirror housings of the cavity mirrors were connected with flexible bellows to the opposite sides of the cross piece, defining a closed cavity of 52 cm in length. In order to protect the mirrors against the dust, a stream of helium was injected into the mirror holder forming very effective "helium curtains". The stream gas was flushing out the mirror and as a result a deposition of contaminants on the surface was significantly prevented. The flow was regulated manually to obtain a pressure in the vacuum chamber at the level of ~0.02 mbar. The alignment of the mirrors was achieved by adjusting high precision

threaded screws. Two tilted quartz windows were fixed outside the cavity to seal the chamber.

4.2.1. Mirrors

The most important part of the cavity, high reflectivity dielectric mirrors, were manufactured by Research Electro Optics Inc, Boulder, Colorado USA. The radius of the curvature of the mirrors used in the experiments was 1 m and diameter 7.75 mm (diameter of coated surface minimum 5 mm). The thickness of the quartz mirror substrate was 4 mm. The width of the multiple dielectric layers is matched to cause positive interference of light reflected from them for a given wavelength range (up to 10% from the specified wavelength). The reflectivity coefficient of the mirrors used in the experiments was around 99.98 - 99.998 %. It depended on the wavelength and the type of the mirror. Such high reflectivity could not be achieved using metal mirrors. Still another advantage of dielectric mirrors is very low absorption. The light which was not reflected, passed through the mirror.

4.3. Detection system

As a light detector a broad band UV-VIS-NIR silicon photodiode (ST336-44BQ Hamamatsu) was used. The sensitivity of the diode was in the range 190-1100 nm and the active area was 3.6x3.6 mm. In order to increase the signal a fast, low noise amplifier LM6365N was applied. In order to cut off the light coming from the plasma and decrease the amplified spontaneous emission level, the filter (transmission $\lambda_0 \pm 20$ nm) was placed in front of the photodiode. The signal was recorded on a 300 MHz digital oscilloscope (LeCroy 9310) where the digitalization of the data took place. 45 laser shots were averaged by the oscilloscope and transmitted via GPIB to a PC computer.

4.4. Data acquisition system

The system of three PC computers was used to run the whole experiment. The CRDS machine was used for main control of the experiment and the data storage. Work of the laser was controlled by PC-107sm. For the triggering and pressure control PC-107motyl was responsible. The software used for the triggering, data acquisition, laser scanning control and steering the experiment was written by Motylewski and is described in details in his Ph. D. thesis [2].

4.5. The vacuum chamber

The vacuum chamber consisted of a large stainless-steel cross-piece (30 cm in diameter and about 20 dm^3 capacity) evacuated by a roots blower system with a total pumping capacity of 2775 m^3/h. The pressure attained in the chamber without the plasma was at the level of ~5.0 * 10^{-3} mbar. The working pressure in the chamber varied from ~0.08 to ~0.25 mbar. The stability of the plasma could be monitored visually through a pyrex window (25 cm in diameter) installed on the one of the sides of the cross piece.

4.6. Discharge source

The carbon chain radicals were produced in a pulsed slit nozzle incorporating a discharge in a high pressure expansion. The orifice was made of two sharp stainless steel jaws forming the actual slit (30 mm × 300 mm), a ceramic insulator, a grounded metal plate and another ceramic insulator. Both insulators and metal parts were mounted to the body of the nozzle with electrically isolated screws. A pulsed negative voltage (ranging from -350 to -1000V) was applied to both jaws via two separate 3.8 kΩ ballast resistors (max. current ~ 300 mA.) The duration of a discharge and gas pulses were 100 - 300 µs and 1.1 ms, respectively. The inner metal plate was grounded while the body floated. The latter was important in order to shield the pulsed valve from internal high voltage arcing. It furthermore prohibited carbon dust formation inside the body. A multichannel system

inside the nozzle regulated the gas flow towards the slit which significantly reduced the Doppler broadening. The distance of the slit nozzle to the optical axis was regulated manually during jet operation and varied from 2 to 10 mm via a translation stage.

4.6.1. Heating system for B_3 production.

The B_3 molecules were produced in the source which was modified because the gaseous gas precursor could not be used in this case. As the solid sample (decaborane, Strem, 98% purity) was used, the heating oven had to be implemented. It consisted of a cylindrical metal reservoir (8 mm in diameter and 20 mm in length) which was placed into the main steel body of the oven (19 mm in diameter and 74 mm in length). The perforation (2 μm pore size) on the bottom of the reservoir allowed an undisturbed flow of the carrier gas. The main body of the oven was heated with a heating system. It consisted of a metal sleeve coiled inside with a coaxial resistant wire. The temperature was set via an external power supply and controlled with a thermocouple. Analogous heating system was used to heat the pulsed valve. The latter had to be heated to avoid the condensation of the boron species in the valve and on the internal edges of the slit nozzle. The transmission of the heat through the metal elements was high enough to maintain the whole production system (the oven, the valve and the body of the nozzle) at the appropriate temperature (~80 °C). The temperature of the valve was also controlled with another thermocouple. The detailed scheme of the source of B_3 is shown in Figure 4.2.

4.6.2. Gas mixing system

The gas mixtures passing through the discharge were prepared in a convenient on-line mixing system. It consisted of a 3.2 dm^3 steel chamber with an electronic pressure meter and three input magnetic valves. Gas bottles were used to supply the input lines with appropriate gases.
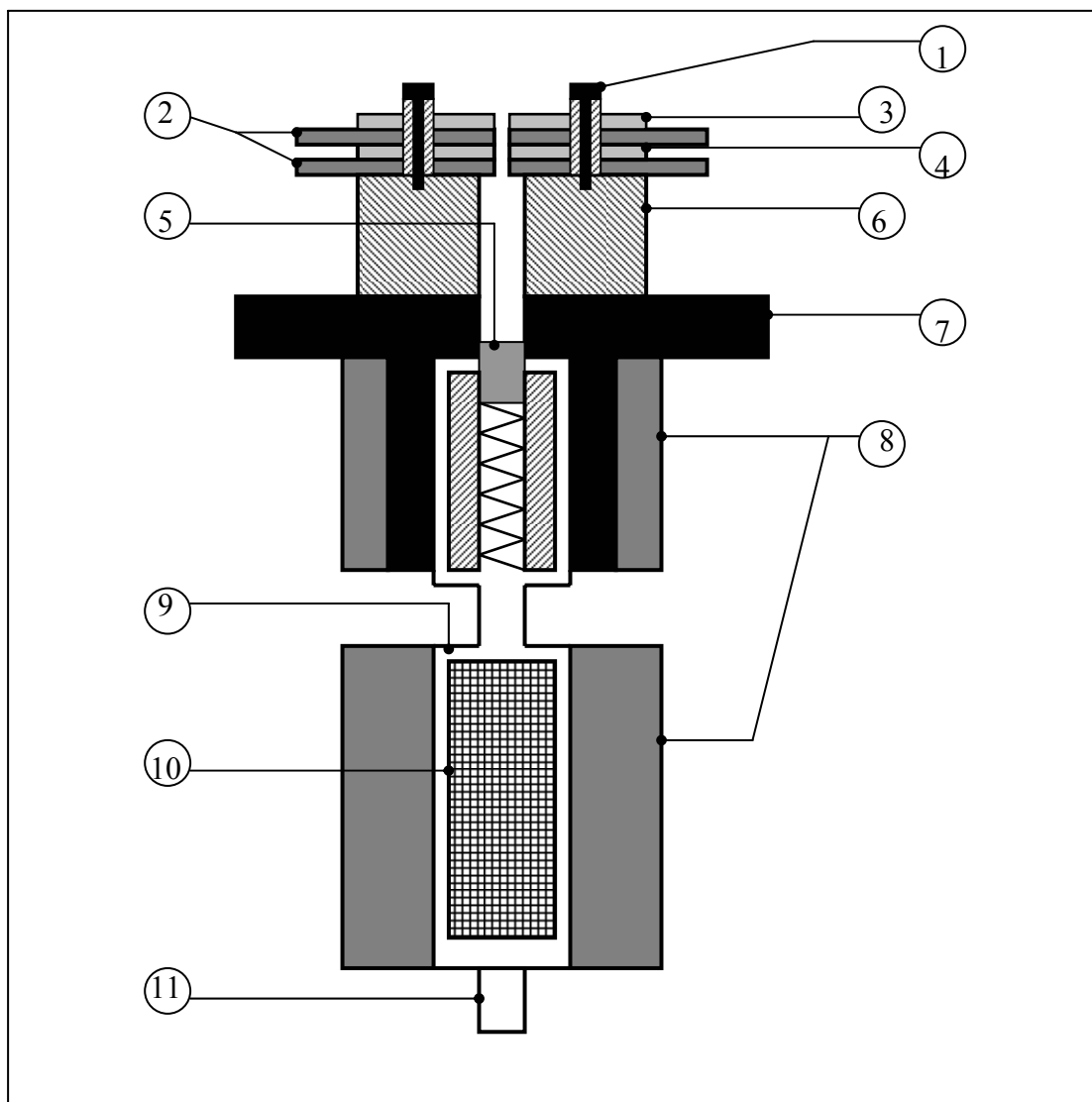
Figure 4.2. Cross section of the high pressure slit nozzle discharge used for the production of the B$_3$ molecules. The orifice consist of two ceramic insulators (2), a metal plate that is grounded (4), two sharp stainless steel jaws (3) that form the actual slit 30mm × 300μm. Both insulators and metal parts are mounted to the body of the nozzle (6) by electrically isolated screws (1). The floating body of the nozzle is connected to an electromagnetic pulsed valve (7). A small plastic poppet (5) controls the gas flow into the nozzle volume. The valve is connected to the oven (9) where the sample basket filled with decaborane is inserted (10). Both the oven and the valve are heated by two independent electric heating systems (8). The system is supplied with the carrier gas (Ne) entering the source through the inlet (11).

Usually they were the 1% mixtures of C_2H_2 or C_2D_2 and pure helium, argon or neon as a carrier gas. The mixing ratio of the gases was equal to the relative frequency of the pulses opening each input valve. The gas pulse duration was supposed to be set manually in such a way that the equal amount of gas entered the chamber in a single pulse of each valve [2]. Typical backing pressure used during the experiments was ~10 bar.

4.6.3. High voltage power supply

The Velonex 345-F high voltage power supply was used to ignite the discharge. The potential applied to the electrodes was controlled by setting an HV pulse amplitude knob. Usually it ranged from −350 to −1000 V. Resistors of 3.8 kΩ were used to limit the maximum current (~300 mA). Duration of a single pulse was 100 - 300 μs.

References

[1] T. Motylewski, H. Linnartz, Rev. Sci. Instrum. 70 (1999) 1305

[2] T. Motylewski, Ph. D. Thesis, University of Basel (2001)

CHAPTER 5

5. Studies of $HC_{2n}H^+$ species

Polyynes and their derivatives have been under examination because they are present in the interstellar medium. It was also proposed that some of polyynes may be responsible for the origin of the diffuse interstellar bands [2-5]. They are also considered as an important intermediate species in plasmas, combustion [1], and interstellar gas-phase ion-molecule reaction schemes. It is important to study electronic transitions of these species in order to understand their role in such environments.

They are open-shell $HC_{2n}H^+$ species with $^2\Pi$ ground state arising from π^3 configuration. $^2\Pi - X\,^2\Pi$ electronic transitions due to the π-π promotion in these species have strong absorptions in the region observed DIBs, i.e., 400-900 nm. The strong electronic transitions have $^2\Pi_u - X\,^2\Pi_g$ symmetry and shift to the red with increasing number of carbon atoms. Members of the series $HC_{2n}H^+$ (n = 2, 3, 4) have been a subject of previous spectroscopic studies in the gas phase. In 1952 Schueler and Reinbeck obtained the first electronic spectrum of a polyacetylene cation [6]. It was assigned by Callomon to the A $^2\Pi_u - X\,^2\Pi_g$ electronic origin band transition of diacetylene cation [7]. This provided the first example of the emission spectrum of an organic cation comprised of more than three atoms. It was also rotationally resolved and analyzed, however, absolute numbering remained ambiguous which led to uncertainty in the derived constants. The situation changed in 1986 when Kuhn et al. discussed and established the absolute rotational numbering of HC_4H^+ and DC_4D^+ [8]. It was done by recording the A $^2\Pi_u - X\,^2\Pi_g$ emission spectrum of the diacetylene and dideuteroacetylene cations at low rotational temperature (~10 K) by means of a supersonic jet expansion. A mixture of diacetylene (or dideuteroacetylene) and helium was expanded through a nozzle into vacuum. The supersonic jet was struck by an electron beam and the resulting fluorescence was detected. This led to an observation of the lowest Q-branch transitions. Their position enabled to choose unambiguously from the two possible sets of rotational

constants. The latter were also obtained anew by analysis of the rotational resolved structure of the origin band in the A $^2\Pi_u$ – X $^2\Pi_g$ laser excitation spectra of HC$_4$H$^+$ and DC$_4$D$^+$. Rotational analysis was carried out by the direct approach whereby the lines positions were fitted to the eigenvalues of an appropriate Hamiltonian matrix [9].

Lecoultre at al. reported the complete r$_s$ structure of the diacetylene cation in the X $^2\Pi_g$ and A $^2\Pi_u$ electronic states [10]. The bond-lengths in the X $^2\Pi_g$ and A $^2\Pi_u$ electronic states were inferred using the method of Kraitchman. The method allows the determination of the position of an atom in a molecule from spectroscopic measurements on its isotopic species [11]. In order to do it, the rotational constants of the isotopic derivatives where the carbon atoms have been substituted by ^{13}C have to be known. It was attained by recording the rotationally resolved origin bands in the A $^2\Pi_u$ – X $^2\Pi_g$ laser excitation spectra of H-^{13}C-C-C-C-H$^+$ and H-C-^{13}C-^{13}C-C-H$^+$ and their subsequent analysis. From the determined rotational constants as well as from those known for HCCCCH$^+$, DCCCCD$^+$, all the bond-lengths in the two electronic states have been inferred. Calculated bond-lengths changes stay in agreement with the study of the Frank Condon factors in the photoelectron spectrum of diacetylene [12] and molecular orbital considerations of the electronic structure [13].

Vaizert et al. also studied HCCCCD$^+$ by means of spectroscopy [14]. The HCCCCD$^+$ cations were produced in a high pressure planar plasma expansion by discharging a gas pulse of HCCH/DCCD mixture in argon in the throat of the slit nozzle [15]. The spectrum was measured using cavity ring down spectroscopy. The analysis of the spectra allowed an accurate determination of the rotational parameters. The change in the overall length of the diacetylene cation upon electronic excitation was calculated using the metod of Kraitchman. Resulting H-H distance in the ground and excited states were in good agreement with the previous isotopic studies [10].

The A $^2\Pi_g$ – X $^2\Pi_u$ band system of triacetylene cation was first detected by their emission spectra of molecular beams excited by controlled electron impact in 1976 by Allan et al. [16]. The identification of the transition was compared with the photoelectron spectrum of triacetylene [13] and the emission spectrum of diacetylene cation [7]. The lifetimes of the lowest vibrational level of the A $^2\Pi_g$ excited state have been also measured. In 1984 more information on the HC$_6$H$^+$ was obtained when the emission and

laser excitation spectra of A $^2\Pi_g$ – X $^2\Pi_u$ transition of the rotationally and vibrationally cooled HC_6H^+ in the gas phase was recorded in analyzed by Klapstein et al. [17]. The emission was excited by electron impact of a seeded supersonic free jet and the fluorescence by laser excitation of the cations formed by Penning ionization in a liquid nitrogen cooled environment. The resolution of the spectra was better than the former one [16] and this made the vibronic analyses possible. The vibrational frequencies of the totally symmetric fundamentals could be inferred for the triacetylene cation in the X $^2\Pi_u$ and A $^2\Pi_g$ states.

The spectrum of the A $^2\Pi_g$ – X $^2\Pi_u$ origin band system of HC_6H^+ and its isotopic derivatives: HC_6D^+ and DC_6D^+ have been also studied at Doppler-limited resolution using frequency modulation absorption spectroscopy by Sinclair et al. [18]. The ions were generated in a liquid nitrogen cooled hollow cathode discharge incorporated in a White cell. A discharge modulation in combination with the frequency modulation technique enhanced the sensitivity of the detection and improved significantly signal-to-noise ratio. Analysis of the rotational structure provided information on the geometry of triacetylene cation together with accurate spin-orbit interaction constants in the two electronic states. Further improvement in the quality of the spectra was possible when frequency modulation absorption technique was combined with a supersonic jet [19].

The tetraacetylene cation was first studied in 1976 in the gas phase through the He 58.4 nm excited photoelectron spectrum of the neutral parent. This study identified the four low $^2\Pi$ states [20]. Electron impact excitation of the neutral tetraacetylene in an effusive source resulted in an observation of the origin band of the A $^2\Pi_u$ – X $^2\Pi_g$ emission [16]. The rotationally resolved A $^2\Pi_u$ – X $^2\Pi_g$ electronic origin band spectrum of HC_8H^+ and its deuterated derivative DC_8D^+ has been recorded in the gas phase by applying both using frequency modulation absorption spectroscopy in a liquid nitrogen cooled hollow cathode discharge and cavity ring down spectroscopy in a supersonic planar plasma [21]. The frequency modulation spectrum was obtained at a high resolution, however determination of an unambiguous numbering in the rotational structure was not possible. The problem was solved when the cavity ringdown spectrum was obtained. It was measured with low resolution but changes in the rotational profile

on cooling the ions to very low rotational temperatures (~15 K) allowed the appearance of the prominent Q-branch to be identified and the absolute numbering to be established.

5.1. Matrix studies

In 1994 Freivogel et al measured in the visible and near infrared region absorption spectra for a series of mass selected $HC_{2n}H^+$ systems (n = 2, 3, 4, 5, 6, 7, 8) isolated in neon matrices at 5 K [22]. The species were produced in a hot-cathode discharge of 30% diacetylene in helium. Subsequently they were deflected, mass-selected in a quadrupole mass filter and trapped in neon matrices where they were characterized through their electronic absorption spectra. Positions of A $^2\Pi$ – X $^2\Pi$ origin bands as well as fundamental vibrational frequencies in the excited state have been obtained. Assignment of band carriers (n = 2, 3, 4) displayed in Figure 5.1 has been determined from experimental and theoretical considerations. Further evidence for their identity was provided by comparison with the gas-phase data. Laser induced fluorescence and emission spectra of diacetylene, triacetylene and tetraacetylene cations were known [16] and agreed quite well with matrix isolation data of the respective mass selected systems. In each case, the gas to neon matrix shift of the band origin was less than one percent of the transition frequency. The correlation between the carbon chain length and the positions of the band origin maxima was also found. It was clearly visible that the origin bands for this set of spectra are shifted by ~100 nm to longer wavelength with each addition of a CC unit. Smith et. al also carried out the matrix study of polyacetylene cations [23]. The species were produced in an electric discharge of acetylene diluted in the matrix gas. Well resolved laser excitation and fluorescence spectra of tri- and tetraacetylen cations were analyzed and compared with available gas phase data, as well as with mass selected matrix results mentioned before [22].
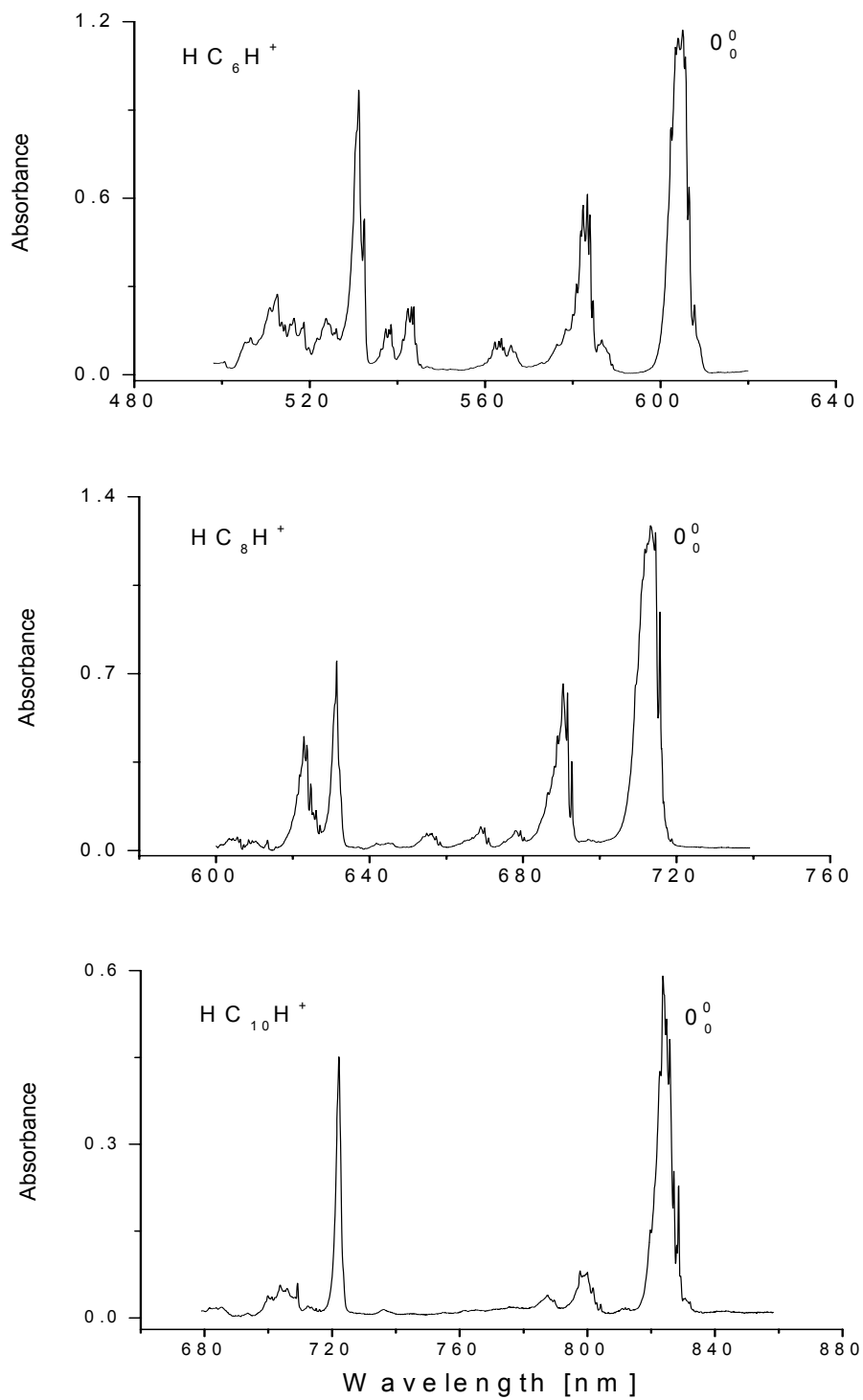
Figure 5.1. The spectra of the A $^2\Pi$ - X $^2\Pi$ transitions of tri-, tetra-, and pentaacetylene cations recorded in the 5 K neon matrices [Ref. 22].

The observed differences in spectra (broader line-widths in the mass selected studies) could be explained with a help of inhomogeneous effects and matrix damage caused by the bombardment with the high energy ionic species.

Sobolewski and Adamowicz calculated the absorption spectra corresponding to the transitions to the lowest electronically excited states of the $HC_{2n}H^+$ species (n=2, 3, 4) using the second order perturbation theory [24]. They used the theoretical scheme which was based on the complete-active-space self-consistent-field (CASSCF) method, with remaining dynamic electron correlation effects added in the subsequent step with the use of the second-order perturbation theory with the CASSCF wave function as the reference state (CASPT2) [25]. These *ab initio* calculations confirmed previous results that the ground states of the polyacetylene cations have the $^2\Pi$ symmetry and the oscillator strength for the dipole allowed transitions from $^2\Pi$ state is relatively high (f > 10 $^{-2}$ for the strongest bands). Energy of the lowest dipole allowed transitions they calculated coincided quite well with the experimental observations. When it comes to the next member in the series, $HC_{10}H^+$, the density functional theory calculations (DFT) were performed in 1998 by Betowski et al. [26] and predicted the linear structure for this molecule.

5.2. Gas-phase study of the pentaacetylene cation

As it was mentioned before, carbon chains are quite feasible candidates for carrier of diffuse interstellar bands. This hypothesis is especially rational for longer molecules [27]. Therefore it seemed reasonable to check if absorption bands of the $HC_{2n}H^+$ species (with high *n*) match some DIBs. Former studies, described earlier in this chapter, showed that in the case of HC_4H^+, HC_6H^+ and HC_8H^+ such a match was not observed. The next molecule in the series, e. i., $HC_{10}H^+$ was a more promising chain as a longer one. On the other hand, it was clear that the resolution of the laser used in the experiment will not yield the rotationally resolved spectrum. (The rotational constant B was much smaller than the resolution of the laser.) Despite this fact it was clear that one should observe two separate bands of the two spin-orbit components. Another difficulty was linked up with

the region in which $HC_{10}H^+$ absorbs. The origin band of pentaacetylene cation lies in the IR region and it caused some technical problems with the alignment of the laser system. Also the performance of the dye left much to be desired. In spite of these problems, based on the work of Freivogel et al. [22], the search for the gas-phase observations of pentaacetylene cation could be started. The matrix spectrum of $HC_{10}H^+$ comprise a strong origin band around 12143 cm^{-1} and a series of weaker bands corresponding to vibrational excitation in the upper electronic state. The gas-phase experiment was focused on the investigation of the origin band. These investigations turned out to be successful and the origin band of $HC_{10}H^+$ in the gas phase was finally recorded. The results of this study are presented below.

Electronic Gas-Phase Spectrum of the Pentaacetylene Cation[†]

P. Cias, O. Vaizert, A. Denisov, J. Mes,[§] H. Linnartz,[#] and J. P. Maier*

Department of Chemistry, Klingelbergstrasse 80, CH 4056 Basel, Switzerland

Received: February 27, 2002; In Final Form: June 25, 2002

The origin band of the $A^2\Pi_u-X^2\Pi_g$ electronic transition of the linear pentaacetelyne cation, $HC_{10}H^+$, and isotopic derivatives, $HC_{10}D^+$ and $DC_{10}D^+$, has been recorded in the gas phase. The absorption spectrum was observed by cavity ring down spectroscopy through a supersonic planar plasma expansion. The spectrum comprises both spin–orbit components with resolved P- and R-branches. Contour fits allow the determination of ground and excited state spectroscopic constants.

Introduction

The polyacetylene cations, HC_nH^+, are open-shell species with a $^2\Pi$ ground state. The strong electronic transitions have $^2\Pi_u-X^2\Pi_g$ symmetry and shift to the red with increasing number of carbon atoms. Rotationally resolved electronic spectra have been recorded previously in the gas phase for the even members with $n = 2$ at 255.7 nm,[1] $n = 4$ at 507.0 nm,[2,3] $n = 6$ at 600.4 nm,[4,5] and $n = 8$ at 707.1 nm.[6] Little is known on the next member in the series, the pentaacetylene cation $HC_{10}H^+$. Density functional theory calculations[7] and ion chromatography[8] predict a linear structure. It was shown that $HC_{10}H^+$ is formed in an ion trap upon collision activated processes on polycyclic aromatic hydrocarbons.[9] Furthermore, this cation may be of interest from an astrophysical point of view. It has been argued that electronic transitions of carbon chains may be among the carriers of unidentified absorption features in diffuse interstellar clouds.[10] Particularly longer chains are of interest as these are expected to be photo stable.

The first experimental observation of the $A^2\Pi_u-X^2\Pi_g$ electronic spectrum of $HC_{10}H^+$ was in a neon matrix using mass selective deposition;[11] the transition was found to comprise a strong origin band around 823.3 nm and a series of weaker bands corresponding to vibrational excitation in the upper electronic state. In the case of the smaller polyacetylene cations, the transitions in the gas phase are typically blue-shifted 100–130 cm^{-1} with respect to the matrix value, that is, the unperturbed origin band of $HC_{10}H^+$ is expected between 814.5 and 816.5 nm.

Experiment

The wavelength range around 815.5 nm was scanned using cavity ring down (CRD) spectroscopy. CRD has become a powerful tool for the study of the structural and dynamical properties of molecules in the gas phase.[12] One of the reasons for this success is the conceptual simplicity of a CRD experiment. A small fraction of laser light is coupled into an optical

cavity of length L consisting of two mirrors with a reflectivity close to unity. The light leaking out of the cavity has an envelope, which is simply a first-order exponential decay, $\exp(-t/\tau)$. The ring down time, τ, reflects the rate of absorption rather than its magnitude, and as such the method is independent of power fluctuations. In addition, very long absorption path lengths are obtained by confining light tens of microseconds to the cavity. A spectrum is recorded by measuring τ as function of the laser frequency.

In the present experiment, a standard pulsed CRD spectrometer with a resolution of 0.15 cm^{-1} is used to sample a pulsed supersonic plasma, generated by discharging a mixture of 0.3% HCCH (or DCCD or both) in He (−600 V, 100 mA) in the throat of a 300 mm × 300 μm multichannel slit nozzle geometry.[13] This system combines high molecular densities and relatively large absorption path lengths with an effective adiabatic cooling. The best S/N ratios are found when the CRD beam intersects the expansion 3 mm downstream from the nozzle orifice. The light exiting the optical cavity is focused via a narrow band-pass filter onto a broad band Si photodiode and is monitored by a fast oscilloscope. Typical ring down times amount to $\tau = 50$ μs. For a cavity of length $L = 52$ cm, this is equivalent to approximately 29 000 passes through the plasma or an effective absorption path length of 865 m. The present data set is calibrated via the internal reference system of the dye laser, yielding an absolute accuracy on the order of 0.5 cm^{-1} around 815 nm.

Results and Discussion

For an $A^2\Pi_u-X^2\Pi_g$ electronic transition of a linear molecule, one expects to observe two separate bands (each consisting of a P-, Q-, and R-branch) of the two spin–orbit transitions $A^2\Pi_{3/2}-X^2\Pi_{3/2}$ and $A^2\Pi_{1/2}-X^2\Pi_{1/2}$. The intensity ratio of the two bands is determined by the spin–orbit temperature (T_{so}) and the spin–orbit splitting in the ground state (A''). The latter is expected to be close to the value found for the tri- and tetraacetylene cations, −31 cm^{-1}. The minus sign indicates that the ground state is inverted—as was observed for the smaller polyacetylene chains[5,6]—i.e., the $\Omega = {}^3/_2$ component is below $\Omega = {}^1/_2$. The separation between the two bands in the spectrum is given by the difference in spin–orbit constants in excited and ground state ($\Delta A = A' - A''$) and is expected to be on the order of 3 cm^{-1}.

The origin band in the $A^2\Pi_u-X^2\Pi_g$ electronic transition of $HC_{10}H^+$ is shown in the left part of Figure 1. The band contour

Spectrum of the Pentaacetylene Cation

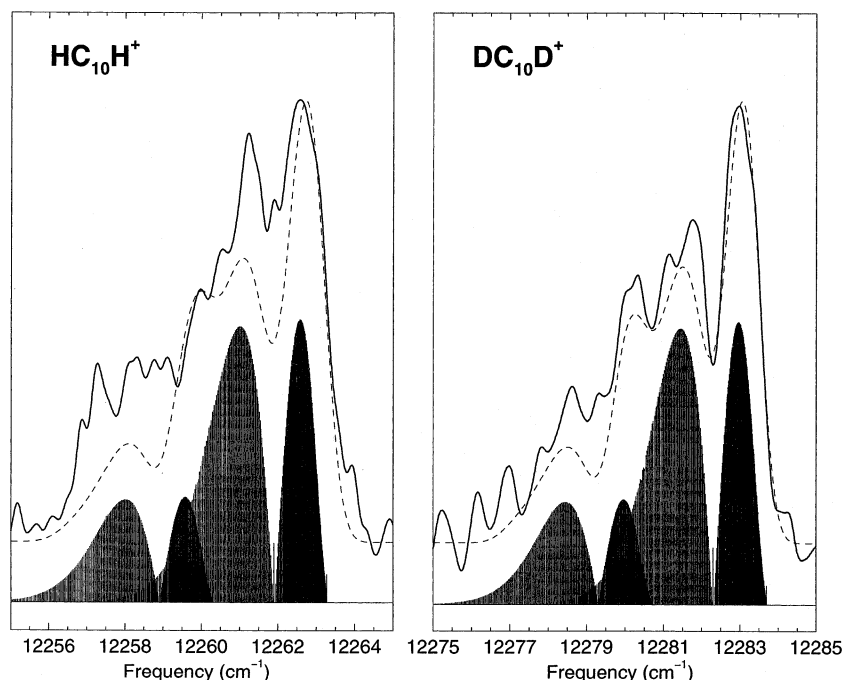*J. Phys. Chem. A, Vol. 106, No. 42, 2002* **9891**

Figure 1. A smoothed laboratory spectrum of the $A^2\Pi_u-X^2\Pi_g$ electronic origin band transition of $HC_{10}H^+$ (left side) and $DC_{10}D^+$ (right side) recorded in absorption using cavity ring down spectroscopy with 0.15 cm^{-1} resolution. Both spin−orbit components are visible, as can be concluded from the stick diagram. The latter shows the simulation for a rotational temperature of $T_{rot} = 45$ K and molecular parameters as listed in Table 1. The dashed line shows the simulation for the unresolved spectrum.

of both spin−orbit components is visible, even though there is some overlap with the absorption lines of another species, presumably C_2. The band is not rotationally resolved because the rotational constant of $HC_{10}H^+$ is on the order of 0.01 cm^{-1} and the best laser resolution obtained with an internal etalon was 0.035 cm^{-1}. In addition, lifetime broadening might occur as result of intramolecular processes. It is possible, however, to interpret the band contours in terms of unresolved P-, Q- and R-branch contours of the $A^2\Pi_{3/2}-X^2\Pi_{3/2}$ and $A^2\Pi_{1/2}-X^2\Pi_{1/2}$ electronic transitions. This is demonstrated in the figure with stick diagrams.

The observed rotational profiles were simulated to determine the band origin position and to estimate the spectroscopic constants, using PGopher.[14] The ground state spin−orbit splitting is assumed to be similar to that found for the tri- and tetraacetylene cations, −31 cm^{-1}. The intensity ratio of the two spin−orbit bands yields $T_{so} = 45(5)$ K, which will be close to the rotational temperature, T_{rot}. This value is higher than that in previous experiments (e.g., ref 15) and a direct consequence of measuring closer to the slit nozzle orifice; further downstream the shoulder at lower energy disappears and only the $A^2\Pi_{3/2}-X^2\Pi_{3/2}$ band is observed. The ground-state rotational constant $B'' = 0.009\ 88$ cm^{-1} is calculated from a recent ab initio density functional theory geometry optimization that gives H−C1 = 1.068 Å, C1−C2 = 1.219 Å, C2−C3 = 1.330 Å, C3−C4 = 1.240 Å, C4−C5 = 1.311 Å, and C5−C6 = 1.246 Å,[7] reflecting a single−triple bond alternation.[16] A good simulation is obtained for an origin band value of $T_0 = 12\ 260.4(5)$ cm^{-1}, blue-shifted 117 cm^{-1} with respect to the matrix value and with excited-state values $A' = -28$ cm^{-1} (i.e., $\Delta A = 3$ cm^{-1}) and $B' = 0.009\ 82$ cm^{-1}. The latter value is expected to be accurate to within a few percent. The ratio $B''/B' = 1.007$ is close to unity; for a chain as long as $HC_{10}H^+$, only a minor change in molecular geometry is expected upon electronic excitation. For smaller chains, the effect is more pronounced. This can be seen from Table 1 in which the parameters of a number of polyacetylene cations HC_nH^+ are compared.

TABLE 1: Comparison of the Spectroscopic Constants of Linear Chains HC_nH^+, DC_nD^+, and HC_nD^{+a}

		HC_nH^+		
	$n = 4^b$	$n = 6^c$	$n = 8^d$	$n = 10^{e,f}$
T_0	19 722.610(2)	16 654.6873(3)	14 143.1815(5)	12 260.4(5)
B''	0.146 888(22)	0.044 594(3)	0.019 078(9)	0.009 88(3)
B'	0.140 083(22)	0.043 792(3)	0.018 867(9)	0.009 82(3)
B''/B'	1.049	1.018	1.011	1.007
A''	−33.5(1.9)	−31.40(28)	(−31)	(−31)
A'	−31.1(2.0)	−28.41(28)	(−28)	(−28)
ΔA			3	3

		HC_nD^+		
	$n = 4^g$	$n = 6^c$	$n = 8^g$	$n = 10^f$
T_0	19 731.725(2)	16 670.6168(3)	14 156.3(3)	12 270.6(5)
B''	0.136 599(30)	0.042 573(8)		
B'	0.130 469(30)	0.041 815(8)		
B''/B'	1.047	1.018		
A''	(−33.3)	−32.37(56)		
A'	(−31.1)	−29.42(56)		
ΔA	2.2			

		DC_nD^+		
	$n = 4^b$	$n = 6^c$	$n = 8^d$	$n = 10^f$
T_0	19 740.683(2)	16 686.5100(3)	14 169.5243(3)	12 280.8(5)
B''	0.127 403(24)	0.040 701(9)	0.017 648(6)	0.009 23(5)
B'	0.121 831(25)	0.039 980(9)	0.017 452(6)	0.009 17(5)
B''/B'	1.046	1.018	1.011	1.007
A''	−33.3(2.0)	−31.31(49)	(−31)	(−31)
A'	−31.1(2.0)	−28.40(49)	(−28)	(−28)
ΔA			3	3

^{a} All values are in cm^{-1}. ^{b} Reference 2. ^{c} Reference 3. ^{d} Reference 4. ^{e} Reference 6. ^{f} This work. ^{g} Reference 19.

For larger n, the rotational constants B decrease, the ratio B''/B' decreases as well, and there is a monotonic shift of the origin band to the red. The oscillator strength increases with n, which holds promise for the extension of the experimental approach to measure the electronic spectrum of even longer species.

A confirmation of the assignment of the observed 815.5 nm band to the pentaacetylene cation is provided by the detection of this transition in the partially ($HC_{10}D^+$) and fully deuterated ($DC_{10}D^+$) species. The latter is shown in the right part of Figure 1, approximately 20 cm^{-1} blue-shifted with respect to the $HC_{10}H^+$ band. A good simulation of the observed spectrum is obtained for $B'' = 0.009\ 23(5)$ cm^{-1}, $B' = 0.009\ 17(5)$ cm^{-1}, and $T_0 = 12\ 280.8(5)$ cm^{-1} (Figure 1). The corresponding stick diagram is shown as well. The spectrum of the monodeuterated chain, $HC_{10}D^+$, has been observed at $12\ 270.6(5)$ cm^{-1} but is rather weak, and a contour simulation is not possible. Table 1 summarizes the determined spectroscopic constants for chains HC_nD^+ and DC_nD^+, with $n = 4, 6, 8,$ and 10.

This work presents the electronic spectrum of the largest polyacetylene cation measured in the gas phase so far. Nevertheless, a comparison with the hitherto reported diffuse interstellar bands in the near infrared[17,18] shows that there is no absorption apparent at the position of the origin band in the electronic spectrum of $HC_{10}H^+$.

References and Notes

(1) Cha, C.; Weinkauf, R.; Boesl, U. *J. Chem. Phys.* **1995**, *103*, 5224.

(2) Callomon, J. H. *Can. J. Phys.* **1956**, *34*, 1046.

(3) Lecoultre, J.; Maier, J. P.; Rösslein, M. *J. Chem. Phys.* **1988**, *89*, 6081.

(4) Sinclair, W. E.; Pfluger, D.; Linnartz, H.; Maier, J. P. *J. Chem. Phys.* **1999**, *110*, 296.

(5) Pfluger, D.; Motylewski, T.; Linnartz, H.; Sinclair, W. E.; Maier, J. P. *Chem. Phys. Lett.* **2000**, *329*, 29.

(6) Pfluger, D.; Sinclair, W. E.; Linnartz, H.; Maier, J. P. *Chem. Phys. Lett.* **1999**, *313*, 171.

(7) Betowski, L. D.; Winnik, W.; Marcus, A. B.; Pyle, S. M. *Int. J. Mass Spectrosc.* **1998**, *173*, 27.

(8) Lee, S.; Gotts, N.; von Helden, G.; Bowers, M. T. *J. Phys. Chem. A* **1997**, *101*, 2096.

(9) Pyle, S. M.; Betowski, L. D.; Marcus, A. B.; Winnik, W.; Brittain, R. D. *J. Am. Soc. Mass. Spectrom.* **1997**, *8*, 183.

(10) Tielens, A. G. G. M., Snow, T. P., Eds. Laboratory studies of proposed carriers. *The diffuse interstellar bands*; Kluwer Academic Publishers: Dordrecht, Netherlands, 1995; pp 175−238.

(11) Freivogel, P.; Fulara, J.; Lessen, D.; Forney, D.; Maier, J. P. *Chem. Phys.* **1994**, *189*, 335.

(12) O'Keefe, A.; Deacon, D. A. G. *Rev. Sci. Instrum.* **1988**, *59*, 2544.

(13) Motylewski, T.; Linnartz, H. *Rev. Sci. Instrum.* **1999**, *70*, 1305.

(14) Western, C. M. *PGOPHER*; School of Chemistry, University of Bristol: Bristol, U.K., 1994 and 1998.

(15) Linnartz, H.; Motylewski, T.; Vaizert, O.; Maier, J. P.; Apponi, A. J.; McCarthy, M. C.; Gottlieb, C. A.; Thaddeus, P. *J. Mol. Spectrosc.* **1999**, *197*, 1.

(16) A nearly identical value is found when extrapolating the values available for the rotational constants of the di-, tri- and tetraacetylene cations.

(17) Jenniskens, P.; Desert, F.-X. *Astron. Astrophys.* **1994**, *106*, 39.

(18) Galazutdinov, G. A.; Musaev, F. A.; Krelowski, J.; Walker, G. A. H. *Publ. Astron. Soc. Pac.* **2000**, *112*, 648.

(19) Vaizert, O.; Furrer, P.; Cias, P.; Linnartz, H.; Maier, J. P. *J. Mol. Spectrosc.* **2002**, *214*, 94.

References

[1] K. H. Homann, Angew. Chem. Intern. Ed. 7 (1968) 414

[2] M.B. Bell, P. A. Feldman, S. Kwok, and H. E. Matthews, Nature 295 (1982) 389

[3] W. Kraetschmer, J. Chem. Soc. Faraday. Trans. 89 (1993) 2285

[4] J. Fulara, D. Lessen, P. Freivogel and J. P. Maier, Nature 366 (1993) 439

[5] A. E. Douglas, Nature 269 (1977) 130

[6] H. Schueler, L. Reinbeck, Z. Naturforsch. 7a (1952) 285

[7] J. H. Callomon, Can. J. Phys. 34 (1956) 1046

[8] R. Kuhn, J. P. Maier, M. Ochsner, Mol. Phys. 59 (1986) 441

[9] R. N. Zare, A. R. Schmeltekopf, W. J. Harrop, D. L. Albritton, J. Mol. Spec. 46, (1973) 37

[10] J. Lecoultre, J. P. Maier, M. Roesslein, J. Chem. Phys. 89 (1988) 6081

[11] J. Kraitchman, Am. J. Phys. 21, (1953) 17

[12] J. Schaeublin, PhD thesis, University of Basel, 1972

[13] F. Brogli, E. Heilbronner, V. Hornung, E. Kloster-Jensen Helv. Chim. Acta 56 (1973) 2171

[14] O. Vaizert, P. Furrer, P. Cias, H. Linnartz, J.P. Maier, J. Mol. Spec. 214, (2002) 94

[15] T. Motylewski, H. Linnartz, Rev. Sci. Instrum. 70 (1999) 1305

[16] M. Allan, E. Kloster-Jensen, J.P. Maier, Chem. Phys. 17 (1976) 11

[17] D. Klapstein, R, Kuhn, J.P. Maier, M. Ochsner, W. Zambach, J. Phys. Chem, 88 (1984) 5176

[18] W.E. Sinclair, D. Pfluger, H. Linnartz, J. P. Maier, J. Chem. Phys 110 (1999) 296

[19] D. Pfluger, W.E. Sinclair, H. Linnartz, J. P. Maier, Chem. Phys. Lett. 313 (1999) 171

[20] M. Allan, E. Heilbronner, E. Kloster-Jensen, J. P. Maier, J. Chem. Phys. Lett. 41 (1976) 228

[21] D. Pfluger, T. Motylewski, H. Linnartz, W.E. Sinclair, J. P. Maier, Chem. Phys. Lett. 329 (2000) 29

[22] P. Freivogel, J. Fulara, D. Lessen, D. Forney, J. P. Maier, Chem. Phys. 189 (1994) 335

[23] A. M. Smith, J. Agreiter, M. Haertle, C. Engel, V.E. Bondybey, Chem. Phys. 189 (1994) 315

[24] A. Sobolewski, L. Adamowicz, J. Chem. Phys. 102 (1994) 394

[25] K. Andersson, P.-A. Malmqvist, B. O. Roos, A. J. Sadlej, K. J. Wolinski, J. Phys. Chem. 94 (1990) 5483

[26] L. D. Betowski, W. Winnik, A. B. Marcus, S. M. Pyle, Int. J. Mass. Spectrosc. 173 (1998) 27

[27] J. P. Maier, G. A. H. Walker, D. A. Bohlender, ApJ 602 (2004) 286

CHAPTER 6

6. Boron and its clusters

Studies of boron clusters and boron-rich materials are currently active areas of both experimental and theoretical study. These systems have many important technological applications, including thermally and chemically stable insulators, high modulus boron fiber composites [1], high temperature semiconductor devices, refractory and thermoelectric materials [2, 3]. Boron chemistry is also of interest in the search for high performance propellants. In particular, the large heat of combustion and the low atomic mass contribute to the interest in boron and boron-containing compounds as high energy density fuels [4-7]. Despite these important technological applications, a number of experimental and theoretical studies of boron clusters is rather limited.

Boron is isovalent with Al, yet the atomic and electronic structures of the two elements are entirely different. Al is a nearly free-electron metal where the valence electrons are delocalized and the solid phase is face centered cubic. Boron-rich solids, on the other hand, are composed of the 12-atom clusters of boron having the structure of icosahedron [8]. Boron's small covalent radius and electron deficiency result in formation of materials involving strong bonds delocalized over several nuclei. The electronic structure of B is characterized by three-center bonding, where three boron atoms share a common pool of charge. It is well known that in covalently bonded materials, the bonding charges are centered between two atoms. Thus the electronic structure of boron is intermediate between covalent and metallic bonding. This behavior renders boron-rich solids some unusual properties. For example, they range from the conducting materials ($B_{1-x}C_x$) to insulating ones ($B_{12}P_2$) [9].

6.1. Experimental and theoretical studies of small boron clusters

In the line of boron clusters its dimer can be considered as the smallest one in the series of B_n. In contrast to other stable first-row homonuclear diatomics, little is known about the B_2 molecule. Its first spectroscopic observation was reported in 1940 by Douglas and Herzberg. In a discharge in helium with a trace of BCl_3 they measured the $^3\Sigma_u^-$ - X $^3\Sigma_g^-$ emission transition of B_2 in the UV region [10]. The absence of a Q-branch and an intensity alteration in the fine structure corresponded to the parallel transition involving a Σ state. On the basis of the molecular orbital theory this so called Douglas-Herzberg emission system was assigned to a $^3\Sigma_u^-$ - X $^3\Sigma_g^-$ transition. This contention was confirmed in 1976 when Graham and Weltner observed this system in an absorption in solid argon at 4-10 K. In their experiment they evaporated elementary boron from a thin-wall tantalum cell. The produced vapor was deposited with argon onto a CaF_2 window. This matrix experiment showed that this transition indeed involved the ground electronic state. However, no ESR spectrum was observed, therefore no definitive determination of the multiplicity of the ground state existed [11]. In 1982 Bredohl et al. recorded the $^3\Sigma_u^-$ - X $^3\Sigma_g^-$ emission spectrum of B_2 at a higher resolution and observed the spin-spin fine structure [12] confirming the assignment of Douglas and Herzberg. The ESR spectrum of the matrix-isolated B_2 obtained by Knight et al. in 1987 [13] also substantiated the former X $^3\Sigma_g^-$ assignment of Douglas and Herzberg.

In 1992 Brazier and Carrick reported the observation of several new electronic transitions of the B_2 molecule. They obtained the spectra by using a corona excited supersonic expansion source [14]. A sample of diborane was seeded in helium which was expanded through a gas nozzle. The DC electric discharge through the throat of the nozzle served to both dissociate the precursor and electronically excite the product molecules. The UV and visible spectra showed six separate electronic transitions, five of which were not known previously. Two of these bands, designated (2) $^3\Pi_u$ – (1)$^3\Pi_g$ and (1)$^1\Delta_u$ – b$^1\Delta_g$, have been fully analyzed by moderate resolution spectra. For these four new electronic states the bond-lengths were determined and compared with theoretically calculated values. The experimental bond-lengths and the tra1nsition energies matched with the theoretical calculations carried out by Langhoff and Bauschlicher [15]. In 1995

the same method was used to obtain the emission spectra of the (1) $^1\Sigma_u^+$ - (1) $^1\Sigma_g^+$ electronic transition of B_2 [16]. The emission spectra of 0-0, 1-1, 2-2, 3-3, and 4-4 vibrational bands have been recorded and analyzed. Bond-lengths were calculated for both states and corresponded to theoretical calculations of Langhoff and Bauschlicher [15].

In 1994 Brazier and Carrick improved their experiment by an implementation of the Fourier transform spectrometer [17]. It increased spectral resolution of the system significantly and provided the capability to resolve the structure of the lowest rotational lines of (2) $^3\Pi_g - A\,^3\Pi_u$ electronic transition of B_2. A full rotational analysis of the 0-0, 0-1, 1-0 and 1-3 bands has been performed. The good match between the experiment and theory has allowed the authors to make a definitive assignment of the observed transition. They also observed a strong perturbation of the (2) $^3\Pi_g$ state by (1) $^3\Pi_g$.

In 2000 Tam et al. reported a couple of absorption spectra of laser ablated boron species trapped in rare gas matrices [18]. In their experiments they used a rotating boron target as a source of the molecules. However, the way in which they produced the matrix varied as their apparatus evolved. In one experiment the laser ablation of the boron species and the matrix deposition were performed in the same vacuum chamber. In another experiment the laser ablation process took place in the different vacuum chamber than the matrix deposition. The advantage of the second approach was to enhance the control over the ablation process. One of the bands they recorded was well known as the Douglas-Herzberg system. Less progression in the 260-300 nm region was assigned to the (2) $^3\Pi_u - X\,^3\Sigma_g^-$ transition of B_2. They also observed a new progression of strong peaks in the region of 180-200 nm which could be due to B_2 molecules, however, it was not assigned.

There were also theoretical studies of B_2. In 1978 an accurate *ab initio* configuration interaction calculation carried out by Dupuis and Liu [19] has established that the ground electronic state of B_2 is of $^3\Sigma_g^-$ symmetry, and that the Douglas–Herzberg emission system near 320 nm is due to transitions from the second $^3\Sigma_u^-$ to the X $^3\Sigma_g^-$ state. The lowest $^5\Sigma_u^-$ state, suggested by previous calculations as the ground state [20, 21], was found about 1300 cm^{-1} above the $^3\Sigma_g^-$ state. The assignment of the Douglas–Herzberg transition was based on the correspondence between calculated and observed molecular

constants. Further confirmation of this assignment was seen in the close agreement between calculated and observed isotope shifts and intensity distributions. Electronic wavefunctions and potential curves for $^3\Sigma_u^-$, $^3\Sigma_g^-$ and $^5\Sigma_u^-$ states of B_2 were calculated using the multiconfiguration self-consistent field and the configuration interaction methods.

Langhoff and Bauschlicher calculated the spectroscopic constants of B_2 by using an extensive Gaussian basis set and multiference configuration interaction approach [15]. They wanted to characterize the spectroscopy and the nature of the bonding in various electronic states of B_2. The singlet, triplet and quintet states of B_2 below ~45000 cm^{-1} have been studied. The analysis of the calculated potential curves and their comparison with those of Al_2 [22] showed that B_2 shows stronger bonding than Al_2. It is consistent with the bond-lengths and weaker bonding in Al_2 resulting from the reduced overlaps.

Examinations and theoretical studies on small boron clusters larger than two atoms, however, are rather rare. In 1981 Whiteside determined ground electronic states, geometries and atomization energies for B_2, B_4 and B_6 using self-consistent field configuration interaction calculations [23]. Another theoretical study of the neutral B_4 carried out by Koutecky et al. [24] gave similar results. In 1984 Lunell's studies have also probed properties of the capped pentagon structure of B_6 but have not attempted to optimize the geometry [25]. B_{12} has been also the subject of several theoretical studies [26]. In 1988 Hanley et al. reported the set of *ab initio* calculations for both neutral and ionic B_n (n=1-6) [27]. Their calculations took the lowest energy geometries for the neutral boron clusters obtained by Whiteside [23] and reoptimized them for the cations with the 6-31G* basis set. B_2^+, B_3^+ and B_4^+ were optimized again with the 6-31G* basis and total energies were obtained by configuration interaction. In the case of B_5^+ they took the linear, symmetric pentagon, square pyramid and bipyramid structures as starting geometries for optimization. The B_6^+ geometry was derived by optimizing the bond-lengths of neutral B_6 structure for B_6^+. To check the accuracy of their calculations they have recalculated the total energies for B_2, B_3, B_4 and B_6 using Whiteside's geometries [23].

It was observed that these two methods usually corresponded one to another. The B_5 geometry was obtained from the local optimization of calculated here B_5^+ structure.

Finally the bond-lengths, spin states, spectroscopic state assignment, and total energies for B_n (n=1-6) and B_n^+ (n=1-6) were obtained. They are given in Table 6.1.

Parent cluster	Bondlength (Å)	Ground state	Total energy (Hartree)		
			Whiteside [Ref. 23]	Hanley et al.	
			6-31G*	6-31G*	6-31G*/CI
B_2	1.60	$^3\Sigma_g^-$	-49.0753	-49.0765	-49.2273
B_2^+	2.00	$^2\Pi_u$		-48.7687	-48.9000
B_3	1.57	$^2A_1{'}$	-73.7721	-73.7402	-73.9101
B_3^+	1.53	$^1A_2{''}$		-73.4270	-73.5574
B_4	1.51	^1A_g	-98.4240	-98.4302	-98.5623
B_4^+	1.53	^2A_g		-98.1327	-98.2444
B_5	1.75	$^2E{'}$		-122.9088	
B_5^+	1.75	$^1A_1{'}$		-122.6662	
B_6	1.62	$^1A_1$	-147.6569	-147.6629	
B_6^+	1.62	$^2A_1$		-147.3547	

Table 6.1. Calculated boron cluster properties and total energies [Ref. 27].

In 1997 Niu et al. performed the calculations using *ab initio* molecular orbital theory (based on both, density functional formalism and quantum chemical methods) [9]. The equilibrium geometries, binding energies, ionization potentials, fragmentation patterns, and electronic structure of neutral and charged boron clusters containing up to six atoms were being calculated.
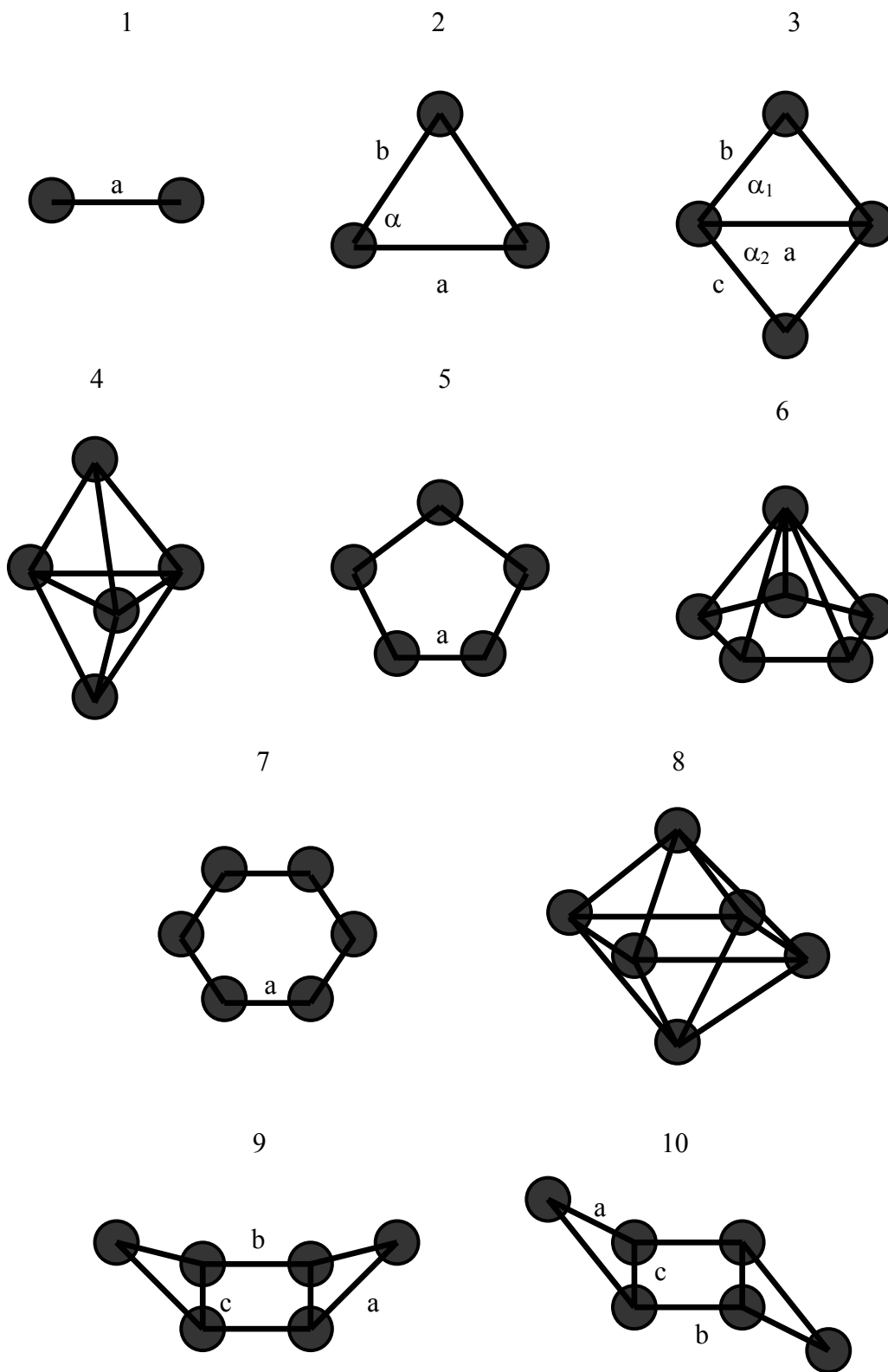
Figure 6.1. Calculated geometries of B_n neutral clusters [Ref. 9].

For the calculation of the total energies, electronic structure and equilibrium geometries they have chosen two different approaches: the HF method followed by a correction through Möller-Plesset fourth order perturbation theory and density functional method with generalized gradient approximation. The equilibrium geometries as well as the geometries of some isomers of neutral B_n clusters (n=2-6) calculated at MP4 level are shown in Figure 6.1. and all geometrical parameters for neutral boron clusters are given in Table 6.2. Results for most of these geometries were also tested using the GGA level of theory under the B3LYP scheme. The equilibrium geometries (with the exception of B_5) and spin multiplicities of clusters using both methods corresponded with each other. The geometrical parameters, i. e., bond-lengths and bond angles as well as the binding energies corresponded as well. Systematic increase in binding energy as a function of the cluster size was observed in both methods.

Cluster	Geometry[a]	Bond-lengths (Å)		Bond angles (°)	
		MP4	B3LYP	MP4	B3LYP
B_2	1	a=1.55	a=1.56		
B_3	2	a=1.52 b=1.52	a=1.52 b=1.52	α=60.0	α=60.0
B_4	3	a=1.79, b=1.51, c=1.51	a=1.82, b=1.51, c=1.51	$\alpha_1=\alpha_2$=53.6 β=180.0	$\alpha_1=\alpha_2$=52.8 β=180.0
B_5	4	a=1.09, b=1.16	a=1.09, b=1.16		
	5	a=1.53	a=1.58		
B_6	6	a=1.39, b=0.89	a=1.37, b=0.92		
	7	a=1.52	a=1.52		
	8	a=1.36, b=0.98			
	9	a=1.49, b=4.63, c=1.57		β=90.1	
	10	a=1.53, b=3.00, c=1.60		β=84.1	

Table 6.2. Geometrical parameters for neutral B_n clusters [Ref. 9]. [a] see Figure 6.1.

The study confirmed the spin triplet configuration of the ground state of the B_2 molecule. The structure of B_3 is an equilateral triangle with a bond-length 1.52 Å at the MP4 level of theory. This is in agreement with the results obtained by Ray et al. [28] and Hanley et al. [27]. The geometry of B_4 which was calculated by Niu et al. differs significantly from those of Ray et al. which can be explained by a less extensive choice of the basis functions (3-21G*). The geometry of B_4 calculated here is a rhombus whereas those calculated before is a linear chain [28]. Hanley et al. obtained the rhombus structure for the B_4 molecule, as well. For the B_5 molecule two isomers were identified among which the triangular bipyramid is more stable using MP4 theory. The equilibrium structure of B_6 is a pentagonal pyramid, however, others isomers were also found i. e., hexagonal, octahedral, the "boat" and the "chair" structures. The calculation of geometries shown that the electronic structure of boron is not typical. If the bonding in B_n clusters would have been a two-centered covalent bond, the octahedral structure would have been the ground state. It is also visible that that the seed for an icosahedric growth pattern is shown at the B_6 cluster stage. It can be finally concluded that the special chemistry which governs the electronic structure of boron-rich solids is also present in small boron clusters.

As an electron is removed from a cluster, the redistribution of charges causes the neutral structure to relax. The difference in the total energy between the neutral and cationic cluster in their respective ground states is the adiabatic ionization potential and was measured by Haneley et al. [27] for boron clusters. They also observed that the fragmentation of B_n^+ clusters for n < 6 proceeded by the emission of a B^+ cation, while in larger clusters the charge resided on the B_{n-1}^+ fragment. The geometries of B_n^+ clusters (n=2-6) were optimized again at the MP4 and B3LYP level of theory [29]. Both methods once again yielded identical geometries and spin multiplication as in the case of the neutral clusters. The schematic equilibrium geometries of the boron-cluster cations are presented in Figure 6.2. and the geometrical parameters for cationic boron clusters are given in Table 6.3.

The comparison of the structures of the neutral and corresponding cationic clusters showed that there is a little change among the geometries of neutral and charged dimers, trimers und tetramers.
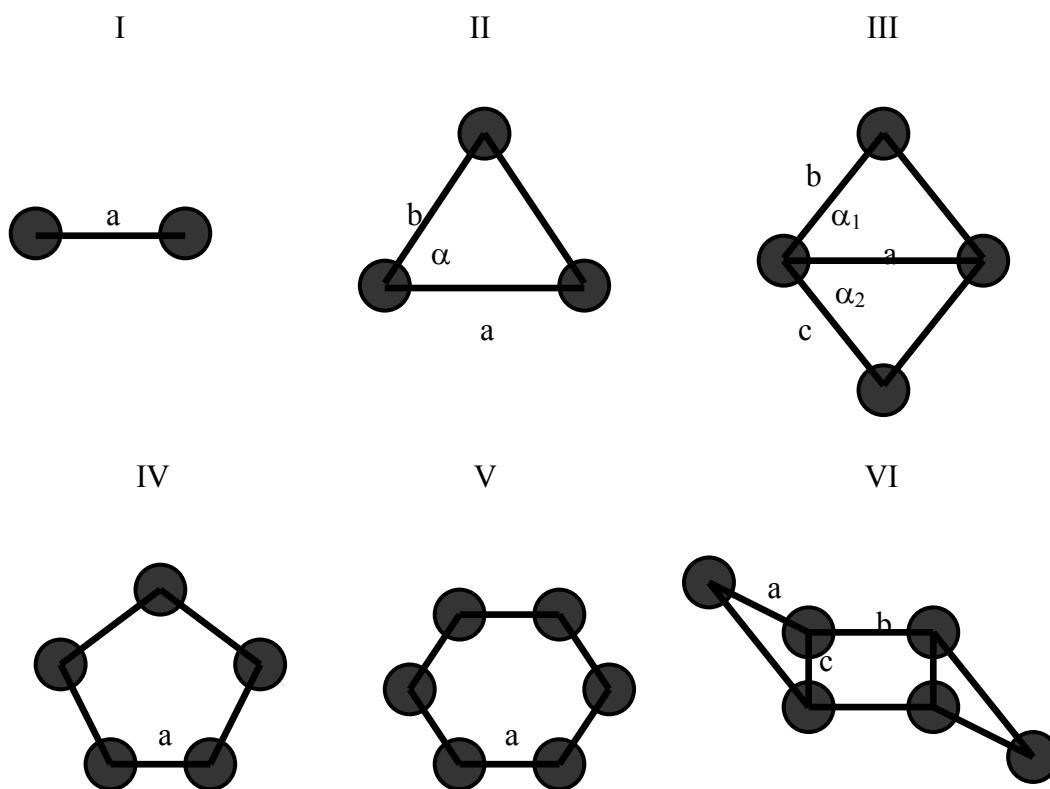
I II III

b

α

a

b

α_1

a

α_2

c

IV V VI

a

a

a

b

c

Figure 6.2. Calculated geometries of B_n^+ clusters [Ref. 9].

Cluster	Geometry[a]	Bond-lengths (Å)		Bond angles (°)	
		MP4	B3LYP	MP4	B3LYP
B_2^+	I	a=1.75	a=1.80		
B_3^+	II	a=1.60 b=1.60	a=1.55 b=1.55	α=60.0	α=60.0
B_4^+	III	a=1.98, b=1.55, c=1.55	a=2.00, b=1.54, c=1.54	$\alpha_1=\alpha_2=50.5$ β=180.0	$\alpha_1=\alpha_2=49.5$ β=180.0
B_5^+	IV	a=1.57	a=1.54		
B_6^+	V	a=1.55	a=1.54		
	VI	a=1.67, b=1.60, c=1.69	a=1.64, b=1.65, c=1.67	β_1 =149.2, β_2=149.2	β_1 =110.1, β_2=110.1

Table 6.3. Geometrical parameters for B_n^+ clusters [Ref. 9]. [a] see Figure 6.2.

The significant changes occur in B_5 and B_6 when an electron is removed. The planar structures are preferred by the cations. It is observed, however, that B-B bond remains close to the one in the neutral clusters in all cases.

As a cluster is doubly ionized, the added repulsion between the two added positive charges tends do destabilize the cluster. This destabilization force is the strongest for the smallest clusters. The calculations at the MP4 level of the theory showed that the doubly charged clusters B_n^{2+} are all linear chains.

6.2. Experimental and theoretical studies of the triatomic boron-rich clusters

The spectroscopic studies of the triatomic clusters containing boron started in the 1960s. In 1962 Varhaegen et al. first observed BC_2 in a mass spectrometric study of the vapor over solid boron carbide at about 2300 K [30, 31]. The principal vapor species were B, BC, BC_2 and B_2C. In 1970 Easley and Weltner studied the vapor in equilibrium with solid boron carbide at 2600 K with X-band ESR spectroscopy and concluded that their spectrum of BC_2 was in accordance with a linear B-C-C structure, corresponding to a $^2\Sigma$ ground state [32]. The *ab initio* studies carried out by Thomson [33] predicted the B-C-C structure to be more stable than C-B-C, however these studies was restricted to the linear isomers. In 1989 Knight et al. did the laser ablation experiment, which indicated that BC_2 actually had the nonlinear symmetric structure C-B-C [34]. Recently Martin et al. in the combined *ab initio* and pulsed laser evaporation studies concluded, that although the global minimum structure of BC_2 is predicted to be an asymmetric triangle, the vibrational averaged structure is an isosceles triangle with a strong symmetric stretching frequency near 1200 cm^{-1}. They observed a 1:4 doublet at 1232.5 and 1194.6 cm^{-1}, with the first band dominating the boron-10 experiments, which they tentatively assigned to the cyclic BC_2. This assignment could not be completely confirmed due to the lack of ^{13}C isotopic data. In 1996 Presilla-Marquez et al. measured a spectrum of BC_2 trapped in argon matrices at 10 K using Fourier transform infrared spectrometer [7]. BC_2 was produced by vaporization boron/carbon mixtures around 3000 K. Analysis of the spectra combined with the predictions of density functional theory calculations resulted

in the assignment of the band previously observed by Martin et al. The band was attributed to the ν_2 fundamental of cyclic BC_2, which was effectively symmetric. The assignment was supported by ^{10}B, ^{11}B and ^{13}C isotopic data (a complete set of measured isotopic shifts) and corresponded to the theoretical predictions.

In 1999 B_2C was studied in an argon matrix [35] and the vibrational spectrum has been observed by Fourier transform infrared spectroscopy. The measured absorption frequencies of the three boron isotopomers of B_2C matched the ab initio predictions of the ν_1 (a_1) fundamental of cyclic symmetric B_2C. The distribution of isotopomers of B_2C matched those of B_2C_2 in three matrices with different isotopic compositions which confirmed the assignment of the band observed at 1392.8 cm^{-1} to the ν_1 (a_1) fundamental of B_2C.

The geometry of the B_2C molecule was calculated in 1994 by Martin and Taylor [36]. The potential energy surface for the ground state has been investigated using full-valence complete active space SCF (CASSCF), augmented by coupled cluster [CCSD(T)] and multiference treatments. The ground state of B_2C is a very stable ring with two electron π systems. The first excited state is linear B-C-B ($^1\Sigma_g^+$), which is biconfigurational due to a ($4\sigma_g$) - ($3\sigma_u$) near degeneracy. In the same work Martin and Taylor calculated also anharmonic spectroscopic constants for B_2C and some isotopomers which can be useful in further investigations.

Knight et al. [37] used a laser vaporization matrix isolation electron spin resonance (ESR) apparatus to study the B-N-B radical. The radical has been generated by the laser vaporization of solid boron nitride and isolated in neon, argon, and krypton matrices at 4 K for detailed ESR investigations. The ESR experimental results and theoretical calculations conducted at the CI level showed that B-N-B has an $X^2\Sigma_u^+$ ground electronic state with a linear centrosymmetric structure. Roland and Wynne [38] described photoionization and photofragmentation of B_xN_y clusters generated by laser vaporization of boron nitride followed by supersonic expansion. Thompson et al. [39, 40] studied the infrared spectra of reaction products of laser ablated boron atoms with ammonia, during condensation with excess argon at 10 K. They observed cyclic and

symmetric linear B_2N together with a series of hydrogen - boron - nitrogen containing species. Asmis et al. [41-44] used a negative ion tandem time-of-flight photoelectron spectrometer to determine adiabatic detachment energies and vibrational frequencies for several low-lying electronic states of BN, B_2N, and B_3N. In particular Asmis et al. found no evidence for a low-lying cyclic isomer of B_2N [43]. They reassigned the matrix IR spectra of Andrews and co-workers [39, 40, 45] to the $^2\Sigma_u^+$ ground state of linear B_2N.

Interesting calculations of boron-nitrogen clusters were also carried out in 1989 by Martin et al. They computed a number of different structures and states of B_2N and BN_2 [46]. Optimum geometries and harmonic spectra were obtained at the HF/6-31G* level of theory. The relative stability of the isomers was determined using full fourth-order Moller-Plesset theory. B_2N has a symmetric linear arrangement in its $^2\Sigma_u^+$ ground state with an extremely low bending frequency (73 cm^{-1}), and an unusually low vertical ionization potential (6.75 eV). Its asymmetric stretching (2021 cm^{-1}) is found to be extremely intense (8782 km mol^{-1}). BN_2 has four rather closely spaced states, of which an isosceles triangle is the absolute minimum ($^2A_1$ state). However, at high temperatures, an asymmetric linear arrangement ($^2\Pi$ state) is of equal importance.

6.3. Theoretical and experimental studies of B_3 and its ions

There are few theoretical *ab initio* calculations of the structure and electronic properties of the B_3 molecule [27, 46-49]. All of them predicted the ground state structure of B_3 to be an equilateral triangle (D_{3h}) with $^2A_1'$ symmetry. Some of the vibrational modes of this molecule in the near infrared and visible regions have been also calculated [46, 48].

A computational study of the structure and properties of the ground and low-lying excited electronic states of the B_3^+ molecule was also carried out in 2001 by Yang et. al [50]. They used sophisticated methods and large basis sets, including the Quadratic CI calculation and cc-pVQZ basis sets. Their results showed that the equilibrium geometry for the singlet $^1A_1'$ ground state of B_3^+ is an equilateral triangle (D_{3h}). However,

it is also found that the energies of state $^3A''_2$ and state $^1A'_1$ alternate when the optimization was performed at different computational levels. This indicated that it is difficult to distinguish these two states only by their total energies. Fortunately, the present calculated harmonic vibrational frequencies are obviously different. As a result, they may be used to identify the ground state $^1A'_1$ from the $^3A''_2$ state. The dissociation energies were also computed at a different level and compared with the other theoretical and experimental work [9, 27].

Despite the growing interest in the structures and energetics of the boron trimer, not many experiments were done. Although the ground-state structures and electronic properties of many metal trimers are known, those of B_3 have not been established experimentally for many years. For the first time B_3 was observed in 1992 by Hamrick et al. [51]. They obtained highly resolved electron-spin-resonance spectrum of boron trimer in rare gas matrices at 3-30 K. The analysis of the spectra allowed the properties of the lowest electronic state to be determined. Comparison of the experimental results and theoretical calculations indicated that B_3 has tree equivalent nuclei e. i., D_{3h} symmetry. It was also confirmed that B_3 has $^2A_1'$ ground state. In 1996 Li et al. obtained the matrix isolation infrared spectra of B_3 in the range from 400 to 5000cm^{-1} [52]. The boron samples were laser-vaporized and trapped in solid argon at 4 K. The absorption spectra were measured using a Fourier transform infrared spectrometer. In this experiment authors observed the ground-state vibrational frequencies which were attributed to the degenerate mode (e') ^{11}B and ^{10}B isotopomers. The experimental data corresponded to the former calculations [46].

In 2003 B_3 and B_3^- were also studied using photoelectron spectroscopy and ab initio calculations [53]. Vibrationally resolved photoelectron spectra were observed for B_3^- at three photon energies (355, 266, and 193 nm), and the electron affinity of B_3 was measured to be 2.82 ± 0.02 eV. An unusually intense peak due to two-electron transitions was observed in the 193-nm spectrum of B_3^- at 4.55 eV and its origin was theoretically characterized, suggesting strong electron correlation effects in the boron trimer. They again confirmed that both B_3^- and B_3 are aromatic systems with D_{3h} symmetry.

In 2003 Wyss et al. reported the experiment in which for the first time the electronic absorption spectra of B_3^- and B_3 have been measured in neon matrices [54].

The B_3^- anions were produced in a cesium sputter ion source that had been built originally for the production of carbon anions. A boron-carbide (B_4C) rod or pressed pure boron powder were used as sputter targets. The ions produced in the source were guided by an electrostatic lens system into a quadrupole mass analyzer, where the B_3^- anions were selected and then codeposited with excess of neon onto a rhodium coated sapphire plate at a temperature of 6 K. A band system with origin at 21412 cm^{-1} was observed and assigned as the $^1E'$- X $^1A_1'$ electronic transition of the cyclic anion. After photobleaching, the $1\ ^2E'$ - X $^2A_1'$ and $2\ ^2E'$ - X $^2A_1'$ band systems of neutral cyclic B_3 were observed. They start around 13587, 21828 cm^{-1}, respectively. The vibrational structure which appears in the observed electronic spectra, is associated with excitation of the two normal modes, v_1 (a_1'), v_2 (e'), in the upper electronic states, because at 6 K the population is essentially in the vibrationless level of the ground state. Since the upper electronic states of B_3 and B_3^- have E' symmetry they are subject to Jahn–Teller distortions which may cause complex vibrational pattern. The second system of B_3, assigned to the $2\ ^2E'$ - X $^2A_1'$ transition, has the most simple pattern. It starts with the origin band at 21828 cm^{-1} and a seemingly regular progression mode is discernible with two spacings that are the same within the error limit. As the origin band is dominant, no large geometry change is expected on passing from the ground to the excited electronic state. In contrast, the vibronic structure of the first system of B_3 assigned to the $1\ ^2E'$ - X $^2A_1'$ transition, indicates a strong Jahn–Teller distortion. The excitation of the degenerate v_2 (e'), Jahn–Teller active mode is evident. The two transition systems are not only very different in complexity but they also show quite different intensities. The spectra indicate an absorbance ratio of one order of magnitude in favor of the second band. The absorption spectrum of B_3^-, assigned to the $1\ ^1E'$ - X $^1A_1'$ transition, shows a complexity similar to the lower transition of B_3.
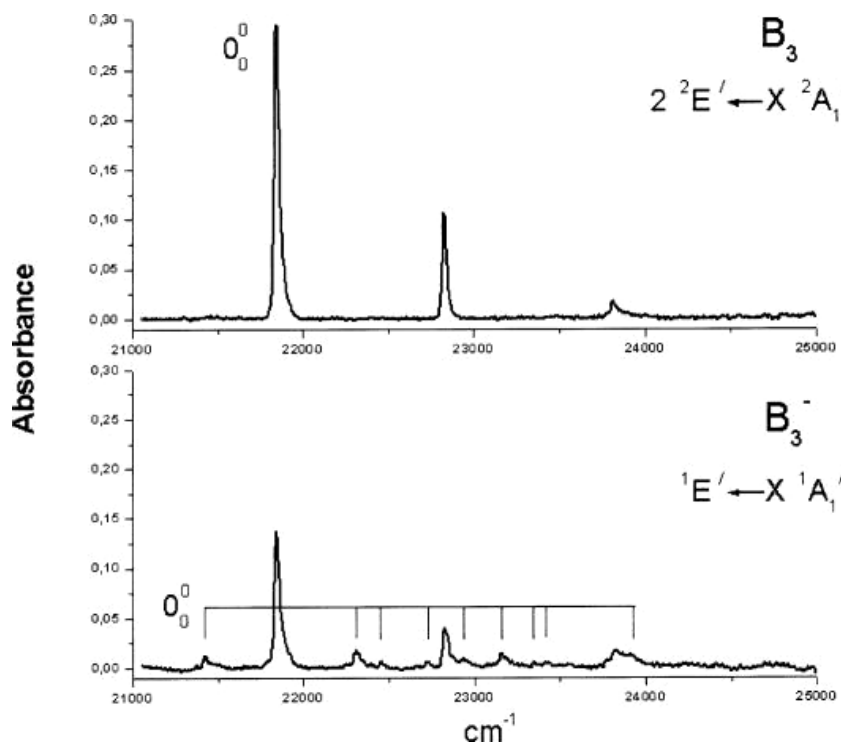
Figure 6.3. Electronic absorption spectra of $2\,^2E'$ - X $^2A_1'$ origin band of B_3 and $^1E'$ - X $^1A_1'$ electronic transition of B_3^- recorded in a 6 K matrix [Ref. 54].
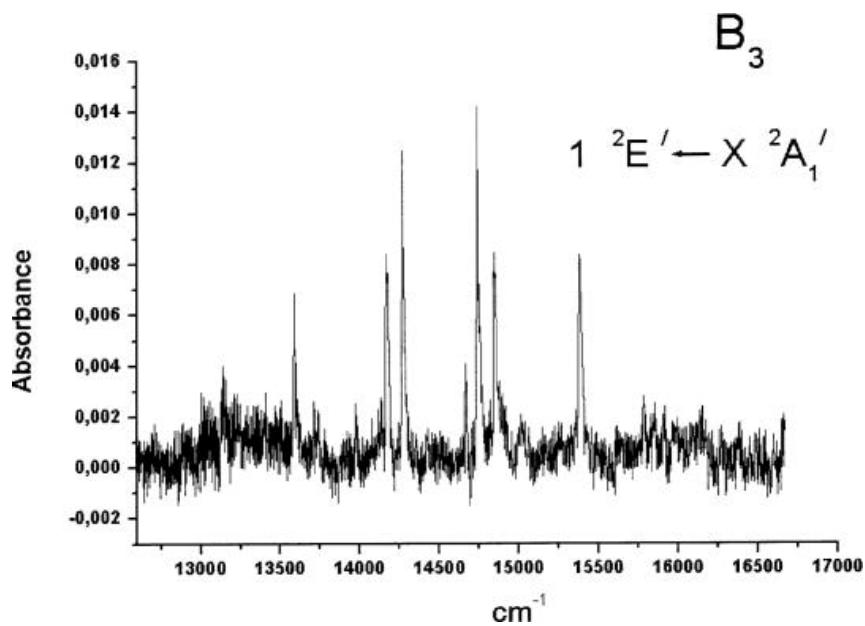

Figure 6.4. The absorption spectrum of the $1\,^2E'$ - X $^2A_1'$ electronic transition of B_3 recorded in a 6 K matrix [Ref. 54].

The patterns of these two systems are complicated and a sensible assignment can only be made on a theoretical base. The spectra are shown in Figures 6.3. and 6.4.

Transition energies, Jahn-Teller distortion energies and equlibrium geometries for the $1\ ^2A_1'$, $1\ ^2E'$ and $2\ ^2E'$ states have been calculated using multireference configuration interaction *ab initio* method. This helped provide symmetry assignments and an interpretation of the complex vibronic structure (due to Jahn –Teller effect) observed in the excited electronic state $1\ ^2E'$ of B_3. The calculated vibrational energies and intensities closely reproduced the complex vibrational structure observed in this state. On the other hand, the calculations confirmed that $2\ ^2E'$ state should undergo only a relatively weak Jahn–Teller distortion as the stabilization and localization energies were quite low. The short progression with an observed frequency of 981 cm^{-1} also corresponded well to the theoretical frequency of 973 cm^{-1}.

6.3.1. Gas-phase study of cyclic B_3

Despite good experimental results and large scale *ab initio* calculations, it is clear that the full analysis of the complex vibronic structure of the spectrum requires theory developments as well as high resolution gas-phase measurements. Although this kind of studies are inherently complicated and perplexing (difficulty in production of the appropriate amount of B_3 in the gas phase), high sensitivity of cavity ringdown method and good efficiency of the slit nozzle discharge source seemed to be a very promising tool in the pursuit of the high resolution spectrum of the B_3 molecule. The goal was really tempting because this spectrum could shed new light on the structure of this interesting cyclic trimer. The search for the $1\ ^2E'$ - $X\ ^2A_1'$ and $2\ ^2E'$ - $X\ ^2A_1'$ bands was carried out and was finally successful in the second case. Despite many efforts, the $1\ ^2E'$ - $X\ ^2A_1'$ electronic transition of B_3 could not be observed in the gas phase. The latest studies of the gas-phase spectrum of the $2\ ^2E'$ - $X\ ^2A_1'$ electronic origin band of cyclic boron trimer are presented below.

Gas phase detection of cyclic B_3: $2\,^2E' \leftarrow X\,^2A_1'$ electronic origin band

P. Cias, M. Araki, A. Denisov and J.P. Maier

Department of Chemistry, University of Basel, Klingelbergstrasse 80,

CH-4056 Basel, Switzerland

Abstract

The rotationally resolved origin band in the $2\,^2E' \leftarrow X\,^2A_1'$ electronic spectrum of cyclic B_3 has been observed by cavity ring down spectroscopy in the gas phase. The B_3 molecule was generated in a supersonic planar plasma containing decaborane ($B_{10}H_{14}$) and neon as a carrier gas. The rotational structure pattern is that of a cyclic molecule. It is analyzed assuming an equilateral triangle in both electronic states. The band origin is determined to be 21853.52 cm^{-1}, and the bond-lengths 1.60377(106) Å in the ground and 1.61907(96) Å in the excited electronic state are inferred from analysis of the rotational structure.

Corresponding author:

Prof. J. P. Maier

Department of Chemistry

University of Basel

Klingelbergstrasse 80

CH 4056 Basel

Switzerland

Phone: +41-61-2673826, Fax: +41-61-2673855

E-mail: J.P.Maier@unibas.ch

I. INTRODUCTION

Well resolved absorption and emission spectra of cyclic trimers have been reported only for few species, including, Al_3,[1] Li_3,[2] Cu_3,[3] H_3^+,[4] and Na_3.[5] As the small boron molecules have applications in industry as chemical insulators, explosives, semiconductors and high energy density materials, their structure is of relevance.[6-7] The boron trimer has been investigated only in rare gas matrices. First came the electron-spin-resonance observation which showed that B_3 contains an unpaired electron and that the three nuclei are equivalent.[8] The infrared spectrum of B_3 was also observed,[1] and recently the $2\,^2E' \leftarrow X\,^2A_1'$ electronic transition of B_3 in a neon matrix was identified using a mass selective approach.[9] However, there is no spectroscopic information on the boron trimer B_3 in the gas phase.

There is interest in the spectrum of cyclic B_3 because several of the excited electronic states are degenerate in D_{3h} symmetry. According to the Jahn-Teller theorem, there exists at least one vibrational mode that removes the electronic degeneracy and results in the stabilization of the lowest component by lowering the symmetry of the equilibrium structure. Most recent theoretical calculations on B_3 predicted an equilateral structure (D_{3h}) with an $^2A_1'$ electronic symmetry in the electronic ground state and an obtuse triangle (C_{2v}) with an apex angle $\geq 60^{\circ}$ for the $2\,^2E'$ excited electronic state.[8,10,11] However, a low stabilization energy (difference between the conical intersection and the minima) compared with zero point energy for the $2\,^2E'$ state is reported.[9] Therefore the B_3 molecule can be considered to have D_{3h} symmetry in the $2\,^2E'$ state as an effective structure and the $2\,^2E' \leftarrow X\,^2A_1'$ electronic system can be considered as a quasi "D_{3h} - D_{3h}" transition.

In the present work we report the observation of the rotationally resolved origin band of the $2\,^2E' \leftarrow X\,^2A_1'$ electronic spectrum of B_3. The analysis of the spectrum gives an estimate of the molecular geometry; the first gas phase structural determination.

II. EXPERIMENT

This consists of a standard cavity ring down set-up sampling a plasma generated in a pulsed supersonic slit jet expansion.[12] A small fraction of pulsed laser light from a tunable dye laser is coupled into an optical cavity consisting of two highly reflective mirrors (R > 99.99%). The fraction of light leaking out of the cavity has an envelope which is a first order exponential decay, $\exp(-t/\tau)$. The ring down time, τ, reflects the absorption coefficient. A spectrum is recorded by measuring τ as function of the wavelength of the laser (running at 30 Hz). 45 ring down events are averaged at each wavelength before the digitized data are downloaded to a workstation. The ~ 0.05 cm^{-1} linewidth of the laser was attained with an internal etalon.

The pulsed slit jet system is located in a vacuum chamber evacuated by a roots blower. The plasma is produced in a nozzle incorporating a discharge in the high pressure expansion. The orifice comprises a metal plate anode and two sharp stainless steel cathodes that form the actual slit (30 mm $\times$ 300 µm). A pulsed negative voltage (-800 V / 100 mA and 100 µs in duration) is applied. The geometry of the orifice is such that the discharge is confined upstream of the supersonic expansion. To produce B_3, solid $B_{10}H_{14}$ is heated in the oven to 70 ± 10 ºC with neon as a carrier gas at a backing pressure of 10 bar. In order to avoid condensation inside the source, the valve and body of the nozzle are heated as shown in Figure 1. The B_3 molecules are efficiently produced at a distance 5 mm down-stream from the slit. The spectrum is calibrated via the neon atomic lines that are observed in the jet expansion.

III. RESULTS

The $2\,^2E' \leftarrow X\,^2A_1'$ electronic spectrum of B_3 was initially identified in absorption in a 6 K neon matrix using mass selection with origin band located at 21828 cm^{-1}.[9] Based on

this the band was sought in the gas phase. The absorption signal was subsequently found near 21900 cm^{-1} (Figure 2) and the observed profile of the band, ~25 cm^{-1} in width, was in a good agreement with preliminary simulations. No other signal could be detected within ± 300 cm^{-1} from the observed band. Though the spectrum visually appears "noisy" (typical S/N of at least 5) all the peaks are genuine. This is shown by the top trace which is an independent recording of this part of the band. Corresponding traces were obtained for other regions proving that all the lines given in Tables 1 and 3 are real.

The spectrum exhibits rotationally resolved P and R branches slightly blended with strong neon atomic lines. The Q-branch is not visible due to a complex splitting and blending with an intense neon line. Actually, it is a composition of four spectra, as two boron isotopes are present. Because the natural isotopic abundance of ^{11}B:^{10}B in the precursor is 4:1, the relative concentration of the two isotopomers $^{33}B_3$:$^{32}B_3$ (two equivalent structures of $^{10}B^{11}B_2$) should be 4:3. The peaks in the spectra of $^{31}B_3$ and $^{30}B_3$ could not be assigned due to their small abundance. As a result, the observed spectrum is essentially an overlap of the two isotopomers $^{33}B_3$ and $^{32}B_3$.

The B_3 cyclic molecule in the excited degenerate state should undergo a deformation due to the Jahn-Teller effect, however, the distortion from an equilateral triangle can be neglected as a result of low stabilization energy (merely 39 cm^{-1} compared with a zero-point energy (1522 cm^{-1}) in the 2 $^2E''$ state[9]). A similar situation was encountered for the cyclic C_3H radical, where deformations of the C_{2v} structure were neglected due to small energy differences between the C_s and C_{2v} forms.[13] Therefore it is reasonable to assume that the effective symmetry of the 2 $^2E'$ state is D_{3h} for the analysis of the rotational structure in the observed spectrum.

The measured positions of the $^{33}B_3$ lines are given in Table 1. The spectral line frequencies were analyzed using a conventional Hamiltonian for a symmetric top molecule. In order to analyze the imperfectly resolved rotational spectrum it was assumed that the

structure of the B_3 molecule has D_{3h} symmetry in both states. This way the number of spectroscopic parameters could be reduced to 3; the bond-lengths r', r'' and band origin T_{00} were then determined directly from a least-squares fit to the line positions.

The results for the $^{33}B_3$ molecule are listed in Table 2. The determined bond-lengths (r_0) are 2% longer than the calculated ones (r_e) [9] in both the ground and excited states. In the ground state this is because of zero-point vibrations as the analysis assumes a negligible inertial defect. The difference in the excited state is additionally caused by imperfections of the simple model used (assuming an equilateral triangle $\theta = 60°$ and ignoring the Jahn-Teller effect) and anharmonicity of the potential.

The observed rotational profile was also simulated with the obtained molecular constants using the program WANG.[14] The simulated spectrum of $^{33}B_3$ is shown in Figure 2. Best agreement with the experiment was attained with a rotational temperature of 30 K. A linewidth of 0.05 cm^{-1} was used for the simulation, though in the observed spectrum it is larger due to Doppler and/or lifetime broadening.

In the case of the $^{32}B_3$ isotopomer the simulation was based on the same geometry and temperature parameters as inferred for $^{33}B_3$ but using a conventional Hamiltonian of an asymmetric top molecule. It was also assumed that only the $B_2 - A_1$ transition, which is a-type, occurs. The rotational constants used for the $^{32}B_3$ molecule were $A : B : C = 1.2696 : 1.1906 : 0.6144$ cm^{-1} for the ground, and $1.2457 : 1.1682 : 0.6029$ cm^{-1} for the excited state. The spectrum of $^{32}B_3$ was then shifted by -1.94 cm^{-1} (from T_{00} of $^{33}B_3$) to get the best agreement with the observation (Figure 2). The isotopic shift of -1.94 cm^{-1} is reasonable for an origin band.

In all, 34 rotational transitions were assigned; 14 of them are attributed to the $^{33}B_3$ molecule and the rest to $^{32}B_3$ (Table 3). The presented rotational assignment and molecular structure of the B_3 molecule should be considered as tentative, because the insufficient S/N ratio of the spectrum decreases the accuracy of the molecular structure determination. Lines

of $^{31}B_3$ (approximately 19 % of the $^{33}B_3$ intensity) disturb the line profiles of $^{32}B_3$ and $^{33}B_3$ transitions. There are few unassigned lines, few missing ones, and some are obscured by intense neon atomic lines (Figure 2). However, the consistency of the whole analysis is sufficient to conclude that the observed rotationally resolved spectrum is indeed the

$2\ ^2E' \leftarrow X\ ^2A_1'$ transition of the cyclic B_3 molecule, and leads to the first structural information in the gas phase.

ACKNOWLEDGMENTS

REFERENCES

[1] S. Li, R.J. Van Zee and W. Weltner, Chem. Phys. Lett. **262**, 298 (1996).

[2] M. Keil, H.-G. Kraemer, A. Kudell, M. A. Baig, J. Zhu, W. Demtroeder, and W. Meyer, J. Chem. Phys. **113**, 7414 (2000).

[3] A. O'Keffe, J. J. Scherer, A. L. Cooksy, R. Sheeks, J. Heath, and R. J. Saykally, Chem. Phys. Lett. **172**, 214 (1990).

[4] A. R. W. McKellar and J. K. G. Watson, J. Mol. Spectrosc. **191**, 215 (1998).

[5] H. A. Eckel, J. M. Gress, J. Biele, and W. Demtroeder, J. Chem. Phys. **98**, 135 (1993).

[6] L. Hanley, J. L. Whitten, and S. L. Anderson, J . Phys. Chem. **92,** 5803 (1988).

[7] J. D. Presilla-Marquez, C. W. Larson, and P. G. Carrick, J. Chem. Phys. **105**, 3398 (1996).

[8] Y. M. Hamrick, R.J. Van Zee, and W. Weltner, J. Chem. Phys. **96**, 1767 (1992).

[9] M. Wyss, E. Riaplov, A. Batalov, J. P. Maier, T. Weber, W. Meyer, and P. Rosmus, J. Chem. Phys. **119**, 9703 (2003).

[10] R. Hernandez and J. Simons, J. Chem. Phys. **94**, 2961 (1991).

[11] J. M. L. Martin, J. P. Francois, and R. Gijbels, J. Chem. Phys. **90**, 6469 (1989).

[12] H. Linnartz, T. Motylewski, and J. P. Maier, J. Chem. Phys. **109**, 3819 (1998).

[13] S. Yamamoto and S. Saito, J. Chem. Phys. **101**, 5484 (1994).

[14] D. Luckhaus and M. Quack, Mol. Phys. **63**, 745 (1989).

Table 1

Frequencies (in cm^{-1}) and assignments in the $2\,^2E' \leftarrow X\,^2A_1'$ absorption spectrum of $^{33}B_3$.

N_K	ν_{obs}	ν_{cal}	$\nu_{obs} - \nu_{cal}$
$1_1 - 2_2$	21850.374	21850.543	-0.169 [a]
$2_2 - 3_3$	21849.223	21849.296	-0.073
$3_3 - 4_4$	21848.070	21848.027	0.043
$4_4 - 5_5$	21846.731	21846.736	-0.005
$6_6 - 7_7$	21844.118	21844.086	0.032
$7_7 - 8_8$	21842.710	21842.727	-0.017
$1_1 - 0_0$	21855.230	21855.305	-0.075
$2_2 - 1_1$	21856.499	21856.440	0.059
$3_3 - 2_2$	21857.600	21857.552	0.048
$4_4 - 3_3$	21858.629	21858.642	-0.013
$5_5 - 4_4$	21859.690	21859.710	-0.020
$8_8 - 7_7$	21862.770	21862.778	-0.008
$9_9 - 8_8$	21863.713	21863.756	-0.043
$10_{10} - 9_9$	21864.749	21864.712	0.037

[a] Not included in the least squares fit.

Table 2

Bond-lengths and spectroscopic constants of the $^{33}B_3$ molecule inferred from the partial rotational analysis of the $2\,^2E' \leftarrow X\,^2A_1'$ electronic origin band.[a]

	$^2A_1'$		$2\,^2E'$	
	Obs.	Cal.[c]	Obs.	Cal.[c]
r_0 (Å)	1.60377(106)		1.61907(96)	
θ_0 (°)	60.0[b]		60.0[b]	
r_e (Å)		1.5706		1.5955
θ_0 (°)		60.0		60.8
T_{00} (cm^{-1})			21853.52[d]	22723
B (cm^{-1})	1.19064(157)[e]		1.16825(138)[e]	
C (cm^{-1})	0.59532(79)[e]		0.58412(69)[e]	

[a] The numbers in parentheses represent the one standard deviation derived from the least square fitting. A rms of the fitting is 0.043 cm^{-1}.

[b] Fixed.

[c] Reference 9.

[d] Error of calibration is around 0.01 cm^{-1}.

[e] The rotational constants were calculated from the determined molecular structures.

Table 3

Frequencies (in cm^{-1}) and assignments in the $2\,{}^2E' \leftarrow X\,{}^2A_1'$ absorption spectrum of ${}^{32}B_3$.[a]

$N_{K_a K_c}$	ν_{obs}	ν_{cal}	$\nu_{obs} - \nu_{cal}$
$2_{12} - 3_{13}$	21847.174	21847.197	-0.023
$2_{02} - 3_{03}$		21847.183	-0.009
$3_{13} - 4_{14}$	21845.859	21845.877	-0.018
$3_{03} - 4_{04}$		21845.876	-0.017
$4_{14} - 5_{15}$	21844.525	21844.544	-0.019
$4_{04} - 5_{05}$			
$5_{15} - 6_{16}$	21843.220	21843.188	0.032
$5_{05} - 6_{06}$			
$6_{16} - 7_{17}$	21841.821	21841.809	0.012
$6_{06} - 7_{07}$			
$7_{17} - 8_{18}$	21840.420	21840.407	0.013
$7_{07} - 8_{08}$			
$4_{14} - 3_{13}$	21856.843	21856.832	0.011
$4_{04} - 3_{03}$		21856.833	0.010
$5_{15} - 4_{14}$	21857.952	21857.934	0.018
$5_{05} - 4_{04}$			
$6_{16} - 5_{15}$	21859.041	21859.013	0.028
$6_{06} - 5_{05}$			
$7_{17} - 6_{16}$	21860.125	21860.068	0.057
$7_{07} - 6_{06}$			

[a] The assignment and calculated frequencies were derived on the assumption that the bond-lengths of ${}^{32}B_3$ and ${}^{33}B_3$ are equal, and the isotopic shift is -1.94 cm^{-1}.

Figure captions

Figure 1

Schematic diagram of the source used to produce B_3. Decaborane was heated up to

$70 \pm 10\ °C$ in the oven. Neon at a backing pressure of 10 bar was used as a carrier gas.

The pulsed plasma was produced by a slit nozzle to which the high voltage was applied.

Figure 2

Rotationally resolved $2\ ^2E' \leftarrow X\ ^2A_1'$ electronic origin band of B_3 in the gas phase measured

by cavity ring down spectroscopy through a supersonic planar plasma. The two upper traces

are independent recordings to show that the peaks are real and not noise. The three bottom

traces are the simulated patterns $^{33}B_3 + {}^{32}B_3$ (in ratio 4:3), $^{32}B_3$ and $^{33}B_3$. The two strong

lines off scale belong to neon. Bands marked with * are unassigned. Lines in the simulation

for which counterparts in the spectrum could not be found are marked with "+".
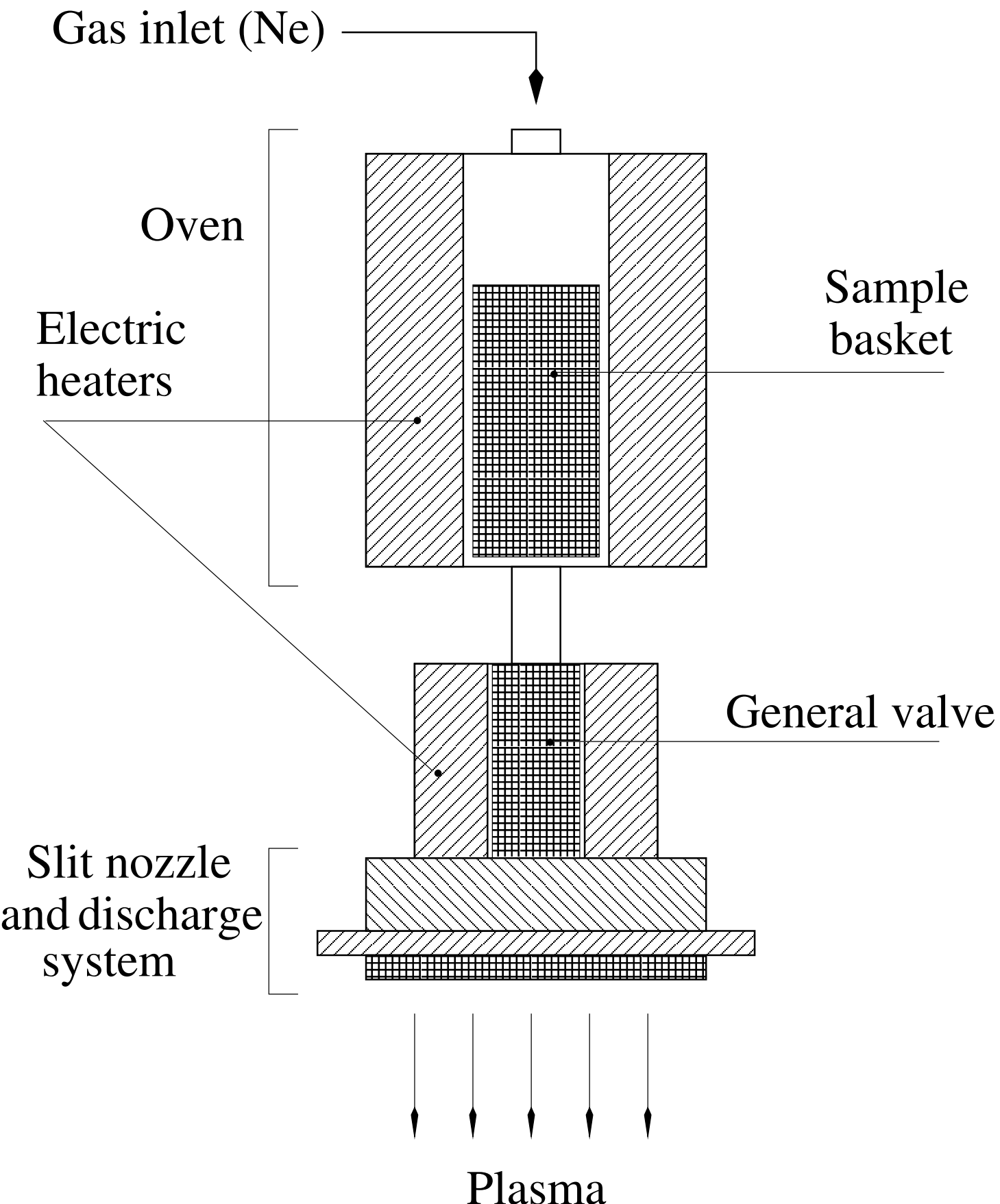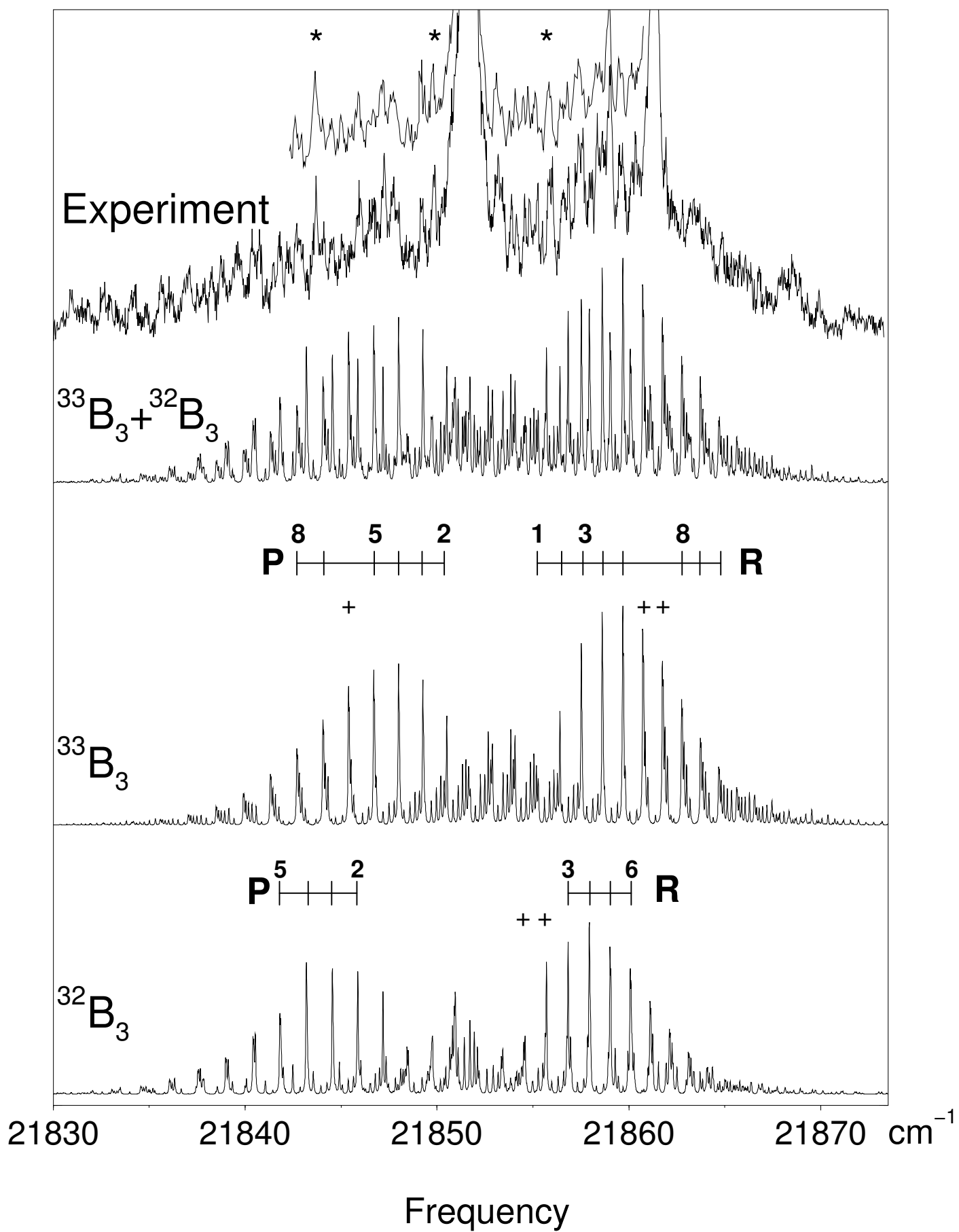
Fig. 1 – Cias et al.

Gas inlet (Ne)

Oven

Electric
heaters

Sample
basket

General valve

Slit nozzle
and discharge
system

Plasma

Fig. 2 – Cias et al.

Experiment

$^{33}B_3 + ^{32}B_3$

P 8 5 2   1 3 8 R

+   + +

$^{33}B_3$

P 5 2   3 6 R

+ +

$^{32}B_3$

21830   21840   21850   21860   21870   cm^{-1}

Frequency

Appendix to chapter 6

Considerable interest has been aroused recently also in the chemistry of mixed boron-carbon-nitrogen compounds. The reason is that some special {B, C, N} compounds were found to show superhardness. These are for example carbon nitride (CN) [55] or boron nitride (BN) [56, 57]. Because hardness is a very important material property which is essential to many high-performance engineering applications, the study of these compounds is of great technological importance. Boron carbide (BC) has potential in such diverse applications such as control rods in nuclear fission reactions [58], target tiles in nuclear fusion reactions [59, 60] and protective coating of carbon fiber materials against atomic oxygen in spacecrafts [61]. They also have a number of highly desirable mechanical, thermal, electrical, and optical properties [57, 62]. In addition, boron-nitrogen clusters have received attention because the existence of fullerens analogues involving boron and nitrogen atoms [63, 64]. In fact boron nitride is a structural analog to carbon, exhibiting bond-length, long-order parameters, and lattice constants to be very similar to those of carbon [57, 65].

The first spectroscopic studies of the smallest in the series of the boron-carbon clusters, diatomic radical BC were reported in 1988 by Knight et al. [34]. They measured ESR spectra of BC in rare gas matrices at 4 K. The $B^{12}C$ and $B^{13}C$ molecules were produced by the laser vaporization of pressed mixtures of $B/^{12}C$ and $B/^{13}C$ mounted in the conventional high temperature oven for thermal outgassing. A quadrupole mass spectrometer was employed to monitor the laser vaporized products during the matrix trapping experiment. The study of the diatomic radical BC confirmed previous theoretical predictions of a $^4\Sigma^-$ electronic ground state. The nuclear hyperfine interactions (A tensors) obtained for ^{11}B, ^{10}B, and ^{13}C from the electron spin resonance (ESR) measurements were compared with extensive *ab initio* CI calculations. The BC molecule is one of the first examples of a small high spin radical for such an in-depth experimental–theoretical comparison. The electronic structure of BC obtained from an analysis of the nuclear hyperfine interaction was compared to that obtained from a Mulliken-type population

analysis conducted on a CI wave function which yielded A_{iso} and A_{dip} results. They corresponded to the observed values.

In 1998 the vibrational spectra of linear BC_3 and B_2C_2 in an argon matrix have been observed for the first time by infrared spectroscopy [66]. Mixtures of boron and carbon powder were vaporized to 3000 K. BC_3 was produced during codeposition of the vapors with argon onto a CsI substrate maintained at 10 K. B_2C_2 was observed only after annealing the matrices. Frequencies measured at 2002.1 and 1512.5 cm^{-1} have been assigned to the $\nu_1(\sigma)$ and $\nu_2(\sigma)$ B–C stretching fundamentals of linear BC_3 and a frequency measured at 955.0 cm^{-1} has been assigned to the $\nu_3(\sigma_u)$ stretching fundamental of linear symmetric BC_2B. These assignments were based on FTIR measurements of the majority of the BC_3 and B_2C_2 isotopomer frequencies and are consistent with the results ab $initio$ study.

Different techniques have been applied to study boron-nitrogen clusters. Becker et al. used laser ionization mass spectrometry to study the formation of $B_nN_m^+$ clusters ions in a laser plasma [67, 68]. They observed that for $B_nN_{m-1}^+$ and $B_nN_{m-2}^+$ cluster ions there is an alternating abundance distribution with the higher intensities of the cluster ions with the odd number of atoms. Hassanzadeh, Andrews and co-workers carried out a reaction of the boron and nitrogen atoms in nitrogen or argon matrices [45, 69]. They identified B-B-N-N, cyclic B_2N, B-N-B, N-N-B-N, and B-N-B-N from mixed isotopic patterns, and isotopic shifts, using Fourier transform infrared spectroscopy and ab $initio$ calculations.

In 1992 Martin et al. have studied the lowest $^1\Sigma^+$ and $^3\Pi$ states of the BN molecule using multireference configuration interaction and averaged coupled-pair functional methods and large atomic natural orbital basis sets, as well as several coupled cluster methods [70]. Their best calculations strongly supported a $^3\Pi$ ground state, but the $^1\Sigma^+$ state was found to lie only 381±100 cm^{-1} higher. The $^1\Sigma^+$ state wave function exhibits strong multireference character and, consequently, the predictions of the perturbationally-based single-reference CCSD(T) coupled cluster method were not as reliable in this case as the multireference results. The best theoretical predictions for the spectroscopic

constants of BN corresponded to the experiment for the $^3\Pi$ state, but strongly suggested a misassignment of the fundamental vibrational frequency for the $^1\Sigma^+$ state.

References

[1] M. S. Reisch Chem. Eng. News. Feb 2, 9 (1987) Technical Bulletin Avco Textron Division

[2] O. Mishima, J. Tanaka, S. Yamaoka, O. Fukunaga, Science 238 (1987) 181

[3] D. Emin, Phys. Today, Jan. 55 (1987) Novel Refractory Semiconductors ; Extended Abstracts of Material Research Society, Spring Meeting

[4] D. Meinkohn, Comb. Flame 59 (1985) 225

[5] L. Pasternack, Comb. Flame 90 (1992) 259

[6] N. Presser, A. T. Pritt, Jr., Proceedings of the High Energy density Materials Contractors Conference, edited by W. J. Lauderdale and W. A. Sowell, USAF Astronautics Laboratory, Edwards AFB, CA (1987)

[7] J. D. Presilla-Marquez, C. W. Larson, P. G. Carrick, C. M. Rittby, J. Chem. Phys. 105 (1996) 3398

[8] D. Emin, Boron Hydride Chemistry, edited by E. L. Mutterties (Academic, New York, 1975)

[9] J. Niu, B. K. Rao, P. Jena, J. Chem. Phys. 107 (1997) 132

[10] A. E. Douglas, G. Herzberg, Can. J. Res. 18 (1940) 165

[11] W. R. M. Graham, W. Weltner, J. Chem. Phys. 65 (1976) 1516

[12] H. Bredohl, I. Dubois, P. Nzohabonayo, J. Mol. Spec. 93 (1982) 281

[13] L. B. Knight, Jr., B. W. Gregory, S. T. Cobranchi, D. Feller, E. R. Davidson, J. Am. Chem. Soc. 109 (1987) 3521

[14] C. R. Brazier, P. G. Carrick, J. Chem. Phys. 96 (1992) 8684

[15] S. R. Langhoff, C. W. Bauschilcher Jr., J. Chem. Phys. 95 (1991) 5882

[16] M. E. DeRose, P. G. Carrick, C. R. Brazier, J. Mol. Spec. 174 (1995) 379

[17] C. R. Brazier, P. G. Carrick, J. Chem. Phys. 100 (1994) 7928

[18] S. Tam, M. Macler, M. E. DeRose, M. E. Fajardo, J. Chem. Phys. 113 (2000) 9067

[19] M. Dupuis, B. Liu, J. Chem. Phys. 68 (1978) 2902

[20] A. A. Padgett, V. Griffing, J. Chem. Phys. 30 (1959) 1286

[21] C. F. Bender, E.R. Davidson, J. Chem. Phys. 46 (1967) 3313

[22] S. R. Langhoff, C. W. Bauschilcher Jr., J. Chem. Phys. 92 (1990) 1879

[23] R. A. Whiteside, Ph. D. Thesis, Carnegie Mellon University, Pittsburgh (1981)

[24] J. Koutecky, G. Pachcioni, G. H. Jeung, E. C. Hass, Surf. Sci. 156 (1985) 651

[25] S. Lunell, Surf. Sci. 141 (1984) 199

[26] R. Hoffman, M. Gouterman, J. Chem. Phys. 36 (1962) 2189

[27] L. Hanley, J. L. Whitten, and S. L. Anderson, J . Phys. Chem. 92 (1988) 5803

[28] A. K. Ray, I. A. Howard, K. M. Kanal, Phys. Rev. B 45 (1992) 14247

[29] Frisch, M. J.; Trucks, G. W.; Schlegel, H. B.; Scuseria, G. E.; Robb, M. A.;
Cheeseman, J. R.; Zakrzewski, V. G.; Montgomery, J. A., Jr.; Stratmann, R. E.;
Burant, J. C.; Dapprich, S.; Millam, J. M.; Daniels, A. D.; Kudin, K. N.; Strain, M.
C.; Farkas, O.; Tomasi, J.; Barone, V.; Cossi, M.; Cammi, R.; Mennucci, B.; Pomelli,
C.; Adamo, C.; Clifford, S.; Ochterski, J.; Petersson, G. A.; Ayala, P. Y.; Cui, Q.;
Morokuma, K.; Malick, D. K.; Rabuck, A. D.; Raghavachari, K.; Foresman, J. B.;
Cioslowski, J.; Ortiz, J. V.; Stefanov, B. B.; Liu, G.; Liashenko, A.; Piskorz, P.;
Komaromi, I.; Gomperts, R.; Martin, R. L.; Fox, D. J.; Keith, T.; Al-Laham, M. A.;
Peng, C. Y.; Nanayakkara, A.; Gonzalez, C.; Challacombe, M.; Gill, P. M. W.;
Johnson, B. G.; Chen, W.; Wong, M. W.; Andres, J. L.; Head-Gordon, M.; Replogle,
E. S.; Pople, J. A. Gaussian 98, revision A.7; Gaussian, Inc.: Pittsburgh, PA, 1998.

[30] G. Verhaegen, F. E. Stafford, M. Ackerman, J. Drowart, Nature 193 (1962) 1280

[31] G. Verhaegen, F. E. Stafford, J. Drowart, J. Chem. Phys. 40 (1964) 1622

[32] W. C. Easley, W. Weltner, Jr. J. Chem. Phys. 52 (1970) 1489

[33] C. Thomson, J. Chem. Phys. 58 (1973) 216

[34] L. B. Knight, Jr., S. T. Cobranchi, J. T. Petty, and E. Earl, D. Feller and E. R.
Davidson, J. Chem. Phys. 90 (1989) 690

[35] C. W. Larson, J. D. Presilla-Marquez, J. Chem. Phys. 111 (1999) 1988

[36] J. M. L. Martin, P. R. Taylor, J. Chem. Phys. 100 (1994) 9002

[37] L. B. Knight, Jr., D. W. Hill, T. J. Kirk, C. A. Arrington, J. Phys. Chem. 96
(1992) 555

[38] P. A. Roland, J. J. Wynne, J. Chem. Phys. 99 (1993) 8599

[39] C. A. Thompson and L. Andrews, J. Am. Chem. Soc. 117 (1995) 10125

[40] C. A. Thompson, L. Andrews, J. M. L. Martin, J. El-Yazal, J. Phys. Chem. 99
(1995) 13839

[41] K. R. Asmis, T. R. Taylor, D. M. Neumark, Chem. Phys. Lett. 295 (1998) 75

[42] K. R. Asmis, T. R. Taylor, D. M. Neumark, Eur. Phys. J. D 9 (1999) 257

[43] K. R. Asmis, T. R. Taylor, D. M. Neumark, J. Chem. Phys. 111 (1999) 8838

[44] K. R. Asmis, T. R. Taylor, D. M. Neumark, J. Chem. Phys. 111 (1999) 10491

[45] L. Andrews, P. Hassanzadeh, T. R. Burkholder, J. M. L. Martin, J. Chem. Phys. 98 (1993) 922

[46] J. M. L. Martin, J. P. Francois, R. Gijbels, J. Chem. Phys. 90 (1989) 6469

[47] F. Marinelli, A. Pellegatti, Chem. Phys. Lett. 158 (1989) 545

[48] R. Hernandez and J. Simons, J. Chem. Phys. 94 (1991) 2961

[49] I. A. Howard, A. K. Ray, Z. Phys. D 42 (1997) 299

[50] C. L. Yang, Z. H. Zhu, J. Mol. Struct. 571 (2001) 225

[51] Y. M. Hamrick, R.J. Van Zee, and W. Weltner, J. Chem. Phys. 96 (1992) 1767

[52] S. Li, R.J. Van Zee and W. Weltner, Chem. Phys. Lett. 262 (1996) 298

[53] H.-J. Zhai, L.-S. Wang, A. N. Alexandrova, A. I. Boldyrev, V. G. Zakrzewski, J . Phys. Chem. A 107 (2003) 9319

[54] M. Wyss, E. Riaplov, A. Batalov, J. P. Maier, T. Weber, W. Meyer, and P. Rosmus, J. Chem. Phys. 119 (2003) 9703

[55] C. M. Niu, Y. Z. Lu, C. M. Lieber, Science 261 (1993) 334

[56] A. Meller in Gemelin's Handbook of Inorganic Chemistry, 8-th ed., 3-rd supplement: Boron compounds (Springer, Berlin, 1988)

[57] J.J. Pouch, S. A. Alterovitz, Synthesis and properties of Boron Nitride, Trans Tech, Zurich, (1990)

[58] F. Kaminaga, S. Sato, Y. Okamoto, J. Nucl. Sci. Tech. 29 (1992) 121

[59] J. P. Coad, B. Farmery, J. Linke, E. Wallura, J. Nucl. Mater 200 (1993) 389

[60] T. Shikama, M. Fujitsuka, H. Araki, T. Noda, J. Nucl. Mater 191 (1992) 611

[61] B. M. Swinyard, J. Spacecr. Rockets, 28 (1991) 730

[62] P. B. Mirkarimi, K. F. McCarty, D. L. Medlin, Mater. Sci. Eng. R. 21 (1997) 47

[63] O. Stephan, Y. Bando, A. Loiseau, F. Willaime, N. Shramchenko, T. Tamiya, T Sato, Appl. Phys. A: Mater. Sci. Process. 67 (1998) 107

[64] D. Golberg, Y. Bando, O. Stephan, K. Kurashima, Appl. Phys. Lett. 73 (1998) 2441

[65] X. Blasé, A. Rubio, S. G. Louie, M. L. Cohen, Europhys. Lett. 28 (1994) 335

[66] J. D. Presilla-Marquez, P. G. Carrick, C. W. Larson, J. Chem. Phys. 110 (1999) 5702

[67] S. Becker, H.-J. Dietze, Int. J. Mass Spectrom. Ion Processes, 73 (1986) 157

[68] S. Becker, H.-J. Dietze, G. Kessler, H.-D. Bauer, W. Pompe, Z. Phys. B: Condens. Matter 81 (1990) 47

[69] P. Hassanzadeh and L. Andrews, J. Phys. Chem. 96 (1992) 9177

[70] J. M. L. Martin, T. J. Lee, G. E. Scuseria, P. R. Taylor, J. Chem. Phys. 97 (1992) 6549

CHAPTER 7

Summary

The work was focused on the spectroscopic study of carbon chain species as well as small boron clusters in the gas phase. The experimental apparatus was built before, however, in order to produce boron species. The source had to be modified as in this case a solid sample of precursor had to be used. Up to now the apparatus could be used to study the electronic transitions of variety of the species producing only by discharging a suitable gas precursor. The heating system built for this purpose worked flawlessly and the first gas-phase electronic spectrum of B_3 could be obtained. This experiment showed that solid-state precursors can be also used for the production of the exotic species in the gas phase, which increases significantly the potential of the CRD experiment. The heated source can be promising for further studies of the bare carbon chains C_6^+, C_7^+ and C_9^+. Their spectra were already measured in the neon matrix and solid precursor (perchloronaphtalene) was used in this case. Since $C_{10}Cl_8$ worked very well in the matrix experiment, it seems reasonable to assume that in the CRD experiment this precursor could work as well.

As mentioned before, cavity ringdown spectroscopy combined with a supersonic slit jet plasma have been applied to obtain gas-phase spectra of the variety of carbon chain species. They ranged from rather short ones like HC_4H^+, to relatively long such as $HC_{10}H^+$. Most of them are linear, however, spectra of the nonlinear carbon chains were also measured ($C_4H_4^+$, $C_6H_4^+$ and $C_8H_4^+$). High sensitivity of the cavity ringdown method and low temperature attained in a jet, in many cases allowed to obtain and analyze rotationally resolved electronic spectra. One of the main results of the work was obtaining the electronic spectrum of the pentaacetylene cation. It turned out to be the largest polyacetylene cation measured in the gas phase so far. Astrophysical relevance of

the $HC_{10}H^+$ was considered, however, the work showed that $HC_{10}H^+$ can not be a carrier of the DIBs. There was no match with the hitherto reported diffuse interstellar bands in the near infrared.

Apart from carbon chain species, the spectrum of the cyclic B_3 molecule was also measured. It was the first detection of this molecule in the gas phase. The analysis of the rotational structure of the spectrum allowed the geometry of the molecule to be inferred, which turned out to be the first structural information on cyclic boron trimer in the gas phase.

8. Publications.

Rotationally resolved $A^3\Sigma_u^- - X^3\Sigma_g^-$ electronic transition of NC5N

H. Linnartz [*], O. Vaizert, P. Cias, L. Grüter, J.P. Maier

Institute for Physical Chemistry, University of Basel, Klingelbergstrasse 80, CH-4056 Basel, Switzerland

Received 18 June 2001; in final form 23 July 2001

Abstract

The rotationally resolved $A^3\Sigma_u^- - X^3\Sigma_g^-$ electronic spectrum of the NC5N radical has been observed in the gas phase by cavity ring down spectroscopy in a supersonic plasma. The origin band is at $v_{00} = 22832.7(1)$ cm^{-1} and a rotational analysis gives constants $B_0'' = 0.02799(4)$ and $B_0' = 0.02778(3)$ cm^{-1}. These are compared to the B_e values available from structures predicted by density functional theory and show that the molecule has a linear and centro-symmetric NCCCCCN structure. © 2001 Elsevier Science B.V. All rights reserved.

1. Introduction

In recent years much progress has been achieved in the study of electronic transitions of highly unsaturated carbon chain radicals. Both matrix [1,2], gas phase [3–8] and theoretical studies [9,10] have been reported. These provide detailed spectroscopic information and allow for the first time a systematic comparison between astrophysical data in the optical range and gas phase laboratory spectra [11–14].

Of particular interest are the cyano- and isocyanopolyynes. Carbon chain radicals of the form HC_nN_m or C_nN_m are remarkably well represented among the species discovered by radio astronomy in interstellar space (e.g. [15,16]). The largest species detected so far in the interstellar medium is the linear $HC_{11}N$ chain [17]. In the laboratory rotational spectra of chains $HC_{2n+1}N$ with n as large as

8 have been recorded by Fourier transform microwave spectroscopy [18] and recently the $A^3\Sigma^- - X^3\Sigma^-$ electronic transition of HC_6N was observed in direct absorption [7]. Significantly less information is available for the dicyano derivatives. An exception is the C_5N_2 species for which optical data have been obtained in an argon matrix [19]. In this study visible absorption, laser-induced fluorescence and laser excitation spectroscopy as well as isotopic substitution were used to identify an intense absorption around 22 737 cm^{-1} as due to C_5N_2. These observations strongly supported a linear centro-symmetric structure, either NCCCCCN or CNCCCNC. In recent density functional theory work the bond lengths and vibrations for these two isomers, as well as for CCNCNCC were calculated [20]. These were optimized for three electronic states: the lowest triplet state ($^3\Sigma_g^-$), the lowest open-shell singlet state ($^1\Sigma_g^-$) and the lowest closed-shell singlet state ($^1\Sigma_u^+$). From a comparison of the calculated and experimentally determined vibrational frequencies for several isotopomers it was

---

[*] Corresponding author. Fax: +41-61-2673855.

E-mail address: henricus.linnartz@unibas.ch (H. Linnartz).

concluded that C_5N_2 is linear with a centro-symmetric NCCCCCN ground state structure. The corresponding triplet and open-shell singlet states were predicted to be very close in energy with the triplet below the singlet state. In the present Letter these conclusions are confirmed from the analysis of the rotationally resolved electronic gas phase spectrum.

2. Experiment

The C_5N_2 radicals are formed by a discharge through a high pressure gas pulse (typically 100 mA at −800 V for a 10 bar backing pressure) of an 0.3% cyanogen/He mixture in the throat of a 3 cm × 300 μm multilayer slit nozzle device. The details of this nozzle and cavity ring down setup have been described before [21]. Rotational temperatures of the order of 10–30 K are routinely obtained in this way. The nozzle is mounted in an optical cavity where the expansion is intersected approximately 8 mm downstream by the pulsed light beam of a dye laser (0.035 cm^{-1} bandwidth). Typically 45 ring down events are averaged at each wavelength. The calibration has been performed using a HeI line at 438.7928 nm. This limits the accuracy with which the absolute frequency can be determined to ∼0.1 cm^{-1}.
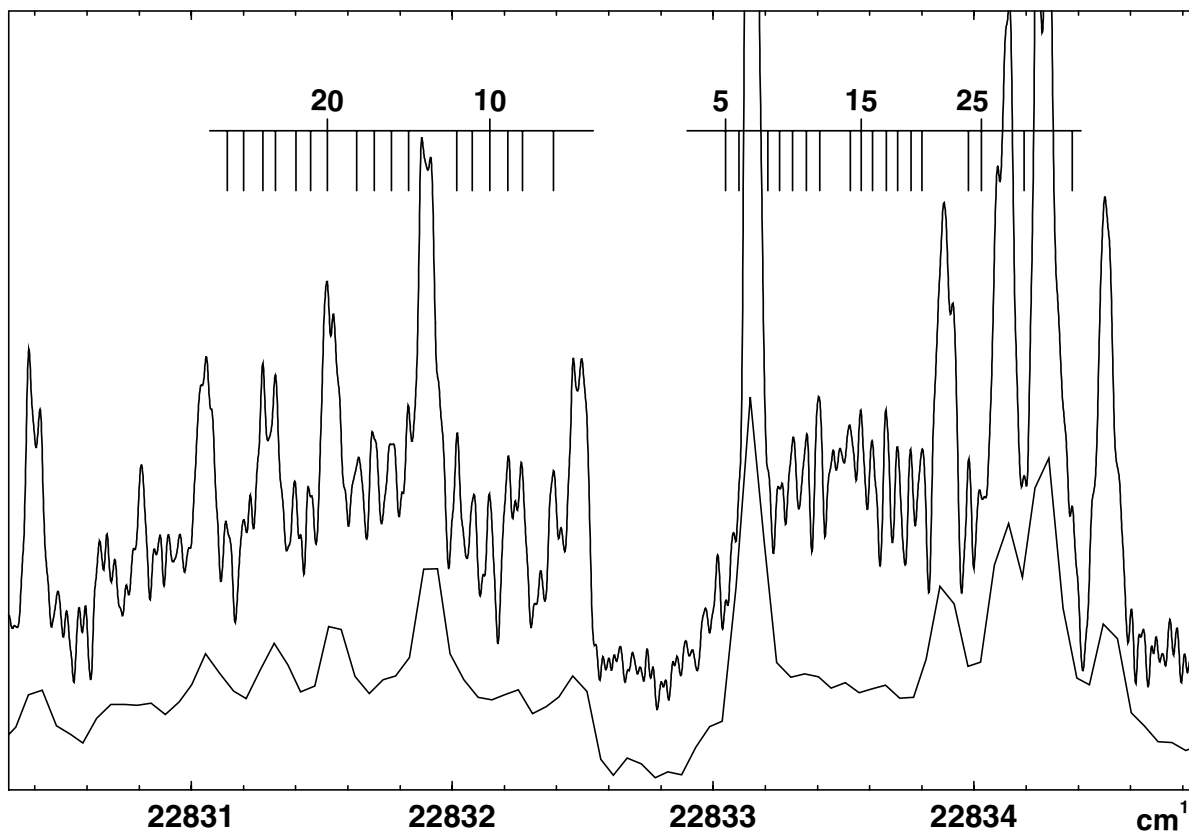

Fig. 1. In the upper trace the origin band of the $A^3\Sigma_u^- - X^3\Sigma_g^-$ electronic spectrum of C_5N_2 is shown, measured in absorption by cavity ring down spectroscopy through a supersonic planar plasma ($T_{rot} \sim 25$ K). The rotational structure is partially blended by absorption features belonging to C_2 or CN, as shown in the lower trace that is recorded at 0.15 cm^{-1} resolution under conditions that do not favour C_5N_2 formation. Nevertheless, a clear rotational progression is observable, as indicated by the solid bars, from which a linear and centro-symmetric NCCCCCN geometry is concluded (see text).

Table 1
Comparison of the experimental and theoretical spectroscopic constants for the $A^3\Sigma_u^- - X^3\Sigma_g^-$ electronic transition of NCCCCCN (cm^{-1})

	Experiment		Theory[a]		
	Ar-matrix[b]	Gas phase[c]	NCCCCCN	CNCCCNC	CCNCNCC
ν_{00}	22 737.3(2)	22 832.7(1)			
ν_{01}	24 697.8(2)	24 791(1)			
B_e'' $(^3\Sigma_g^-)$			0.02787	0.03014	0.03190
B_e'' $(^1\Sigma_g^-)$			0.02790	0.03019	0.03192
B_0''		0.02799(4)			
B_0'		0.02778(3)			

[a] Ref. [20].
[b] Ref. [19].
[c] This work.

3. Results

In Fig. 1 (upper trace) the rotationally resolved origin band of the $A^3\Sigma_u^- - X^3\Sigma_g^-$ electronic transition of NC_5N is shown. This spectrum resembles spectra recently recorded for the $A^3\Sigma - X^3\Sigma$ electronic transition of the iso-electronic HC_6N [7] and HC_7H [4,7] chains with origin bands around 471 and 505 nm. All these spectra show clearly resolved P and R branches, partially blended by transitions belonging to C_2 or CN, as shown in the lower trace of Fig. 1 for conditions that do not favour C_5N_2 formation. A Q branch is not present. Each rotational level is split into three fine structure levels characterized by the total angular momentum J ($J = N + 1$, N and $N - 1$, except for $N = 0$ where $J = 1$). This spin structure is not discernible but influences the rotational contour of the band system. A rotational N-numbering [1], is indicated in Fig. 1. In total 17 transitions in the P branch and 18 transitions in the R branch have been observed. [2] The absolute N assignment is hampered as transitions starting from low lying levels are not detected. In addition, a precise interpretation of the band gap requires knowledge of the spin–spin coupling constants in both electronic states, because the spin splittings are most significant for the lowest J-levels. Therefore, the num-

bering is based on the simulation of the band contour. For this λ'' was fixed to the ground state value recently determined for the iso-electronic HC_6N (0.36 cm^{-1} [22]) and λ' was optimized, yielding $\lambda' = 0.435(10)$ cm^{-1}. The rotational analysis of the observed spectrum was carried out using Pgopher [23]. The transitions were fitted using ν_{00}, B_0'' and B_0' as parameters. The fit has an rms of less than 0.01 cm^{-1}. Inclusion of centrifugal distortion effects does not improve the fit. The resulting values are listed in Table 1.

The ratio B_0''/B_0' is 1.0076 and reflects a small lengthening of the chain upon electronic excitation. This value is comparable to the ratios found for the corresponding transition in HC_6N (1.0051), DC_6N (1.0060) and HC_7H (1.0043) [7]. The fit yields a band origin of $\nu_{00} = 22\,832.7(1)$ cm^{-1}. The error is limited by the accuracy with which the absolute frequency can be determined. The band origin is ~95 cm^{-1} to the blue of the band observed in the argon matrix and ~60 cm^{-1} compared with unpublished spectra observed in a neon environment [24].

The fit can be used to determine the isomeric structure. Using the calculated bond lengths [20], B_e'' values are calculated for the NCCCCCN, the CNCCCNC and the CCNCNCC isomeric forms, in their electronic triplet and singlet states. The results are summarized in Table 1. Clearly, the present B_0'' value fits best to B_e'' calculated for the NCCCCCN isomer. Constraining B_0'' in the fit of the rotational line positions to the B_e'' value of one of the two other isomers gives significantly larger

---

[1] The output of the rotational fit is largely independent of the exact values of λ'' and λ' (see [7]).
[2] A list with line positions is available on request.

rms. This comparison gives additional evidence that a linear and centro-symmetric NCCCCCN structure is responsible for the $22\,737$ cm^{-1} band observed in the argon matrix spectrum [19], rather than any of the other isomers.

The ab initio work [20] predicts the two lowest electronic states, the triplet $^3\Sigma_g^-$ and open-shell singlet $^1\Sigma_g^-$, to be very close in energy. Although the triplet state was calculated to be lower, no definite conclusion was made on the nature of the ground state. The present experiment, however, confirms the triplet character of the ground state, even though triplet splittings are not resolved. Apart from the similarities with the $A^3\Sigma$–$X^3\Sigma$ electronic transition observed for the iso-electronic HC_6N and HC_7H, it also seems to be the only way in which the lack of a 2:1 spin statistical alternation for adjacent rotational levels can be explained. Only in the case of an overlap of rotational and triplet structures a loss in intensity alternation becomes possible, assuming a centro-symmetric structure. This can also explain spectral fading, as discussed in [7]. In a singlet state, however, this effect cannot take place and consequently an alternation should have been observed.

Besides the $A^3\Sigma_u^-$–$X^3\Sigma_g^-$ origin band a transition involving excitation of a CC or CN triple bond stretching vibration in the upper electronic state (labelled 1_0^1 in [19]) has been observed. This two to three times weaker band is located in the gas phase at $24\,791(1)$ cm^{-1}. [3] This corresponds to a vibrational frequency of 1958 cm^{-1} in the upper electronic state, close to the 1961 cm^{-1} value found in the argon matrix [19].

Acknowledgements

---

[3] This band is blended by a strong C_3 band and it is not possible to get a more accurate determination of the band origin.

References

[1] J.P. Maier, J. Phys. Chem. A. 102 (1998) 3462.
[2] I. Cermak, M. Forderer, I. Cermakova, S. Kalhofer, H. Stopka-Ebeler, G. Monninger, W. Kratschmer, J. Chem. Phys. 108 (1998) 10129.
[3] T.R. Taylor, C.S. Xu, D.M. Neumark, J. Chem. Phys. 108 (1998) 10018.
[4] C.D. Ball, M.C. McCarthy, P. Thaddeus, J. Chem. Phys. 112 (2000) 10149.
[5] D. Pfluger, T. Motylewski, H. Linnartz, W.E. Sinclair, J.P. Maier, Chem. Phys. Lett. 329 (2000) 29.
[6] N.M. Lakin, F. Guthe, M. Tulej, M. Pachkov, J.P. Maier, Faraday Discuss. 115 (2000) 383.
[7] O. Vaizert, T. Motylewski, M. Wyss, E. Riaplov, H. Linnartz, J.P. Maier, J. Chem. Phys. 114 (2001) 7918.
[8] T. Pino, H.B. Ding, F. Guthe, J.P. Maier, J. Chem. Phys. 114 (2001) 2208.
[9] Z.X. Cao, S.D. Peyerimhoff, Phys. Chem. Chem. Phys. 3 (2001) 1403.
[10] Z.X. Cao, S.D. Peyerimhoff, J. Phys. Chem. A 105 (2001) 627.
[11] M. Tulej, D.A. Kirkwood, M. Pachkov, J.P. Maier, Astrophys. J. 506 (1998) L69.
[12] C.D. Ball, M.C. McCarthy, P. Thaddeus, Astrophys. J. Lett. 529 (1999) L61.
[13] T. Motylewski, H. Linnartz, O. Vaizert, J.P. Maier, G.A. Galazutdinov, F.A. Musaev, J. Krelowski, G.A.H. Walker, D.A. Bohlender, Astrophys. J. 531 (2000) 312.
[14] P. Brechignac, T. Pino, N. Boudin, Spectrochim. Acta A 57 (2001) 745.
[15] M. Guélin, N. Neininger, J. Cernicharo, Astron. Astrophys. 335 (1998) L1.
[16] M.B. Bell, J.K.G. Watson, P.A. Feldman, M.J. Travers, Astrophys. J. 508 (1998) 286.
[17] M.B. Bell, P.A. Feldman, M.J. Travers, M.C. McCarthy, C.A. Gottlieb, P. Thaddeus, Astrophys. J. 483 (1997) L61.
[18] M.C. McCarthy, W. Chen, M.J. Travers, P. Thaddeus, Astrophys. J. Suppl. Ser. 129 (2000) 611.
[19] A.M. Smith, C. Engel, A. Thoma, G. Schallmoser, B.E. Wurfel, V.E. Bondybey, J. Chem. Phys. 184 (1994) 233.
[20] J. Tittle, D. Merkoziaj, R. Liu, Chem. Phys. Lett. 305 (1999) 451.
[21] T. Motylewski, H. Linnartz, Rev. Sci. Instrum. 70 (1999) 1305.
[22] V.D. Gordon, M.C. McCarthy, A.J. Apponi, P. Thaddeus, Astrophys. J. 540 (2000) 286.
[23] C.M. Western, School of Chemistry, University of Bristol, UK, PGOPHER, 1994 and 1998.
[24] A.M. Smith-Gicklhorn, M. Lorenz, M. Frankowski, R. Kolos, V.E. Bondybey, Chem. Phys. Lett. (submitted).

Rotationally resolved $A^2\Pi_u \leftarrow X^2\Pi_g$ electronic transition of NC_6N^+

H. Linnartz,[a] D. Pfluger, O. Vaizert, P. Cias, P. Birza, D. Khoroshev, and J. P. Maier

Institute for Physical Chemistry, Klingelbergstrasse 80, CH-4056 Basel, Switzerland

The rotationally resolved $A^2\Pi_u \leftarrow X^2\Pi_g$ electronic origin band spectrum of dicyanodiacetylene cation, NC_6N^+, has been recorded in the gas phase using frequency-production double modulation spectroscopy in a liquid nitrogen cooled hollow cathode discharge and cavity ring down spectroscopy in a supersonic plasma. The analysis of the complementary results provides accurate molecular parameters for the two spin-orbit components in both electronic states. © 2002 *American Institute of Physics.* [DOI: 10.1063/1.1427710]

I. INTRODUCTION

In recent years several cyanopolyacetylene radicals (HC_nN) have been studied by Fourier transform microwave spectroscopy[1,2] and, following their laboratory detection, species as large as $HC_{11}N$ have been identified by radio astronomy in the interstellar medium.[3] The dicyano derivatives (NC_nN) may be comparably abundant in space, but are unsuitable for microwave detection due to absence of a dipole moment. In this case accurate spectroscopic information can be obtained from high resolution studies of vibrational or electronic transitions in the gas phase. The latter are available for a series of carbon chain radicals. Examples are the nonpolar NC_5N (Ref. 4) and HC_7H,[5,6] as well as chains that were already detected in dense interstellar clouds such as HC_6N (Ref. 6) and C_6H.[7] These species are formed in ion-molecule reactions and consequently spectroscopic information on carbon chain ions is needed as well, but high resolution data are rare and pure rotational spectra are limited to a few species.[8]

This is particularly true for the (di)cyanopolyacetylene cations. Electronic spectra have been recorded in neon matrices for $NC_{2n}N^+$ ($n=2-6$) and $HC_{2n+1}N^+$ ($n=2-6$).[9–12] Following these and low resolution emission studies[13–15] the rotationally resolved electronic gas phase spectrum of the cyanodiacetylene (HC_5N^+) and dicyanoacetylene (NC_4N^+)[16] as well as the cyanotriacetylene (HC_7N^+)[17] were reported. In the present work the rotationally resolved spectrum of the next larger member in the dicyano-series, NC_6N^+, is presented. The results are compared with the results of density functional theory calculations[18] and the spectroscopic parameters available for the iso-electronic chains HC_7N^+ (Ref. 17) and HC_8H^+.[19]

II. EXPERIMENT

The spectra are recorded using two complementary experimental approaches. These are frequency production double modulation (FPM) spectroscopy of a static plasma generated in a discharge cell ($T_{rot} \sim 150$ K) and cavity ring-down (CRD) spectroscopy sampling a supersonic planar

plasma ($T_{rot} = 15$ K), yielding spectra with significantly different rotational profiles. Both experimental techniques have been described. In the FPM experiment[20] mixtures of 0.5%–0.6% cyanogen/He are discharged in a liquid nitrogen cooled hollow cathode incorporated into a White-type multiple reflection cell ($L_{tot} \sim 100$ m). Production modulation is obtained by applying a rectified 17 kHz ac voltage (−500 to 700 V). The laser beam is electro-optically modulated at a radio frequency of 192 MHz and detected by a fast photodiode. Subsequent phase sensitive demodulation of the high frequency portion of the signal during a production cycle gives absorption bands that have a derivativelike shape. The resolution is Doppler limited and typically of the order of 550 MHz.

In the CRD setup[21] the NC_6N^+ radicals are formed by a discharge through a high pressure gas pulse (typically 100 mA at −1000 V for a 12 bar backing pressure) of an 0.2% cyanogen/He mixture in the throat of a 3 cm×300 μm multilayer slit nozzle device. A standard CRD spectrometer is used to detect the signals in direct absorption. The resolution is limited by the bandwidth of the laser to ~0.035 cm^{-1}. In both experiments iodine spectra are used for an absolute frequency calibration.

III. RESULTS AND DISCUSSION

An overview scan of the $A^2\Pi_u \leftarrow X^2\Pi_g$ electronic origin band transition of NC_6N^+ recorded by FPM in the discharge cell is shown in Fig. 1. In the range 15 240–15 248 cm^{-1} approximately 200 individual absorption lines are resolved. These transitions belong to the P-, Q- and R-branches of two subbands corresponding to the parallel $A^2\Pi_{3/2} \leftarrow X^2\Pi_{3/2}$ and $A^2\Pi_{1/2} \leftarrow X^2\Pi_{1/2}$ electronic transitions. The intensity ratio of the two bands is determined by the "spin-orbit temperature" and the value of the spin-orbit splitting (A'') in the ground state. The latter is estimated from previous studies to be of the order of $-40(5)$ cm^{-1},[16] the minus indicating that the $\Omega = \frac{3}{2}$ spin-orbit component is lower in energy than the $\Omega = \frac{1}{2}$. At the high ambient temperature in the cell both spin-orbit components are equally intense. The rotational population is distributed over many levels and the intensity of both Q-branches and transitions starting from low J-levels is low. Clear band heads, however, are missing. Moreover, the spin-
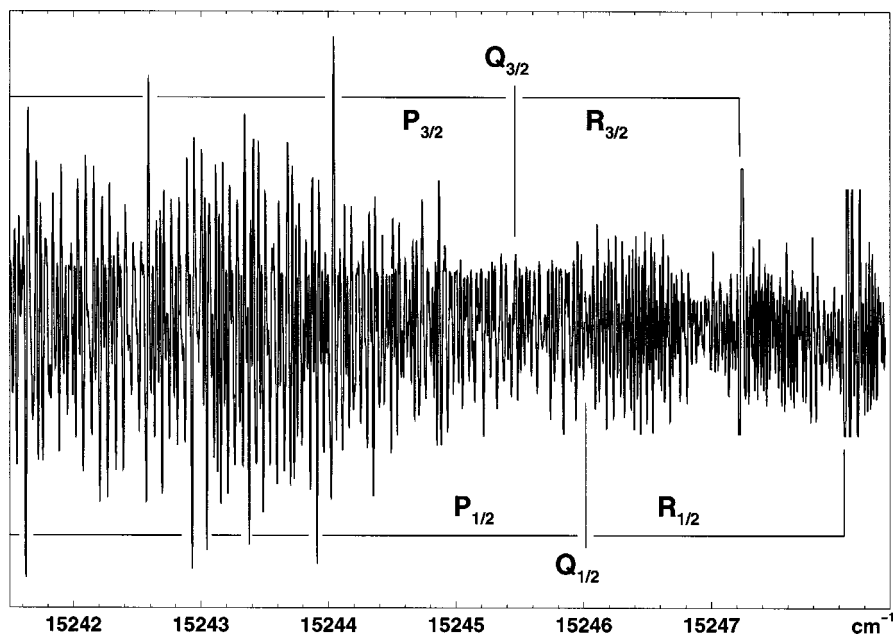
FIG. 1. Rotationally resolved frequency production double modulation absorption spectrum of the $A^2\Pi_u \leftarrow X^2\Pi_g$ electronic origin band of NC_6N^+ measured in a liquid-nitrogen cooled hollow cathode discharge ($T_{rot} \sim 150$ K). The P-, Q- and R-branches of the $A^2\Pi_{3/2} \leftarrow X^2\Pi_{3/2}$ and $A^2\Pi_{1/2} \leftarrow X^2\Pi_{1/2}$ subbands are indicated.

orbit components overlap as the difference in spin-orbit splittings in ground and excited state, ΔA, appears to be small. All these factors together lead to ambiguity in the assignment of the rotational lines. What is missing is a clearly defined starting point. This is provided by the jet spectrum.

In Fig. 2 part of the spectral region of Fig. 1 is shown. The spectrum is recorded by CRD in the plasma expansion. Only the lower subband, $A^2\Pi_{3/2} \leftarrow X^2\Pi_{3/2}$, is clearly visible now, as the population of the upper spin-orbit component is low. Besides unresolved P- and R-branches,[22] a clear Q-branch is observed starting at $15\,245.46(3)$ cm^{-1}. This branch is not visible in Fig. 1, but the CRD position allows the assignment of transitions belonging to the $A^2\Pi_{3/2} \leftarrow X^2\Pi_{3/2}$ subband within ± 1 J quantum numbering in the FPM spectrum. The band gap is $\sim 10B$ [with $B \sim 0.019$ cm^{-1} (Ref. 18)] reflecting that the lowest rotational transitions cor-

respond to $P(\frac{5}{2})$ and $R(\frac{3}{2})$. Adjacent transitions are separated by $\sim 2B$. In this way more than $80(40)$ transitions have been assigned in $P(R)$-branch of the $A^2\Pi_{3/2} \leftarrow X^2\Pi_{3/2}$ band with J-values up to 90.5.[23] These values are then fitted with PGopher[24] using ν_0, B_0'', B_0', D_0'' and D_0' as variables yielding a rms of 0.002 cm^{-1}. The resulting constants are listed in Table I. The value for $B_0'' = 0.018\,753\,3(55)$ cm^{-1} is close to the B_e-value of $0.018\,67$ cm^{-1} as obtained from density functional calculations.[18] A simulation using these constants proves that the stronger feature in Fig. 1 at $15\,247.23(3)$ cm^{-1} corresponds to the R-branch band head of the $A^2\Pi_{3/2} \leftarrow X^2\Pi_{3/2}$ system. A similar feature is observed at $15\,247.85$ cm^{-1} and is tentatively assigned to the R-branch band head of the second spin-orbit system.

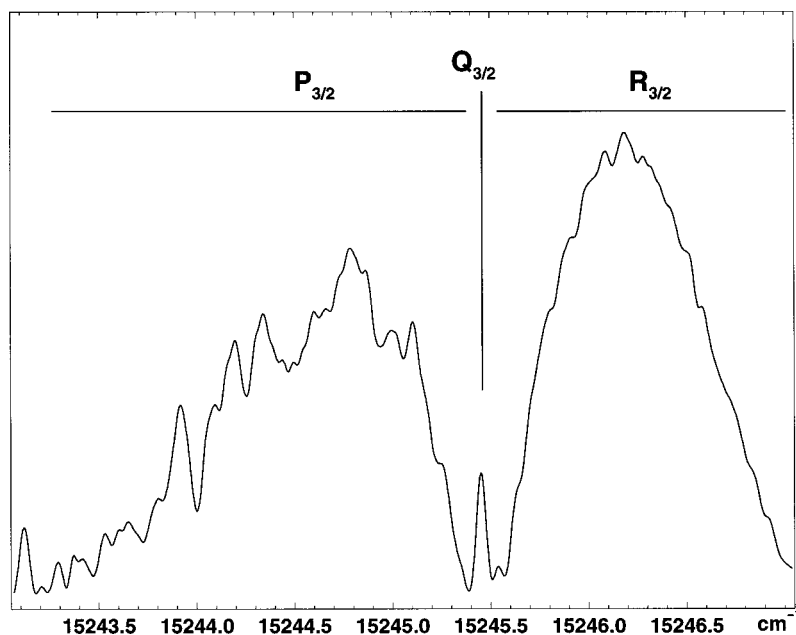The lines that are left over are mainly due to the $\Omega = \frac{1}{2}$

FIG. 2. Cavity ring down absorption spectrum of the $A^2\Pi_{3/2} \leftarrow X^2\Pi_{3/2}$ electronic origin band of NC_6N^+, recorded through a supersonic plasma. The second spin-orbit component is not visible at the low temperature in the jet ($T_{rot} \sim 15$ K). The Q-branch position is used to assign the FPM spectrum.

TABLE I. Molecular constants (in cm^{-1}) for the $A^2\Pi_{3/2}-X^2\Pi_{3/2}$ and for the $A^2\Pi_{1/2}-X^2\Pi_{1/2}$ electronic origin band transition of NC_6N^+. The molecular parameters for the $A^2\Pi_u \leftarrow X^2\Pi_g$ electronic origin band transition of the iso-electronic HC_7N^+ (Ref. 17) and HC_8H^+ (Ref. 19) species are listed for comparison.

| | NC_6N^+ | | HC_7N^+ | HC_8H^+ |
	$\Omega=3/2$	$\Omega=1/2$	$\Omega=3/2$	$\Omega=3/2$ and $1/2$
B_0''	0.018 753 3(55)	0.018 707(19)	0.018 966 5(71)	0.019 077 9(93)
D_0''	$6.7(15).10^{-9}$	$6.2(38).10^{-9}$		
B_0'	0.018 558 5(56)	0.018 565(19)	0.018 773 1(72)	0.018 867 3(94)
D_0'	$7.1(16).10^{-9}$	$8.3(39).10^{-9}$		
ΔB	-0.00019	-0.00014	-0.00019	-0.00021
ΔA	$+0.56$		-2.04	-3.00
ν_0	15 245.737(1)		14 925.423(4)	14 143.1815(5)

component. The rotational assignment is problematic now as information on the Q-branch of the $A^2\Pi_{1/2} \leftarrow X^2\Pi_{1/2}$ band is missing. The difference between the band heads, however, indicates that the $Q_{1/2}$-branch is expected around 15 246.1 cm^{-1}. In addition, only minor differences between the rotational constants for the two spin-orbit systems are expected. In previous studies transitions originating from different spin-orbit components were fitted with one single set of rotational parameters.[7,16,19] In the present experiment this turns out not to be possible. However, as long as the effect of spin uncoupling is small, i.e., $2BJ \ll |A|$, B is best replaced by effective parameters $B_{eff}(^2\Pi_{1/2})$ and $B_{eff}(^2\Pi_{3/2})$. In second order perturbation theory the difference ΔB_{eff} is given by

$$\Delta B_{eff} = \frac{2B^2}{\bar{A}}, \tag{1}$$

where $\bar{A} = A - 2B$.[25] A is expected to be of the order of $-40(5)$ cm^{-1} (Ref. 16) which puts an additional constraint to the fit. The line positions and most likely assignment for

transitions belonging to the $A^2\Pi_{1/2} \leftarrow X^2\Pi_{1/2}$ system are available from (Ref. 26). The resulting molecular parameters are given in Table I. The quality of the fit will be worse as only a few transitions share a common level (rms ~ 0.004 cm^{-1}).[26] Nevertheless, using Eq. (1) an A''-value between -15 and -32 cm^{-1} is calculated.[27] The simulation confirms that the band head position coincides with the feature at 15 247.85 cm^{-1}.

The spectral features of NC_6N^+ are expected to be qualitatively similar to those of the iso-electronic cyanotriacetylene cation[17] and tetraacetylene cation.[19] The molecular parameters of the $A^2\Pi_u \leftarrow X^2\Pi_g$ electronic origin bands of these two ions are listed in Table I as well. These bands are shifted to lower energy, by 320 cm^{-1} for HC_7N^+ and by 1103 cm^{-1} for HC_8H^+. The ΔA value of HC_7N^+ (-2.04 cm^{-1}) is comparable to that of HC_8H^+ (-3.00 cm^{-1}), but the corresponding value for NC_6N^+ is significantly smaller and, moreover, is positive ($+0.56$ cm^{-1}). This value, however, is very close to the $\Delta A = +0.53$ cm^{-1} found for NC_4N^+.[16] There it was concluded that this anomaly is due to a spin-orbit induced interaction of the upper $A^2\Pi_{1/2}$ electronic state with another low lying electronic state, presumably of $^2\Sigma$ character, whereas the $A^2\Pi_{3/2}$ state is not affected. This becomes clear from the different values for $\Delta B = B_0' - B_0''$: for the $\Omega = \frac{3}{2}$ component a value of 0.000 19 cm^{-1} is found, similar to the values determined for HC_7N^+ (0.000 19 cm^{-1}) and HC_8H^+ (0.000 21 cm^{-1}), but for $\Omega = \frac{1}{2}$ the value decreases to 0.000 14 cm^{-1}. The second-order spin-orbit contribution to the rotational constant for a Π state is given by[28,29]

$$B^{(2)} = \Sigma_{n \neq 0} \frac{4B^2}{E_0^0 - E_n^0}. \tag{2}$$

With $|\Delta E| = 40$ cm^{-1} this gives $B^{(2)} \sim 0.000 04$ cm^{-1}, i.e., an unperturbed value for ΔB of 0.000 18 cm^{-1}, close to the value of the other spin-orbit component.

In the case of NC_4N^+ it was also found that the $^2\Sigma - ^2\Pi$ interaction removes the degeneracy of the e- and
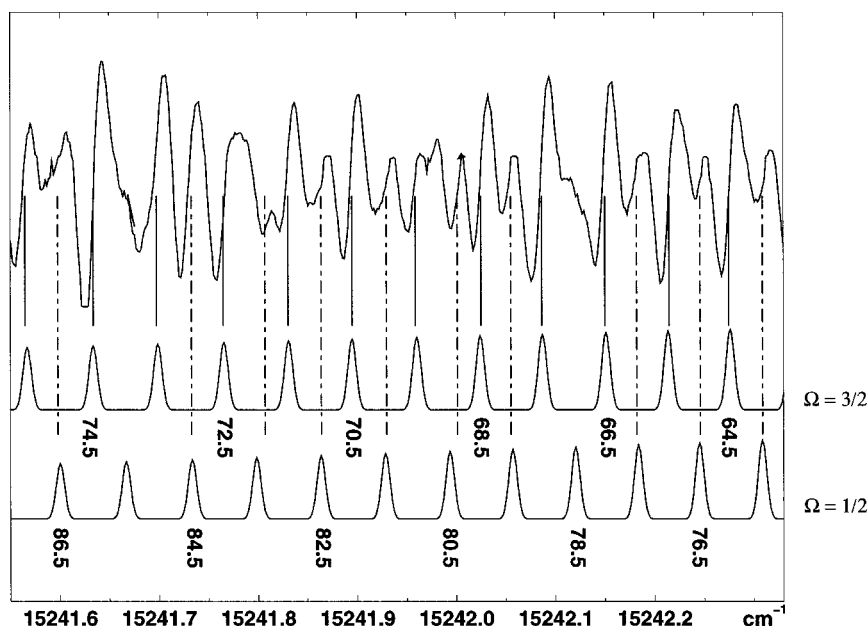

FIG. 3. High J-level transitions with their typical $1f$ derivative line shapes recorded in the FPM experiment. The simulated spectrum is shown for both spin-orbit components. There is no evidence for Λ-doubling (see the text).

f-symmetry, resulting in a resolvable Λ-doubling. This effect is not observed here. In Fig. 3 part of the P-branch range for high J-levels in both spin-orbit components is shown. The simulated spectrum is given as well. Clearly, there is no evidence for Λ-doubling within the experimental resolution: the size of the splitting would have been J-dependent and the expected 2:1 spin-statistical alternation is lacking. This is also expected: the rotational constant of NC_6N^+ is 2.5 times smaller than that of NC_4N^+ (~ 0.044 cm^{-1}) and since the Λ-type doubling constants p and q are proportional to B and B^2, respectively, splittings will be considerably smaller.

ACKNOWLEDGMENTS

[1] M. C. McCarthy, J. U. Grabow, M. J. Travers, W. Chen, C. A. Gottlieb, and P. Thaddeus, Astrophys. J. **494**, L231 (1998).

[2] M. C. McCarthy and P. Thaddeus, Chem. Soc. Rev. **30**, 177 (2001).

[3] M. B. Bell, P. A. Feldman, M. J. Travers, M. C. McCarthy, C. A. Gottlieb, and P. Thaddeus, Astrophys. J. **483**, L61 (1997).

[4] H. Linnartz, O. Vaizert, P. Cias, L. Grüter, and J. P. Maier, Chem. Phys. Lett. **345**, 89 (2001).

[5] C. D. Ball, M. C. McCarthy, and P. Thaddeus, J. Chem. Phys. **112**, 10149 (2000).

[6] O. Vaizert, T. Motylewski, M. Wyss, E. Riaplov, H. Linnartz, and J. P. Maier, J. Chem. Phys. **114**, 7918 (2001).

[7] H. Linnartz, T. Motylewski, O. Vaizert, J. P. Maier, A. J. Apponi, M. C. McCarthy, C. A. Gottlieb, and P. Thaddeus, J. Mol. Spectrosc. **197**, 1 (1999).

[8] C. A. Gottlieb, A. J. Apponi, M. C. McCarthy, P. Thaddeus, and H. Linnartz, J. Chem. Phys. **113**, 1910 (2000).

[9] J. Agreiter, A. M. Smith, M. Härtle, and V. Bondybey, Chem. Phys. Lett. **225**, 87 (1994).

[10] D. Forney, P. Freivogel, J. Fulara, and J. P. Maier, J. Phys. Chem. **102**, 1510 (1995).

[11] J. Agreiter, A. M Smith, and V. Bondybey, Chem. Phys. Lett. **241**, 317 (1995).

[12] A. M. Smith, J. Agreiter, and V. Bondybey, Chem. Phys. Lett. **244**, 379 (1995).

[13] E. Kloster-Jensen, J. P. Maier, O. Marthaler, and M. Mohraz, J. Chem. Phys. **71**, 3125 (1979).

[14] G. Bieri, E. Kloster-Jensen, S. Kvisle, J. P. Maier, and O. Mathaler, J. Chem. Soc., Faraday Trans. **76**, 676 (1980).

[15] J. P. Maier, L. Misev, and F. Thommen, J. Phys. Chem. **86**, 54 (1982).

[16] W. E. Sinclair, D. Pfluger, and J. P. Maier, J. Chem. Phys. **111**, 9600 (1999).

[17] W. E. Sinclair, D. Pfluger, D. Verdes, and J. P. Maier, J. Chem. Phys. **112**, 8899 (2000).

[18] S. Lee, J. Phys. Chem. **100**, 13959 (1996).

[19] D. Pfluger, T. Motylewski, H. Linnartz, W. E. Sinclair, and J. P. Maier, Chem. Phys. Lett. **329**, 29 (2000).

[20] W. E. Sinclair, D. Pfluger, H. Linnartz, and J. P. Maier, J. Chem. Phys. **110**, 296 (2000).

[21] T. Motylewski and H. Linnartz, Rev. Sci. Instrum. **70**, 1305 (1999).

[22] No rotational resolution has been obtained, presumably because of residual Doppler broadening.

[23] See EPAPS Document No. E-JCPSA6-116-004204 for a list with line positions and observed-calculated values. This document may be retrieved via the EPAPS homepage (http://www.aip.org/pubserv/epaps.html) or from ftp.aip.org in the director /epaps/. See the EPAPS homepage for more information.

[24] C. M. Western, School of Chemistry, University of Bristol, UK, PGOPHER, 1994 and 1998.

[25] H. W. Kroto, *Molecular Rotation Spectra* (Wiley, New York, 1975), p. 232.

[26] See Ref. 23.

[27] Shifting the rotational assignment by ± 1 J gives values of -7 and -115 cm^{-1}.

[28] J. H. van Vleck, Rev. Mod. Phys. **23**, 213 (1951).

[29] R. F. Curl, Mod. Phys. **9**, 585 (1965).

NOTE

Rotationally Resolved $\tilde{A}\,^2\Pi_u$–$\tilde{X}\,^2\Pi_g$ Electronic Transition of HC$_4$D$^+$

Key Words: diacetylene cation.

The diacetylene cation, HC$_4$H$^+$, is considered to be a reactive intermediate in plasma, combustion, and astrochemical reaction schemes and has been the topic of several spectroscopic studies (*1–4*). The first assigned gas phase spectrum dates back to 1956 (*1*) when previously observed emission spectra (*2*) were identified as the origin band of the $\tilde{A}\,^2\Pi_u \leftarrow \tilde{X}\,^2\Pi_g$ electronic transition. In subsequent emission studies the absolute rotational numbering was verified (*3*) and the bond lengths in the $\tilde{X}\,^2\Pi$ ground and $\tilde{A}\,^2\Pi$ electronically excited state were determined for the vibrational ground state upon isotopic substitution (*4*). The only main isotopic geometry not studied spectroscopically so far is the mixed diacetylene cation: H^{12}C$_4$D$^+$. In this note the line positions and a rotational analysis of the origin band of the $\tilde{A}\,^2\Pi_u \leftarrow \tilde{X}\,^2\Pi_g$ electronic spectrum of this molecule are presented.

The HC$_4$D$^+$ cations were generated in a high pressure planar plasma expansion by discharging a gas pulse of a 0.25% HCCH and 0.25% DCCD mixture in argon in the throat of a 3-cm × 300-μm multilayer slit nozzle geometry (*5*). Cavity ring down spectroscopy was used to observe the species in direct absorption (*6*). An iodine spectrum was recorded simultaneously for absolute frequency calibration.

In the upper trace of Fig. 1 part of the $\tilde{A}\,^2\Pi_u \leftarrow \tilde{X}\,^2\Pi_g$ electronic origin band transition of HC$_4$D$^+$ is shown, recorded under conditions that are optimized for strong rotational cooling (T$_{rot}$ = 15 K). The lower trace shows the same spectral region for a higher rotational temperature of about 50 K. In the cold spectrum mainly the lower spin–orbit component ($\tilde{A}\,^2\Pi_{3/2}$–$\tilde{X}\,^2\Pi_{3/2}$) is observed; the population of the other spin–orbit component is moderate for the low rotational temperatures in the jet and a ground state spin–orbit splitting that amounts to approximately $A'' = -31$ cm^{-1} (*4*). In the warmer spectrum transitions originating from the second spin–orbit component ($\tilde{A}\,^2\Pi_{1/2}$–$\tilde{X}\,^2\Pi_{1/2}$) are visible as well. The higher temperature is reflected in the appearance of more pronounced
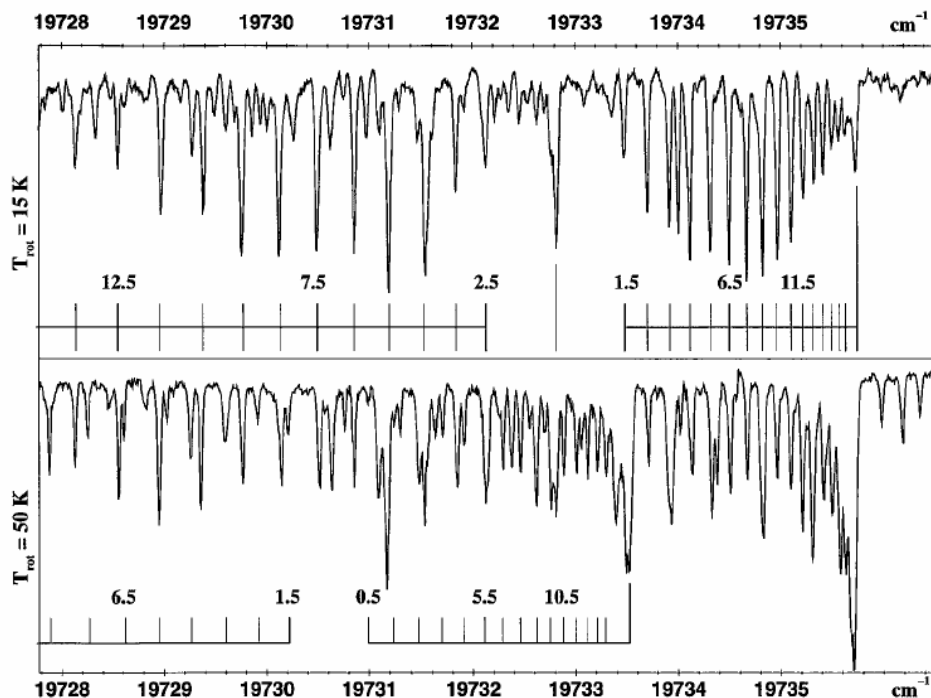
FIG. 1. The origin band in the $\tilde{A}\,^2\Pi_u \leftarrow \tilde{X}\,^2\Pi_g$ electronic origin band transition of HC$_4$D$^+$, measured by cavity ring down spectroscopy through a supersonic planar plasma. The upper trace is recorded for T$_{rot} \sim$ 15 K, the lower trace for T$_{rot} \sim$ 50 K. In the cold spectrum mainly transitions of the $\tilde{A}\,^2\Pi_{3/2}$–$\tilde{X}\,^2\Pi_{3/2}$ component are seen. In the warmer spectrum transitions belonging to the upper spin–orbit system, $\tilde{A}\,^2\Pi_{1/2}$–$\tilde{X}\,^2\Pi_{1/2}$, become visible.

TABLE 1
Line Positions (in cm⁻¹) for the Origin Band of the $\tilde{A}\,^2\Pi_u \leftarrow \tilde{X}\,^2\Pi_g$ Electronic Transition of HC₄D⁺

	$\Omega = 3/2$				$\Omega = 1/2$			
J	P-branch	o-c^a	R-branch	o-c^a	P-branch	o-c^a	R-branch	o-c^a
0.5							19730.99	−14
1.5			19733.48	10	19730.20	1	19731.24	−7
2.5	19732.13	−11	19733.70	0	19729.92	13	19731.47	−9
3.5	19731.84	2	19733.92	3	19729.60	−2	19731.70	2
4.5	19731.53	7	19734.12	−2	19729.27	−14	19731.91	6
5.5	19731.20	4	19734.32	6	19728.95	−5	19732.11	11
6.5	19730.86	4	19734.50	6	19728.62	7	19732.29	9
7.5	19730.50	−5	19734.67	7	19728.27	11	19732.46	9
8.5	19730.14	−1	19734.82	2	19727.89	−2	19732.62	12
9.5	19729.77	5	19734.96	−2	19727.51	−4	19732.75	−4
10.5	19729.38	3	19735.10	7	19727.12	−3	19732.88	−7
11.5	19728.96	−16	19735.21	−3	19726.70	−19	19733.00	−7
12.5	19728.55	−13	19735.31	−9			19733.12	−6
13.5	19728.14	2	19735.41	−4			19733.21	−2
14.5	19727.70	−1	19735.49	−7	19725.44	4	19733.30	−6
15.5	19727.25	−2	19735.57	3	19724.98	−3		
16.5			19735.63	5	19724.52	1		
17.5					17924.05	8		
18.5					19723.56	7		
19.5					19723.06	9		

^{a} Observed minus calculated in units of 10^{-3} cm⁻¹.

bandheads and a weaker Q-branch for the $\Omega = \frac{3}{2}$ component. The cold spectrum allows an unambiguous rotational assignment of the $\tilde{A}\,^2\Pi_{3/2}$–$\tilde{X}\,^2\Pi_{3/2}$ band system with a band gap of approximately 10 B. The warmer spectrum provides line positions for higher J-levels in the $\Omega = \frac{3}{2}$ component as well as transitions originating from the $\Omega = \frac{1}{2}$ component. The rotational assignment

TABLE 2
Rotational Constants (in cm⁻¹) for the Origin Band of the $\tilde{A}\,^2\Pi_u \leftarrow \tilde{X}\,^2\Pi_g$ Electronic Transition of HC₄D⁺

ν_{00}	19731.725(2)
B_0''	0.136 599(30)
$D_0''\ (10^{-8})$	2.1(3)
B_0'	0.130 469(30)
$D_0'\ (10^{-8})$	2.1(3)
ΔA	2.2(1)

is given for $\Omega = \frac{3}{2}$ in the upper trace and for $\Omega = \frac{1}{2}$ in the lower trace. Some remaining lines, particularly in the warmer spectrum, are due to transitions originating from HC₄H⁺ and DC₄D⁺ as can be concluded from the line positions given in Ref. (4).

A combined analysis of the two spectra with about 60 transitions (Table 1) allows an accurate determination of the rotational parameters. The rotational analysis of the data has been performed using the program PGopher (7). The line positions were fitted with an effective Hamiltonian where both spin–orbit components were considered simultaneously. The band origin and rotational B-constants were varied. The centrifugal distortion constants were fixed to the values found for HC₄H⁺ and DC₄D⁺ (4). As the spin–orbit splittings A'' and A' are highly correlated in the fit, ΔA has been determined instead. The fit has an rms of 0.007 cm⁻¹, significantly smaller than the observed linewidth of approximately 0.035 cm⁻¹ (FWHM). The resulting constants are listed in Table 2. These values are in between the values found for the two other main isotopes, HC₄H⁺ and DC₄D⁺ (4), as may be expected.

The rotational constants found here allow an additional check of the change in overall length of the diacetylene cation upon electronic excitation, using Kraitchman's equations (8). This yields an H–H distance in the $\tilde{X}\,^2\Pi_g$ ($\tilde{A}\,^2\Pi_u$) state of 592 (600) pm, which is in perfect agreement with the values derived from the previous isotopic studies: 591 (599) pm (4).

REFERENCES

1. J. H. Callomon, *Can. J. Phys.* **34**, 1046–1076 (1956).
2. H. Schüler and L. Reinbeck, *Z. Naturforsch. A* **7**, 285–289 (1952).
3. R. Kuhn, J. P. Maier, and M. Ochsner, *Mol. Phys.* **59**, 441–448 (1986).
4. J. Lecoultre, J. P. Maier, and M. Rösslein, *J. Chem. Phys.* **89**, 6081–6085 (1988).
5. T. Motylewski and H. Linnartz, *Rev. Sci. Instrum.* **70**, 1305–1312 (1999).
6. A. O'Keefe and D. A. G. Deacon, *Rev. Sci. Instrum.* **59**, 2544–2551 (1988).
7. C. M. Western, School of Chemistry, University of Bristol, England, PGOPHER, v3.73 (1994).
8. J. Kraitchman, *Am. J. Phys.* **21**, 17–24 (1953).

O. Vaizert
P. Furrer
P. Cias
H. Linnartz
J. P. Maier

Institute for Physical Chemistry
University of Basel, Klingelbergstrasse 80
CH 4056 Basel, Switzerland

Received February 20, 2002; in revised form April 3, 2002

High-resolution electronic spectroscopy of a nonlinear carbon chain radical $C_6H_4^+$

Mitsunori Araki,[a] Harold Linnartz,[b] Pawel Cias, Alexey Denisov, Jan Fulara, Anton Batalov, Ivan Shnitko, and John P. Maier
Department of Chemistry, Klingelbergstrasse 80, CH-4056 Basel, Switzerland

A high-resolution gas-phase spectrum of a molecular absorption band around 604 nm is assigned as due to an electronic transition of a nonlinear $C_6H_4^+$ planar species starting from its $^2A''$ electronic ground state. The spectrum is observed in direct absorption by cavity ringdown spectroscopy through a supersonic planar discharge through a mixture of acetylene in helium. The spectrum has a clear rotational and K-type structure. This allows an accurate determination of the B and C rotational constants and an estimate for the A rotational constant in ground and electronically excited states. The resolved spectrum of the fully deuterated species $C_6D_4^+$ has been obtained as well. The results are compared both to the outcome of *ab initio* geometry optimizations and low-resolution absorption spectra in 6 K neon matrices obtained after mass-selective deposition. © *2003 American Institute of Physics.* [DOI: 10.1063/1.1575736]

I. INTRODUCTION

In recent years many experimental studies have been reported presenting high-resolution spectra of pure and highly unsaturated carbon chain radicals. Microwave,[1] infrared,[2] and UV–VIS spectra[3,4] are available both from matrix and gas-phase studies, all of them having in common that the major part of the observed geometries is linear. Even for very long chains, such as $HC_{22}H$ (Ref. 5) and $HC_{17}N$ (Ref. 6), linear structures have been found. Theoretical studies, however, predict for longer chains cyclic structures as well.[7] In the case of C_{13}, for example, theory[8] predicts a cyclic ground-state structure, but the experimentally observed IR spectrum is clearly that of a linear chain.[9] A reason for this discrepancy might be simply that the experimental techniques—supersonic jet expansions or matrix deposition experiments—favor the production of linear species, because large-amplitude bending motions (that are necessary to close the ring) are frozen in the production process. A similar situation might apply to the interstellar medium, where many linear carbon chain species already have been identified and the number of cyclic structures is still rather limited.[10]

In this work the electronic spectrum of a member of a so-far-unstudied class of carbon chain radicals is presented: a nonlinear and noncyclic species. The spectrum was observed more or less accidentally around 604 nm when scanning for coincidences with diffuse interstellar band features in a hydrocarbon plasma. The observed spectrum has a clear rotational and K-type structure. Simulation of the spectrum allows an accurate determination of the molecular constants of the carrier. Study of the partially and completely deuterated species gives information on the number of (equivalent) hy-drogen atoms. Final identification becomes possible following semiempirical and *ab initio* geometry optimizations for a number of species. These indicate that the band at 604 nm is due to the carbon chain cation $C_6H_4^+$ with a nonlinear $H-C\equiv C-C\equiv C-CH=CH_2^+$ planar molecular geometry. This is confirmed by the observation of their transition in the absorption spectrum obtained after mass-selective deposition of $C_6H_4^+$ ions generated in a hydrocarbon plasma in a 6 K neon matrix.

Spectroscopic data for species of the form $C_6H_4^{(+)}$ are so far missing. Only a photodissociation study has been reported in which $C_6H_4^+$ was generated following a ring opening reaction in cyanobenzene.[11] In the latter study geometry optimizations are reported using MNDO calculations, which result in a series of equilibrium structures for the cation in which the heat formation of the possible acyclic structures is about 150 kJ mol^{-1} lower than that of benzene-type structures. Among these is a geometry that is confirmed in the present study, a linear noncyclic structure that is very close to the geometry proposed for the neutral species: 1-hexene-3,5-diyne.[12,13]

II. EXPERIMENT

The experimental method has been described and uses cavity ringdown (CRD) spectrometer sampling a supersonic planar plasma.[14] The plasma is generated by a discharge through a gas pulse (-300 V, 30 Hz repetition rate) of a 0.5% C_2H_2 (and/or C_2D_2) in He mixture with a backing pressure of 10 bars in the throat of a 3 cm×100 μm multilayer slit nozzle geometry. Rotational temperatures of the order of 20–40 K are routinely achieved. The nozzle is mounted in an optical cavity where the expansion is intersected approximately 2 mm downstream by the pulsed light of a tunable dye laser (resolution 0.15 cm^{-1}). The light leaking out of the cavity is detected with a photodiode, and the resulting ring-down event is used as input for a standard ringdown

[a] Author to whom correspondence should be addressed. Fax: +41 61 2673855. Electronic mail: mitsunori.araki@unibas.ch
[b] Present address: Department of Physical Chemistry, Vrije Universiteit, De Boelelaan 1083, NL 1081 HV Amsterdam, the Netherlands.
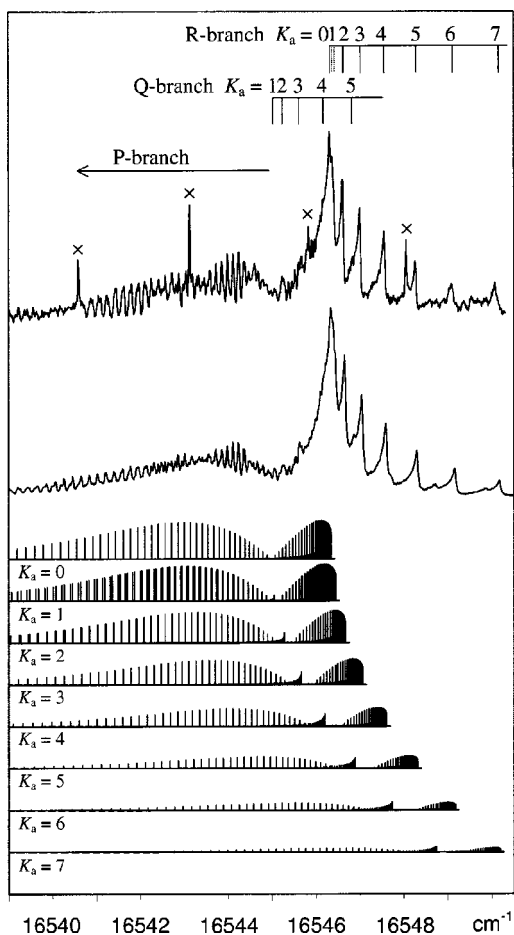
FIG. 1. Band observed at 604 nm using CRD spectroscopy through a supersonic planar plasma expansion. The rotational and K-type structure that is observed experimentally (top trace) can be simulated with a rotational temperature of 40 K, using constants derived from geometry optimizations for the nonlinear planar and noncyclic $C_6H_4^+$ carbon chain cation (second trace). The assignment is indicated in the figure and further illustrated by stick diagrams of each individual K_a. Lines marked with $\times$ are due to another carrier.
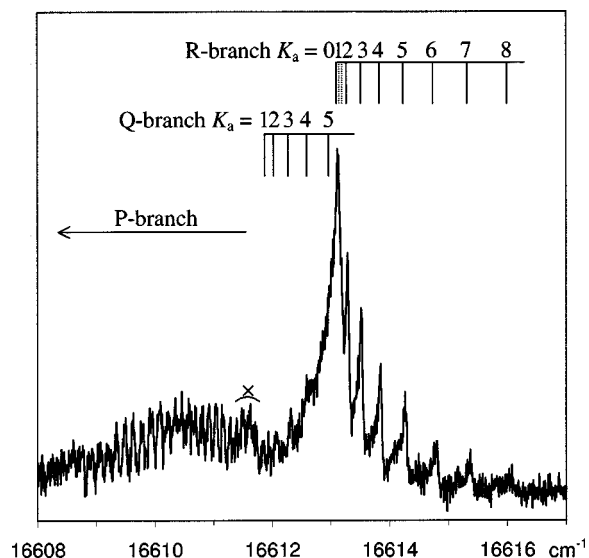

FIG. 2. Spectrum for the fully deuterated $C_6D_4^+$ species, blueshifted by approximately 67 cm^{-1} with respect to the $C_6H_4^+$ cation. Lines marked with $\times$ are due to another carrier.

analysis.[15] A spectrum is recorded by determining an averaged ringdown time as a function of the laser frequency and calibrated by simultaneously recording an iodine spectrum.

III. RESULTS AND DISCUSSION

The CRD gas-phase spectrum of the band around 604 nm is shown in Fig. 1. A series of overlapping rotational transitions is observed as well as a K-type structure ($K = 0-7$), typical for a nonlinear species. Using C_2D_2 instead of C_2H_2 yields a 67 cm^{-1} blueshifted spectrum with nearly identical spectral features, as shown in Fig. 2. This indicates that the carrier is of the form C_nH_m or $C_nH_m^{+/-}$.[16] In order to determine the values for n and m, a C_2H_2/C_2D_2 mixture has been used. A low-resolution scan, in which mainly the strong peaks for $K = 0$ and 1 will be visible, gives five broadbands including bands originating from fully H- (16 546 cm^{-1}) and fully D- (16 613 cm^{-1}) substituted species. Three remaining bands located at 16 500 cm^{-1} (a), 16 560 cm^{-1} (b), and 16 595 cm^{-1} (c) are due to partially deuterated species. From this it can be concluded that $m = 4$: the a, b, and c bands correspond to species with one, two, and three D

atoms, respectively. The one-, two-, and threefold-deuterated species should have four, six, and four peaks by statistical arguments, but three, four, and three peaks are observed. This indicates that two of the four hydrogen atoms are rather similar.

The rotational analysis of the spectra with C_2H_2 and C_2D_2 as precursors allows the determination of the number of carbon atoms (n) in the chain. The stick diagrams (Fig. 1) show how the observed spectrum can be dissected into rotational transitions belonging to individual K values. The P branch consists of a series of transitions that are closely overlapping, causing some fluctuations in overall intensity, but which give a good indication for the value of B'' (C''). The change in rotational constants upon electronic excitation is reflected by a change of line distances, particularly for higher J levels on the P branch and gives values for B' (C'). The R-branch region consists of a series of unresolved bands with clear bandheads corresponding to $K = 0-7$ as indicated in Fig. 1. The distance between the bandheads is a good indication for the value $\Delta A - \Delta B = (A'' - A') - (B'' - B')$, and the intensity ratio can be used to estimate A''. The Q-branch bands are rather weak and cannot be assigned directly. The overall pattern indicates a rotational temperature of the order of 40(5) K.

The spectra of $C_nH_4^{(+)}$ ($C_nD_4^{(+)}$) can now be rather well reproduced with rotational B and C constants of the order of 0.045 cm^{-1} (0.040 cm^{-1}) and an A constant of approximately 1.2 cm^{-1} (0.9 cm^{-1}) using WANG.[17] In view of the available constants for different kinds of carbon chain radicals determined in previous studies[18–20] this makes it very likely that $n = 6$ or 7. Therefore possible equilibrium structures have been calculated for isomers of $C_6H_4^{(+)}$ and $C_7H_4^{(+)}$ (and fully deuterated isotopes) using MOPAC (Ref. 21) (PM3/UHF). The structure that gets closest to the observations is that of the nonlinear chain H–C≡C–C≡C–CH=CH$_2^+$ (Fig. 3) for which $A'' = 1.230$ cm^{-1}, $B'' = 0.0465$ cm^{-1}, and $C'' = 0.0448$ cm^{-1}. This struc-

J. Chem. Phys., Vol. 118, No. 23, 15 June 2003

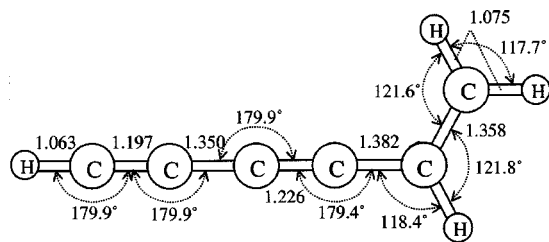Spectroscopy of a carbon chain   10563

FIG. 3. Optimized molecular structure of $C_6H_4^+$ using *ab initio* calculations. The bond lengths are given in Å.

ture corresponds to one of the geometries calculated in Ref. 11 and is close to the previously proposed geometry of the neutral C_6H_4. Other isomeric structures yield sets of substantially different constants, particularly for the fully deuterated species, whereas the corresponding D–C≡C–C≡C–CD=CD$_2^+$ gives $A''=0.889$ cm^{-1}, $B''=0.0414$ cm^{-1}, and $C''=0.0395$ cm^{-1}, close to the simulated values for the spectrum observed here.

In order to improve the geometry optimization *ab initio* calculations have been performed using GAMESS.[22] In previous work ROHF/6-31G** calculations have been reported on the isomerization of C_4H_4 radical cations.[23] An identical method is applied here to $C_6H_4^+$. Rotational constants of $C_6H_4^+$ were determined using the *ab initio* optimized structure with bond lengths and angles as indicated in Fig. 3. The resulting constants are summarized in Table I and are close to the MOPAC results, as may be expected. The simulated spectrum, using the *ab initio* results, is plotted in Fig. 1 both as stick diagrams for individual K values and as an overall spectrum with an assumed resolution of 0.05 cm^{-1}. The calculated and observed spectra match very well apart from minor intensity deviations and a few lines that may belong to another carrier.

At this stage, however, two points remain unclear. First, it is not possible to discriminate between the neutral and cationic species from the rotational analysis alone. However, the neutral C_6H_4 is a closed-shell system and as a consequence it is unlikely that a strong electronic band is found at

a rather low energy of 604 nm. In this case electronic transitions are expected in the UV. Indeed, the experimental conditions are in favor of a charged species. Second, it is not clear whether the band observed here is the origin band or a band that involves excitation of a vibrational mode in the upper electronic state—even though such bands are generally rather weak;[3] i.e., the origin band may be redshifted by a few thousands cm^{-1}. The change in rotational constants upon electronic excitation is minor and reflects a small elongation of the molecule in the upper electronic state. It is hard to conclude from these values that no vibrational excitation is involved. However, the present band is close to the well-studied and closely related $A\ ^2\Pi_g–X\ ^2\Pi_u$ electronic origin band transition of the linear triacetylene cation ($C_6H_2^+$) that has been located at 600 nm.[24] In analogy with the latter system, which is due to a transition from a $\cdots\pi_g^4\pi_u^3$ to a $\cdots\pi_g^3\pi_u^4$ configuration, it is very likely that the upper state of the observed band of the nonlinear $C_6H_4^+$ will have $^2A''$ symmetry. In this case the origin band of $C_6H_4^+$ is expected to be rather close to that of $C_6H_2^+$, as is observed.

Proof comes from a mass-selective matrix study that was performed following the gas phase analysis. This experiment combines mass selection and matrix isolation spectroscopy and has been described.[25] The $C_6H_4^+$ ($C_6D_4^+$) cations were produced from a phenylacetylene–deuterated-2,4-hexadiyne–) helium mixture in a hot cathode discharge source. A 90° deflector and a quadrupole mass spectrometer are used to steer the ion beam onto the matrix, where the mass-selected ions are codeposited with excess of neon at 6 K. The absorption spectra are recorded by guiding mono-chromatized light (0.1 nm bandpass) through the matrix onto a photomultiplier. The resulting spectra for matrices prepared with mass of $C_6H_4^+$ or $C_6D_4^+$ are shown in Fig. 4. Two strong bands are observed, one around 609 nm and one around 585 nm, for $C_6H_4^+$. No strong bands are observed to lower energy; i.e., the band at 609 nm corresponds to the origin band. The main structures to the blue of the dominant peaks (609 nm for $C_6H_4^+$ and 606 nm for $C_6D_4^+$) are matrix artifacts, site structure. The 114 cm^{-1} blueshift of the gas-phase spectrum with respect to the matrix band at 609 nm is typical for a chain of this size and in this frequency regime.[3] The band at 585 nm is due to another isomer of $C_6H_4^+$, since the relative intensity of the two bands varies strongly with different precursors. Upon deuteration the band at 609 nm shifts by 62(3) cm^{-1} to the blue—i.e., close to the 67 cm^{-1} shift observed in the gas phase upon deuteration. The band observed at 585 nm in the matrix only shifts 17(3) cm^{-1} upon deuteration. Subsequent neutralization of the trapped species by irradiation of the matrix with a medium-pressure mercury lamp leads to the disappearance of both bands. This confirms that the carrier of the 609 nm matrix and the 604 nm gas-phase carrier is a $C_6H_4^+$ cation, as was concluded from the gas-phase spectrum.

TABLE I. Observed and calculated molecular constants of $C_6H_4^+$ and $C_6D_4^+$.

| | $C_6H_4^+$ | | $C_6D_4^+$ | |
	Obs.[a]	*Ab initio*[b]	Obs.[a]	*Ab initio*[b]
A''	1.24	1.217	0.89	0.889
B''	0.0467	0.0471	0.0416	0.0420
C''	0.0449	0.0453	0.0400	0.0401
$A'-A''$	0.0767		0.0450	
B'	0.0452		0.0403	
C'	0.0434		0.0387	
$(A'-A'')-(B'-B'')^c$	0.0782		0.0463	
T_{00}	16 544.980		16 611.91	

[a]Expected errors of the rotational constants are 0.1 cm^{-1} in A and 0.001 cm^{-1} in B and C, whereas 0.0006 cm^{-1} and 0.001 cm^{-1} for $B-C$ and $(A'-A'')-(B'-B'')$. Expected errors of T_{00} are 0.01 cm^{-1} for $C_6H_4^+$ and 0.1 cm^{-1} for $C_6D_4^+$.
[b]Equilibrium values.
[c]Assuming $B'-B''=C'-C''$.

IV. ASTROPHYSICAL RELEVANCE

All the spectroscopic information is in favor of the identification of the band observed at 604 nm as due to the $^2A''–X\ ^2A''$ electronic origin band transition of the nonlinear
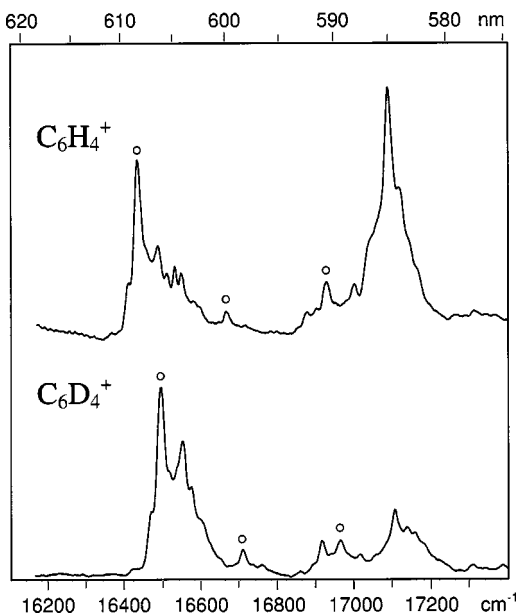
FIG. 4. Electronic absorption spectra of $C_6H_4^+$ (upper trace) and $C_6D_4^+$ (lower trace) measured in 6 K matrices after codeposition of mass-selected cations with excess of neon. The bands at 609 nm of $C_6H_4^+$ and at 606 nm of $C_6D_4^+$ correspond to the gas-phase spectra shown in Figs. 1 and 2. The weaker bands at 600 and 591 nm for $C_6H_4^+$ and 599 and 590 nm for $C_6D_4^+$ (indicated by ○) exhibit an identical chemical behavior as the 609 nm band on $C_6H_4^+$ and the 606 nm band on $C_6D_4^+$ and are due to transitions to vibrationally excited levels in the upper $^2A''$ state. The bands at 585.3 and 584.7 nm of $C_6H_4^+$ and $C_6D_4^+$ are due to another isomer.

planar $H-C{\equiv}C-C{\equiv}C-CH{=}CH_2^+$ carbon chain cation. The inferred rotational constants may guide a search for this species by millimeter-wave spectroscopy to allow a more accurate geometry determination. This is of interest as the number of microwave studies of carbon chain cations is still rather limited.[26] It furthermore would make a radio-astronomical search for this species in dense interstellar clouds possible. The optical spectrum obtained here allows a comparison with the available lists of diffuse interstellar
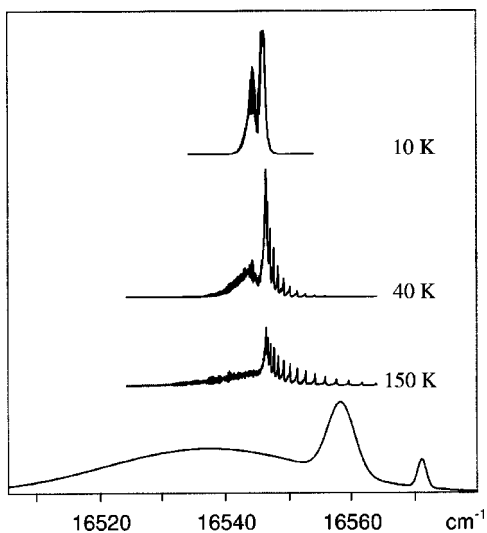

FIG. 5. Artificial DIB spectrum (Ref. 27) in the 604 nm range (lowest trace) and the simulated $C_6H_4^+$ spectra for 10, 40, and 150 K (upper three traces).

band (DIB) positions.[27,28] A comparison with the hitherto reported DIBs shows that there exists an overlap between the band observed around 16 545 cm^{-1} and a broad DIB [full width at half maximum (FWHM) $\sim$14 cm^{-1}] reported at 16 537.3 cm^{-1}. In order to check whether this discrepancy of 8 cm^{-1} might be due to a temperature effect, a comparison has been made between an artificial DIB spectrum in the 604 nm range and the $C_6H_4^+$ spectrum for low (10 K), intermediate (40 K), and high (150 K) temperatures (Fig. 5). Although it is clear that for higher temperatures the spectrum of the nonlinear $C_6H_4^+$ might start filling up the broadband around 16 545 cm^{-1}, it is hard to account for the difference in intensity of the P and R branches. This is not reflected in the DIB spectrum.

ACKNOWLEDGMENTS

[1] M. C. McCarthy and P. Thaddeus, Chem. Soc. Rev. **30**, 177 (2001).

[2] A. van Orden and R. J. Saykally, Chem. Rev. **98**, 2313 (1998).

[3] J. P. Maier, J. Phys. Chem. A **102**, 3462 (1998).

[4] H. Linnartz, D. Pfluger, O. Vaizert, P. Cias, P. Birza, D. Khoroshev, and J. P. Maier, J. Chem. Phys. **116**, 924 (2002) and references therein.

[5] T. Pino, H. B. Ding, F. Guthe, and J. P. Maier, J. Chem. Phys. **114**, 2208 (2001).

[6] M. C. McCarthy, J. U. Grabow, M. J. Travers, W. Chen, C. A. Gottlieb, and P. Thaddeus, Astrophys. J. Lett. **494**, L231 (1998).

[7] K. Aoki and S. Ikuta, J. Mol. Struct.: THEOCHEM **310**, 229 (1994).

[8] J. M. L. Martin, J. P. Francois, R. Gijbels, and J. Almlöf, Chem. Phys. Lett. **187**, 367 (1991).

[9] T. F. Giesen, A. Vanorden, H. J. Hwang, R. S. Fellers, R. A. Provencal, and R. J. Saykally, Science **265**, 756 (1994).

[10] P. Thaddeus and M. C. McCarthy, Spectrochim. Acta, Part A **57**, 757 (2001).

[11] W. J. van der Hart, E. Oosterveld, T. A. Molenaar-Langeveld, and N. M. M. Nibbering, Org. Mass Spectrom. **24**, 59 (1989).

[12] C. A. Arrington, C. Ramos, A. D. Robinson, and T. S. Zwier, J. Phys. Chem. A **103**, 1294 (1999).

[13] T. Bohm-Gossl, W. Hunsmann, L. Rohrschneider, W. Schneider, and M. Ziegenbein, Chem. Ber. **96**, 2504 (1963).

[14] T. Motylewski and H. Linnartz, Rev. Sci. Instrum. **70**, 1305 (1999).

[15] A. O'Keefe and D. A. G. Deacon, Rev. Sci. Instrum. **59**, 2544 (1998).

[16] The density of anions in the plasma is generally low, and therefore these are not considered.

[17] D. Luckhaus and M. Quack, Mol. Phys. **63**, 745 (1989).

[18] P. Cias, O. Vaizert, A. Denisov, J. Mes, H. Linnartz, and J. P. Maier, J. Phys. Chem. A **106**, 9890 (2002).

[19] H. Linnartz, D. Pfluger, O. Vaizert, P. Cias, P. Birza, D. Khorosev, and J. P. Maier, J. Chem. Phys. **116**, 924 (2002).

[20] M. C. McCarthy, M. J. Travers, A. Kovacs, C. A. Gottlieb, and P. Thaddeus, Astrophys. J. **113**, 105 (1997).

[21] J. J. P. Stewart, computer code MOPAC, a semiempirical molecular orbital program, QCPE, 455, 1983; version 6.0, 1990.

[22] M. W. Schmidt, K. K. Baldridge, J. A. Boatz, *et al.* J. Comput. Chem. **14**, 1347 (1993).

[23] G. Koster and W. J. van der Hart, Int. J. Mass Spectrom. Ion Processes **163**, 169 (1997).

[24] M. Allan, E. Kloster-Jensen, and J. P. Maier, Chem. Phys. **17**, 11 (1976).

[25] P. Freivogel, J. Fulara, D. Lessen, D. Forney, and J. P. Maier, Chem. Phys. **189**, 335 (1994).

[26] C. A. Gottlieb, A. J. Apponi, M. C. McCarthy, P. Thaddeus, and H. Linnartz, J. Chem. Phys. **113**, 895 (2000).

[27] P. Jenniskens and F.-X. Désert, Astron. Astrophys., Suppl. Ser. **106**, 39 (1994).

[28] S. Ó. Tuairisg, J. Cami, B. H. Foing, P. Sonnentrucker, and P. Ehrenfreund, Astron. Astrophys., Suppl. Ser. **142**, 225 (2000).

Electronic spectroscopy of the nonlinear carbon chains C$_4$H$_4^+$ and C$_8$H$_4^+$ [1]

Mitsunori Araki, Pawel Cias, Alexey Denisov, Jan Fulara, and John P. Maier

Abstract: The electronic spectrum of a nonlinear carbon chain radical C$_4$H$_4^+$ was observed after mass-selective deposition in a 6 K neon matrix. The corresponding gas-phase spectra of C$_4$H$_4^+$ and C$_4$D$_4^+$ have been observed in the 512 to 513 nm region and at 710 nm for C$_8$H$_4^+$. These were detected in direct absorption by cavity ring down spectroscopy through a supersonic planar discharge. The electronic transition energies of these nonlinear carbon chain radicals correlate well with those of the polyacetylene cations HC$_n$H$^+$ (n = 4, 6, 8). The observed profiles are reproduced with rotational constants obtained by ab initio geometry optimizations and extrapolation between the ground and excited electronic states.

Key words: nonlinear carbon chain, carbon cation, electronic transition, diffuse interstellar bands, molecular structure.

Résumé : On a observé le spectre électronique d'un cation C$_4$H$_4^+$ correspondant à une chaîne carbonée non linéaire déposée par un procédé sélectif en fonction de la masse dans une matrice de néon, à 6 K. Les spectres correspondants en phase gazeuse des cations C$_4$H$_4^+$ et C$_4$D$_4^+$ ont été observés dans la région de 512–513 nm et à 710 nm dans le cas du C$_8$H$_4^+$. Ces spectres ont été détectés par absorption directe par spectroscopie avec l'anneau de la cavité vers le bas grâce à une décharge supersonique planaire. Il existe une bonne corrélation entre les énergies de transition électronique de ces cations à chaîne carbonée non linéaire et celles des cations polyacétyléniques HC$_n$H$^+$ (n = 4, 6, 8). Les profils obtenus peuvent être reproduits à l'aide de constantes rotationnelles obtenues par des optimisations ab initio de géométrie et une extrapolation entre les états électroniques excités et fondamentaux.

Mots clés : chaîne carbonée non linéaire, cation carbone, transition électronique, bandes interstellaires diffuses, structure moléculaire.

[Traduit par la Rédaction]

Introduction

High-resolution spectroscopy of unsaturated carbon chain radicals is of interest in view of interstellar chemistry, as well as terrestrial discharge and flame processes. Electronic transitions of the polyacetylene cations HC$_n$H$^+$ (1–4) and radicals C$_n$H (5) with even number carbons have now been studied. Recently a nonlinear planar carbon chain radical C$_6$H$_4^+$, H-C≡C-C≡C-CH=CH$_2^+$, was detected in a supersonic planar discharge with cavity ring down spectroscopy in the 604 nm region (6). Therefore, the related C$_4$H$_4^+$ and C$_8$H$_4^+$ nonlinear chains were expected to be produced in the plasma discharge in a sufficient concentration for detection.

Hydrogenated nonlinear chains can exist in dark interstellar clouds as well as linear ones, e.g., the column densities of C$_2$O, H$_2$CCO, and CH$_3$CHO are of the same order of

magnitude in Taurus Molecular Cloud-1 (7). However, the intensity of rotational transitions for a linear molecule with a smaller rotational partition function is stronger than for an asymmetric top, and thus, a long nonlinear carbon chain has not yet been detected by radio astronomy, even though the population may be comparable. In the case of electronic transitions, an asymmetric top molecule is not at a disadvantage compared with the linear one. Thus, the nonlinear chains can be considered as candidates, causing the diffuse interstellar band (DIB) absorptions in much the same way as the linear series (8).

The short nonlinear carbon chain H-C≡C-CH=CH$_2$ is predicted to be an intermediate between acetylene and polyaromatic hydrocarbons in the interstellar chemistry of circumstellar envelopes (9). Laboratory experiments indicate that photodissociation of aromatic molecules produces a nonlinear carbon chain (10). The potential energy surface for three C$_4$H$_4$ isomers is also of relevance in the fields of organic chemistry and reaction dynamics (11). Therefore, species and their ions having H-C$_n$-CH=CH$_2$ (n = 2, 4, 6,...) nonlinear chain structures are of interest, and information by high-resolution spectroscopy is needed.

The 604 nm origin of the ^{2}A″–X^{2}A″ transition of C$_6$H$_4^+$ (6) is close to the 600 nm $^2\Pi_u$–X$^2\Pi_g$ one of HC$_6$H$^+$ (2). Both transitions involve the same π ← π excitation. The transition energy difference in a homologous series should be comparable because C$_6$H$_4^+$ and HC$_6$H$^+$ are produced by an extension of the acetylene chain from C$_4$H$_4^+$ or HC$_4$H$^+$ (12). The

Fig. 1. (a) Energies of the origin bands in the $^2\Pi_u$–$X^2\Pi_g$ transition of HC_nH^+ and the $^2A''$–X^2A'' transition of $C_nH_4^+$. For HC_nH^+ (n = 4, 6, 8) and $C_6H_4^+$, those are the observed values reported in refs. 1–3 and 6, respectively. The transitions of $C_4H_4^+$ and $C_8H_4^+$ were estimated by shifting the HC_4H^+ and HC_8H^+ values down by the difference of HC_6H^+ to $C_6H_4^+$; (b) Observed transition-energy differences between HC_nH^+ and $C_nH_4^+$ with the same number of carbon atoms.
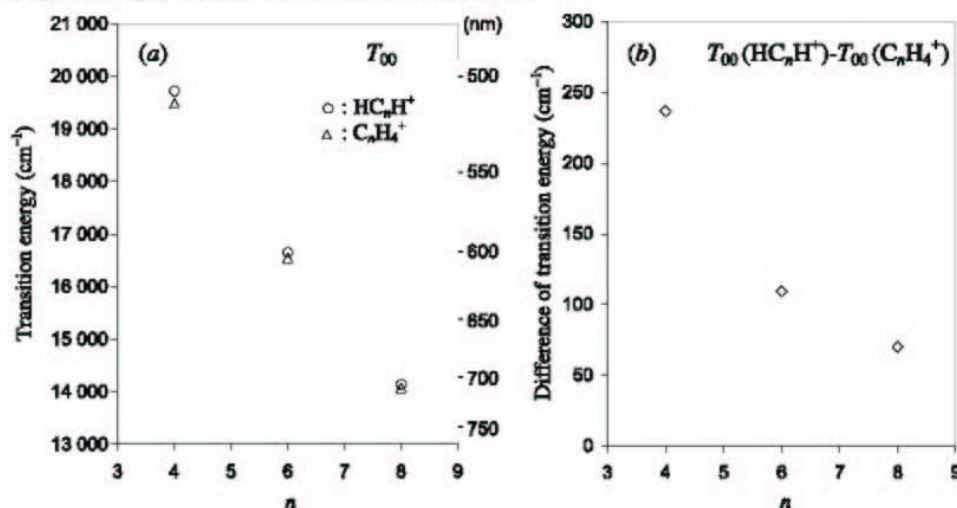

same argument may be applied to the six- and eight-carbon chain species. This trend is shown in Fig. 1a, and the transition energies of $C_4H_4^+$ and $C_8H_4^+$ are consequently estimated to lie near 510 and 712 nm, respectively.

The electronic transition of mass-selected $C_4H_4^+$ was subsequently observed in a neon matrix with origin band at 515 nm, in good agreement with the estimated value. Based on this, the gas-phase spectrum was searched for in a cavity ring down spectrometer, and the origin band was observed at 513 nm. Similarly the electronic transition of $C_8H_4^+$ was also detected in the gas phase in the expected 712 nm region. The observed rotational structure in the gas-phase spectra indicates that these are due to the nonlinear, planar carbon chains H-C≡C-CH=CH$_2^+$ and H-C≡C-C≡C-C≡C-CH=CH$_2^+$.

## Experimental observations

To locate the electronic transition of $C_4H_4^+$, neon-matrix isolation spectroscopy in combination with mass selection was used at first. The $C_4H_4^+$ cation was produced from a benzene–helium mixture in a hot cathode discharge source. A 90° deflector and a quadrupole mass spectrometer were used to steer the ion beam onto the substrate, where the mass-selected ions were codeposited with excess of neon at 6 K (13). The absorption spectra were recorded by guiding monochromatized light (0.1 nm bandpass) through the matrix onto a photomultiplier. The observed spectrum is shown in Fig. 2. All bands observed in the absorption spectrum disappeared upon UV irradiation of the matrix, a test used to indicate that the species is a cation. Three bands of $C_4H_4^+$ were observed; the one at 19 416 cm^{-1} can be assigned to the origin of the electronic transition and the 19 931 and 20 229 cm^{-1} ones to transitions to excited levels in the upper electronic state corresponding to vibrational frequencies of 515 and 813 cm^{-1}, because the population of the species at 6 K is entirely in the lowest level of the ground state.

Fig. 2. The electronic absorption spectrum of $C_4H_4^+$, measured in a 6 K matrix after codeposition of mass-selected cations with excess of neon. The band at 19 416 cm^{-1} corresponds to the gas-phase spectrum shown in Fig. 3. The weaker bands at 19 931 and 20 229 cm^{-1} decrease at the same rate as the 19 416 cm^{-1} one upon UV radiation and are due to transitions to vibrationally excited levels in the upper $^2A''$ state. The three peaks (□) 100 cm^{-1} to the blue from the dominant ones are matrix artefacts, site structure. The bands at 19 630 and 20 440 cm^{-1} are due to the diacetylene cation HC_4H^+.
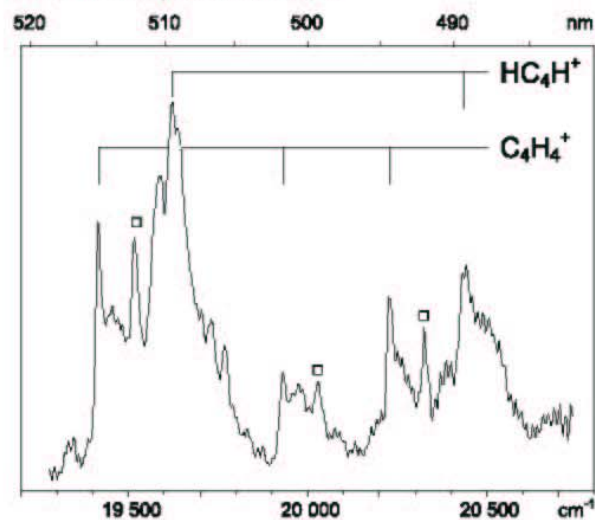
The gas-phase measurement used a cavity ring down spectrometer sampling a supersonic planar plasma (14). The latter was generated by a discharge through a gas pulse (30 Hz repetition rate) of a sample in a buffer gas mixture with a backing pressure of 1000 kPa in the throat of a 3 cm ×

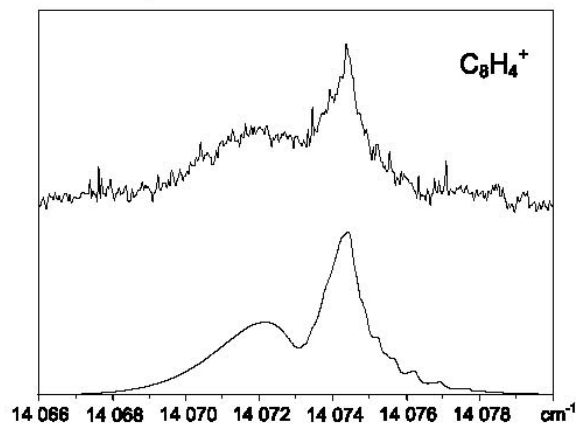**Fig. 3.** The origin bands of the $^2A''-X^2A''$ electronic transition for $C_4H_4^+$ and $C_4D_4^+$ observed using cavity ring down spectroscopy through a supersonic planar plasma expansion. The rotational structure observed (traces a and c) can be simulated with a temperature of 30 K using constants derived from geometry optimization by ab initio calculation (traces b and d). Bands marked with * are due to another carrier. The peaks going off-scale are due to the Swan bands of C_2 and were used for the frequency calibration. The spectrum of $C_4D_4^+$ is shifted by -51.64 cm^{-1} for comparison with $C_4H_4^+$.

Fig. 4. The $^2A''-X^2A''$ origin band in the electronic transition for $C_8H_4^+$ observed using cavity ring down spectroscopy through a supersonic planar plasma expansion. The rotational structure observed (upper trace) can be simulated (lower trace) using constants derived from geometry optimization by an ab initio calculation and a temperature of 50 K.
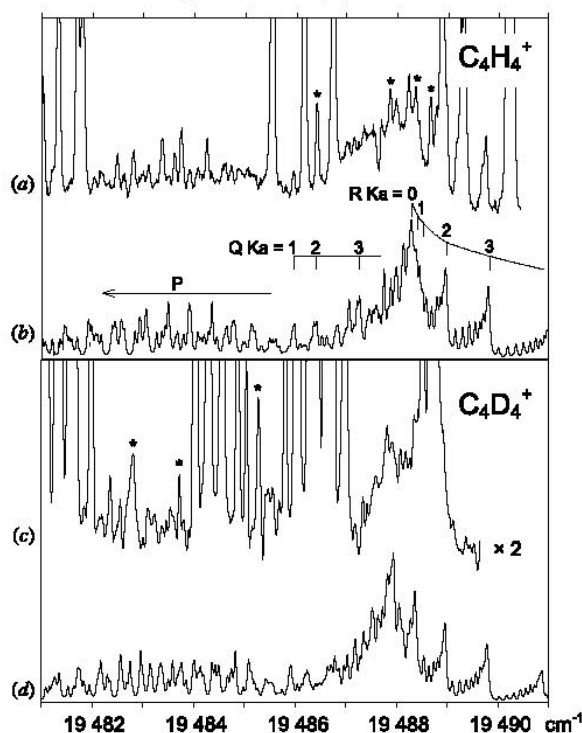

100 μm multilayer slit-nozzle geometry. Rotational temperatures of the order 30–50 K are routinely achieved. The nozzle was mounted in an optical cavity where the expansion was intersected ~2 mm downstream by the pulsed light of a tunable dye laser. The line width of the dye laser was 0.15 cm^{-1} when scanning with a grating and 0.04 cm^{-1} with an intracavity etalon. The light leaking out of the cavity was detected with a photodiode and was used as input for a standard ring down analysis (15). A spectrum was recorded by determining an averaged decay time as a function of the laser frequency.

The origin transition of $C_4H_4^+$ was searched for around the 19 416 cm^{-1} region, and a band having P- and R-branches was found at 19 486 cm^{-1}, as shown in Fig. 3a. When C_2D_2 was used as the sample gas, another band, having a similar profile, was detected around 19 537 cm^{-1} (Fig. 3c). The shift on deuteration is 51 cm^{-1}, which is comparable with the 67 cm^{-1} one for the $C_6H_4^+-C_6D_4^+$ pair (6). The 19 486 cm^{-1} band lies 70 cm^{-1} to the red in a neon matrix, comparable with the 79 cm^{-1} shift in HC$_4$H$^+$ (12). The optimized condition for the production of $C_4H_4^+$ used a mix-

ture of 0.5% C_2H_2 in argon and a -700 V discharge while sampling 2 mm downstream from the discharge slit. The signals could not be detected when helium was used as the buffer gas. The behaviour of the HC$_4$H$^+$ absorption signals was similar.

The energy of the electronic transition of $C_8H_4^+$ was expected around 14 030 cm^{-1} by reference to Fig. 1. One band was found in the gas phase at 14 073 cm^{-1}, as shown in Fig. 4. The optimized condition was quite similar to that for $C_6H_4^+$, a -300 V discharge through a mixture of 0.5% C_2H_2 in helium and with probing 1.5 mm downstream from the slit.

Results and discussion

The differences in frequency between the observed origin bands of $C_4H_4^+$, $C_6H_4^+$, and $C_8H_4^+$ and of the corresponding HC$_n$H$^+$ series (1–3) are 237, 110, and 70 cm^{-1}, as shown in Fig. 1b. The shifts decrease with increasing number of carbon atoms. This indicates that the contribution of the nonlinear part, -CH=CH$_2$, to the molecular orbital decreases on extension of the carbon chain. This trend in the two homologous series suggests that the observed bands can be assigned to $C_4H_4^+$ and $C_8H_4^+$ with the common chain structures. $C_8H_4^+$ has five isomers constructed by combination of ethylene and acetylene, as shown in Fig. 5. Structure (b) is intermediate between a prolate and an oblate top, but the observed spectrum has the profile of a typical near-prolate top and a-type transition. In the view of this, structure (b) is rejected as the carrier of the observed spectrum. Geometries (b) and (c) do not have eight carbons in a line but instead have a branching structure. Owing to the correlation of the transition energy of $C_n H_4^+$ and HC$_n$H$^+$ (Fig. 1), these should be π–π type electronic excitations in the conjugated system. Transition energies of the structures (b) and (c) would not show the correlation with the HC$_n$H$^+$ series. Structures (d) and (e) are cis and trans isomers, and both should have

Fig. 5. Optimized molecular structure in the ground state of $C_4H_4^+$ and $C_8H_4^+$ using ab initio calculations. The bond lengths are given in Å. Other isomers of $C_8H_4^+$ are indicated by simple pictures.
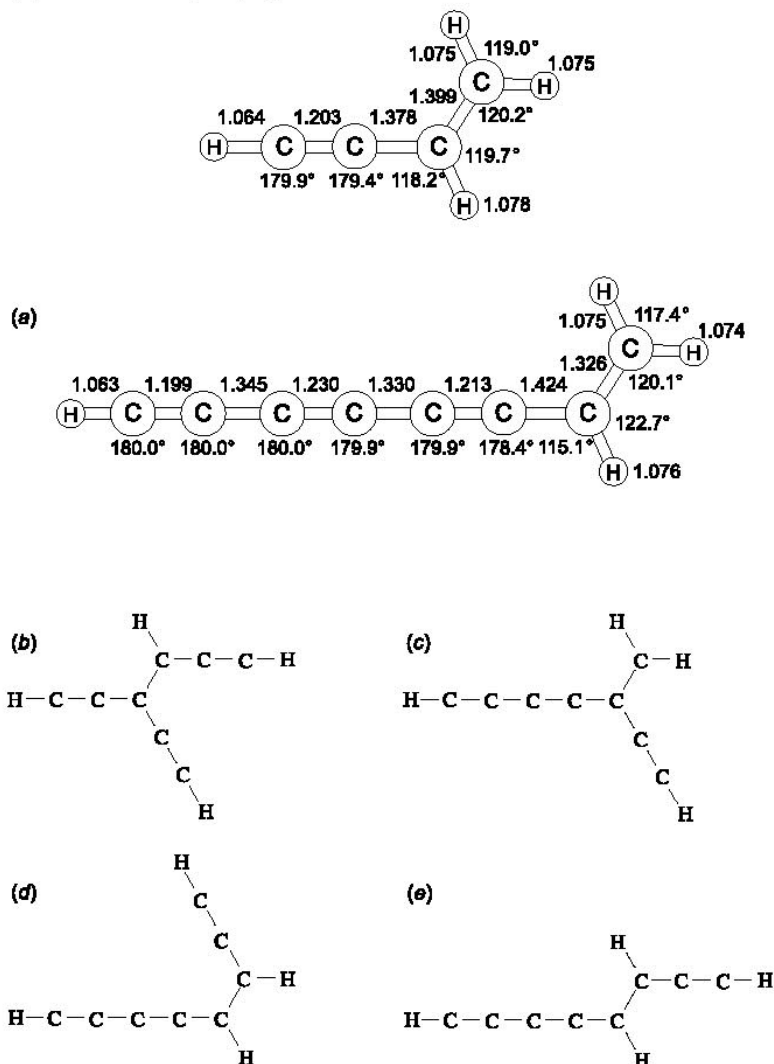
their electronic transition close to each other. No other signal could be detected within ±100 cm^{-1} from the observed band. Thus, the structures (c), (d), and (e) can be rejected as candidates for the observed spectrum. There remains structure (a), which would correlate with the HC_nH^+ series, and therefore this is the best candidate for the assignment. Consequently the symmetry of the electronic transitions observed for $C_4H_4^+$ and $C_8H_4^+$ is $^2A''-X^2A''$.

Determination of the rotational constants from the observed spectra is difficult because of overlap by the Swan bands of C_2 (16) in the case of $C_4H_4^+$ (Fig. 3) and the non-resolved rotational contour on $C_8H_4^+$ (Fig. 4). Thus, the rotational constants and molecular structure in the ground state of $C_4H_4^+$ and $C_8H_4^+$ were determined by ab initio calculations using GAMESS (17) with ROHF/6-31G**, the same method used in previous works (6, 18). The optimized

bond lengths and angles are given in Fig. 5. From the latter, the rotational constants were calculated (Table 1).
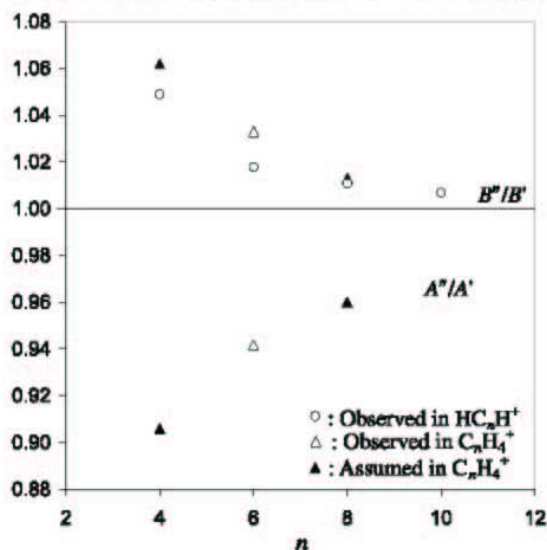
In the case of the polyacetylene cations HC_nH^+, the ratio B''/B' of rotational constants between the ground and excited states decreases and approaches 1.0 on extension of the carbon chain (Fig. 6). The ratios B''/B' and C''/C' for the $C_nH_4^+$ series should follow the same trend and converge to the HC_nH^+ value for the long chains. Ratio A''/A' should increase and approach 1.0 on extension of the carbon chain. These trends were assumed in order to estimate the rotational constants in the excited states of $C_4H_4^+$ and $C_8H_4^+$ (Table 1). The profiles of the origin bands in the electronic transitions of $C_4H_4^+$ and $C_8H_4^+$ were then simulated using the ground-state rotational constants given by the ab initio calculation and the extrapolated excited-state values from the $C_6H_4^+$ data. The observed profiles are then well repro-

Table 1. Calculated rotational constants and assumed ratios between the ground and excited states.

	$C_4H_4^+$	$C_4D_4^+$	$C_6H_4^{+a}$	$C_8H_4^+$
A'' (cm^{-1})	1.562	1.075	1.217	1.220
B'' (cm^{-1})	0.162	0.138	0.0471	0.0193
C'' (cm^{-1})	0.147	0.122	0.0453	0.0190
A''/A'		0.91	0.94^b	0.96
B''/B', C''/C'		1.06	1.03^b	1.01

[a]Reference 6.
[b]Experimentally determined.

Table 2. Comparison of the origins (cm^{-1}) of the $^2A''-X^2A''$ electronic transition of $C_nH_4^+$ and $^2\Pi_u-X^2\Pi_g$ of HC_nH^+.

n	HC_nH^+	$C_nH_4^+$ ($C_nD_4^+$)	ΔT_{00}
4	$19\,722.61^a$	19 485.80 (19 537.45)	236.81
6	$16\,654.69^b$	$16\,544.98^c$ ($16\,611.91)^c$	109.71
8	$14\,143.18^d$	14 073.00	70.18

[a]Reference 1.
[b]Reference 2.
[c]Reference 6.
[d]Reference 3.

Fig. 6. Ratios of rotational constants between the ground and excited states for HC_nH^+ and $C_nH_4^+$. A''/A' are <1.0 whereas B''/B' are >1.0, and it is assumed that $B''/B' = C''/C'$ in $C_nH_4^+$.

Fig. 7. Artificial diffuse interstellar band absorptions in the 709–714 nm range (lower trace reproduced from ref. 20) and the simulated $C_8H_4^+$ laboratory spectra at 10, 40, and 150 K (upper traces).

duced (Figs. 3 and 4) using the WANG program (19). By comparison of the simulated and observed spectra, the assignments were confirmed, and more accurate transition frequencies were inferred. These are given in Table 2.

Astrophysical relevance

The optical spectrum obtained for $C_8H_4^+$ allows a comparison with the available lists of DIB positions (20, 21). This shows that there is an overlap between the band observed around 14 073 cm^{-1} and two DIBs reported at 14 068.9 and 14 078.4 cm^{-1}. To check whether these differences in frequency might be due to a temperature effect, a comparison was made between an artificial DIB spectrum in the 709–714 nm range and the simulated $C_8H_4^+$ spectrum for low (10 K), intermediate (40 K), and high (150 K) temperature. This is shown in Fig. 7. From this it is clear that the absorption band of the nonlinear $C_8H_4^+$ does not fit the DIB absorption at any temperature.
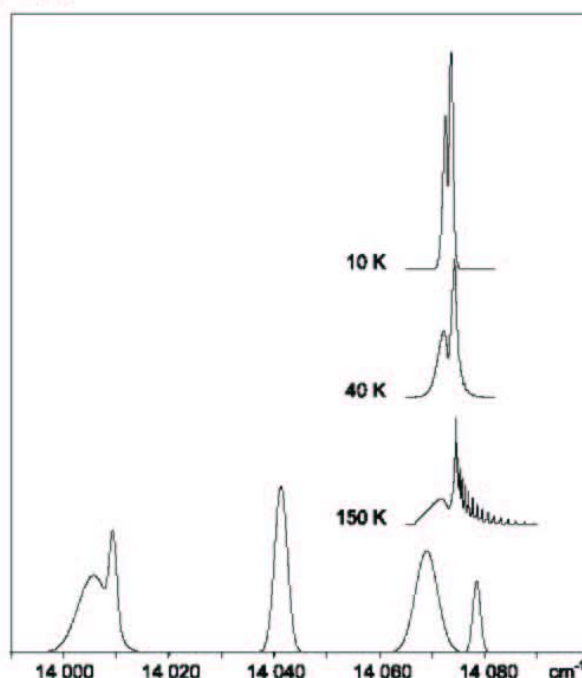
A DIB having a double peak structure and similar rotational profile (with P- and R-branches) to that observed for $C_8H_4^+$ is located between 14 000 and 14 010 cm^{-1} (Fig. 7).

However, no absorption was detected in this region in the laboratory measurements. In the case of the $C_4H_4^+$ absorptions, there are no overlaps with DIBs.

An upper limit of the column density for the $C_nH_4^+$ series in diffuse clouds can be estimated by comparison of the laboratory and DIB data in a similar fashion to that used before (22). For this, it is assumed that the oscillator strengths of the 0–0 band in the $^2A''-X^2A''$ transition for $C_nH_4^+$ ($n = 4$, 6, 8) and $A^2\Pi_u-X^2\Pi_g$ for HC_nH^+ (22) are equal (i.e., 0.04, 0.06, and 0.08 for $C_4H_4^+$, $C_6H_4^+$, and $C_8H_4^+$) and that a signal-to-noise ratio of 5 is required for detection of a DIB absorption. The fwhm of the bands is about 2 Å, and the sensitivity limit for a DIB detection is 0.002 Å (20). This leads to upper limits for their column densities of 2×10^{12}, 1×10^{12}, and 0.6×10^{12} cm^{-2} for $C_4H_4^+$, $C_6H_4^+$, and $C_8H_4^+$, respectively.

Acknowledgement

References

1. J. Lecoultre, J.P. Maier, and M. Rösslein. J. Chem. Phys. **89**, 6081 (1988).
2. W.E. Sinclair, D. Pfluger, H. Linnartz, and J.P. Maier. J. Chem. Phys. **110**, 296 (1999).
3. D. Pfluger, T. Motylewski, H. Linnartz, W.E. Sinclair, and J.P. Maier. Chem. Phys. Lett. **329**, 29 (2000).
4. P. Cias, O. Vaizert, A. Denisov, J. Mes, H. Linnartz, and J.P. Maier. J. Phys. Chem. A, **106**, 9890 (2002).
5. See for example: H. Linnartz, T. Motylewski, and J.P. Maier. J. Chem. Phys. **109**, 3819 (1998).
6. M. Araki, H. Linnartz, P. Cias, A. Denisov, J. Fulara, A. Batalov, I. Shnitko, and J.P. Maier. J. Chem. Phys. **118**, 10 561 (2003).
7. M. Ohishi, W.M. Irvine, and N. Kaifu. *In* Astrochemistry of cosmic phenomena. *Edited by* P.D. Singh. Kluwer, Dordrecht. 1992. pp. 171–177.
8. A.E. Douglas. Nature (London), **269**, 130 (1977).
9. M. Frenklach and E.D. Feigelson. Astrophys. J. **341**, 372 (1989).
10. See for example: W.J. van der Hart, E. Oosterveld, T.A. Molenaar-Langeveld, and N.M.M. Nibbering. Org. Mass Spectrom. **24**, 59 (1989).
11. R. Wrobel, W. Sander, D. Cremer, and E. Kraka. J. Phys. Chem. A, **104**, 3819 (2000).
12. J.P. Maier. Chem. Soc. Rev. **26**, 21 (1997).
13. P. Freivogel, J. Fulara, D. Lessen, D. Forney, and J.P. Maier. Chem. Phys. **189**, 335 (1994).
14. H. Linnartz, T. Motylewski, and J.P. Maier. J. Chem. Phys. **109**, 3819 (1998).
15. A. O'Keefe and D.A.G. Deacon. Rev. Sci. Instrum. **59**, 2544 (1988).
16. G.M. Lloyd and P. Ewart. J. Chem. Phys. **110**, 385 (1999).
17. M.W. Schmidt, K.K. Baldridge, J.A. Boatz, S.T. Elbert, M.S. Gordon, J.H. Jensen, S. Koseki, N. Matsunaga, K.A. Nguyen, S.J. Su, T.L. Windus, M. Dupuis, and J.A. Montgomery. J. Comput. Chem. **14**, 1347 (1993).
18. G. Koster and W.J. van der Hart. Int. J. Mass Spectrom. Ion Processes, **163**, 169 (1997).
19. D. Luckhaus and M. Quack. Mol. Phys. **63**, 745 (1989).
20. P. Jenniskens and F.-X. Désert. Astron. Astrophys. Suppl. Ser. **106**, 39 (1994).
21. S.Ó. Tuairisg, J. Cami, B.H. Foing, P. Sonnentrucker, and P. Ehrenfreund. Astron. Astrophys. Suppl. Ser. **142**, 225 (2000).
22. T. Motylewski, H. Linnartz, O. Vaizert, J.P. Maier, G.A. Galazutdinov, F.A. Musaev, J. Krełowski, G.A.H. Walker, and D.A. Bohlender. Astrophys. J. **531**, 312 (2000).

Curriculum Vitae

Personal information

Name	Pawel Cias
Place of birth	Konskie, Poland
Nationality	Polish
Marital status	Single

Education

	Primary School No. 2, Konskie
	Secondary Technical School, Konskie
1994 – 2000	Jagiellonian University, Department of Chemistry, Krakow, Poland
	MSc title in Chemistry
2000 – 2004	University of Basel, Department of Chemistry, Switzerland
	Ph.D. work in the group of Prof. John. P. Maier

List of publications

1. Rotationally resolved A $^3\Sigma_u^-$ – X $^3\Sigma_g^-$ electronic transition of NC_5N.

   H. Linnartz, O.Vaizert, P. Cias, L. Grueter, J.P. Maier, Chem. Phys. Lett. **345** (2001) 89.

2. Rotationally resolved A $^2\Pi_u$ – X $^2\Pi_g$ electronic transition of NC_6N^+.

   H. Linnartz, D. Pfluger, O. Vaizert, P. Cias, P. Birza, D. Koroschev, J.P. Maier, J. Chem. Phys. **116** (2002) 924.

3. Rotationally resolved A $^2\Pi_u$ – X $^2\Pi_g$ electronic transition of HC_4D^+.

   O. Vaizert, P. Furrer, P. Cias, H. Linnartz, J.P. Maier, J. Mol. Spec. **214,** (2002) 94.

4. Electronic gas-phase spectrum of pentaacetylene cation.

   P. Cias, O. Vaizert, A. Denisov, J. Mes, H. Linnartz, J.P. Maier, J. Phys. Chem. **106,** (2002) 9890.

5. High resolution electronic spectroscopy of a nonlinear carbon chain radical $C_6H_4^+$.

   M. Araki, H. Linnartz, P. Cias, A. Denisov, J. P. Maier, J. Chem. Phys. **118** (2003) 10561.

6. Electronic spectroscopy of the nonlinear carbon chains $C_4H_4^+$ and $C_4H_8^+$.

   M. Araki, P. Cias, A. Denisov, J. Fulara, J. P. Maier, Can. J. Chem. **82** (2004) 1.

7. Gas phase detection of cyclic B_3: $2\,^2E^{'} - X\,^2E_1^{'}$ electronic origin band.

   P. Cias, M. Araki, A. Denisov, J. P. Maier, J. Chem. Phys. (submitted).

8. New laboratory data of a molecular band at 4429 Å.

   M. Araki, H. Linnartz, P. Kolek, H. Ding, A. Denisov, A. Boguslavskiy, T. W. Schmidt, T. Motylewski, P. Cias, J. P. Maier, ApJ. (submitted).